1993

Effects of randomly rough surfaces on ultrasonic inspection

Mehmet Bilgen
Iowa State University

Order Number 9413958

Effects of randomly rough surfaces on ultrasonic inspection

Bilgen, Mehmet, Ph.D.

Iowa State University, 1993

U·M·I
300 N. Zeeb Rd.
Ann Arbor, MI 48106

Effects of randomly rough surfaces on ultrasonic inspection

by

Mehmet Bilgen

A Dissertation Submitted to the

Graduate Faculty in Partial Fulfillment of the

Requirements for the Degree of

DOCTOR OF PHILOSOPHY

Interdepartmental Program:	Biomedical Engineering
Department:	Electrical Engineering and Computer Engineering
Co-Majors :	Biomedical Engineering
	Electrical Engineering (Communication and Signal Processing)

Approved:

Signature was redacted for privacy.

In Charge of Major Work

Signature was redacted for privacy.

For the Interdepartmental Program

Signature was redacted for privacy.

For the Major Department

Signature was redacted for privacy.

For the Graduate College

Iowa State University
Ames, Iowa

1993

TABLE OF CONTENTS

GENERAL INTRODUCTION

Nondestructive evaluation has been used for various science and engineering applications. For example high frequency sound waves (ultrasound) are used to detect subsurface defects such as cracks, voids and inclusions. The inspection of industrial parts for such flaws is carried out either during manufacturing or periodically during the use of the part. Inspection is necessary for quality control and more importantly for failure prevention in safety related areas. The surface finish of the part affects its ultrasonic inspection and consequently the surfaces are often machined smooth before the inspection. Inspection through smooth surfaces have been well studied and understood. A theoretical basis has been established for the characterization of interior flaws and a large literature exists. However, much less is known about quantitative ultrasonic inspection of such defects in part with rough surfaces, e. g. machine marks or "as-cast" surfaces. A question arises "When can an industrial part with randomly rough surfaces be inspected robustly using ultrasound?". This dissertation is aimed at: (1) developing a rigorous theory for immersion ultrasonic inspection through randomly rough surfaces, (2) providing a concrete understanding of the physics of the received signal and its dependence on changes in the probe's parameters as well as the statistics of the rough surface, and (3) giving simple formulas suitable for engineering use. The results presented in this dissertation can provide considerable insight into the development of experiments and the interpretation of measurements.

Ultrasonic nondestructive inspections typically use phase-coherent probes described by radius, focal length and center frequency. Typical frequencies range from 1 to 50 MHz, with wavelength ranging from 30 μm to 6 mm. Transducer radii are on the order of centimeters as are the various path lengths in the problem. Typical microstructures range from 10 μm to 1 mm in radius. A part's rough surfaces are usually characterized by a stationary Gaussian random process with zero mean and correlation functions of either

Gaussian or exponential type. The rms height of the roughness typically varies between 1 and 500 μm, while the surface correlation length varies from 100 μm to several millimeters.

Figure 1 depicts geometry of a typical set-up designed to perform ultrasonic inspection through randomly rough surfaces in the pulse-echo mode. The probe illuminates the rough surface with a broadband pulse at normal incidence. The same probe detects the scattering induced from the interaction of the incident beam with the rough surface, the microstructure (noise) and any flaw located within the part (signal). Figure 2 shows signals recorded experimentally from a brass sample. The brass sample was specially prepared; one surface was roughened randomly, the opposite surface was machined smooth and a hole drilled between these two surfaces. The top two signals in Fig. 2 were obtained using an unfocused probe and lower two were recorded using a focused probe. The signals in Figs. (2a) and (2c) were measured through the smooth surface of the sample and the ones in Figs. (2b) and (2d) were received through the rough side. The incoherent backscatter from the microstructure produces a more-or-less random signal, "material noise", which is weakly modified by the surface roughness for both types of probes. On the other hand, reflections from the drilled hole are greatly attenuated by the surface roughness. These results imply significant reduction of the signal-to-noise ratio and hence a lowering of the probability of detection. The degradation in the signal-to-noise ratio is more severe for the unfocused probe; in this case the noise masked the attenuated flaw signal completely. Consequently, it is of considerable interest to determine quantitatively the effects of randomly rough surfaces on the signal-to-noise ratio. Hence, this dissertation addresses this problem by modeling the probe signal and then analyzing it statistically.

In its general setting, the theoretical modeling of ultrasonic inspection beneath rough surfaces is difficult and involved due to the inherent elastic nature and the different orientations and phases of the microstructures within the specimen. The dissertation addresses this problem by making certain simplifying assumptions and approximations

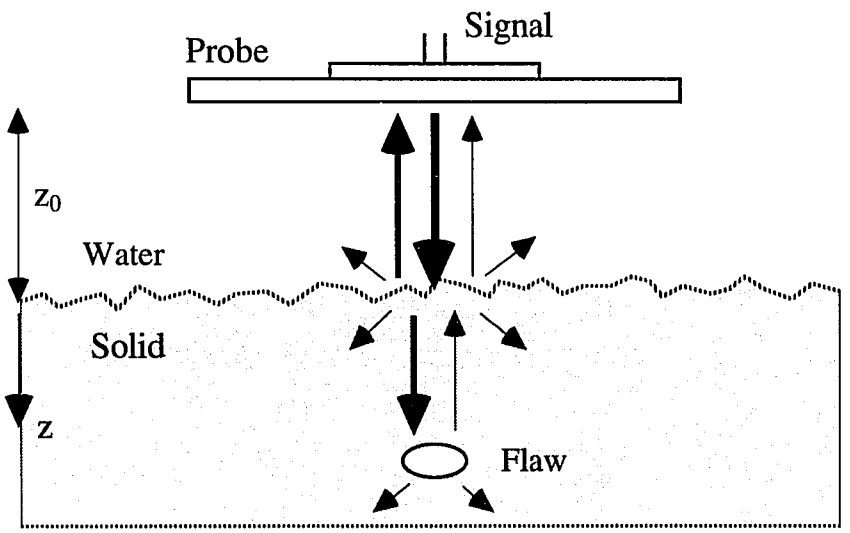

Figure 1. Schematic geometry of immersion type ultrasonic inspection set-up.

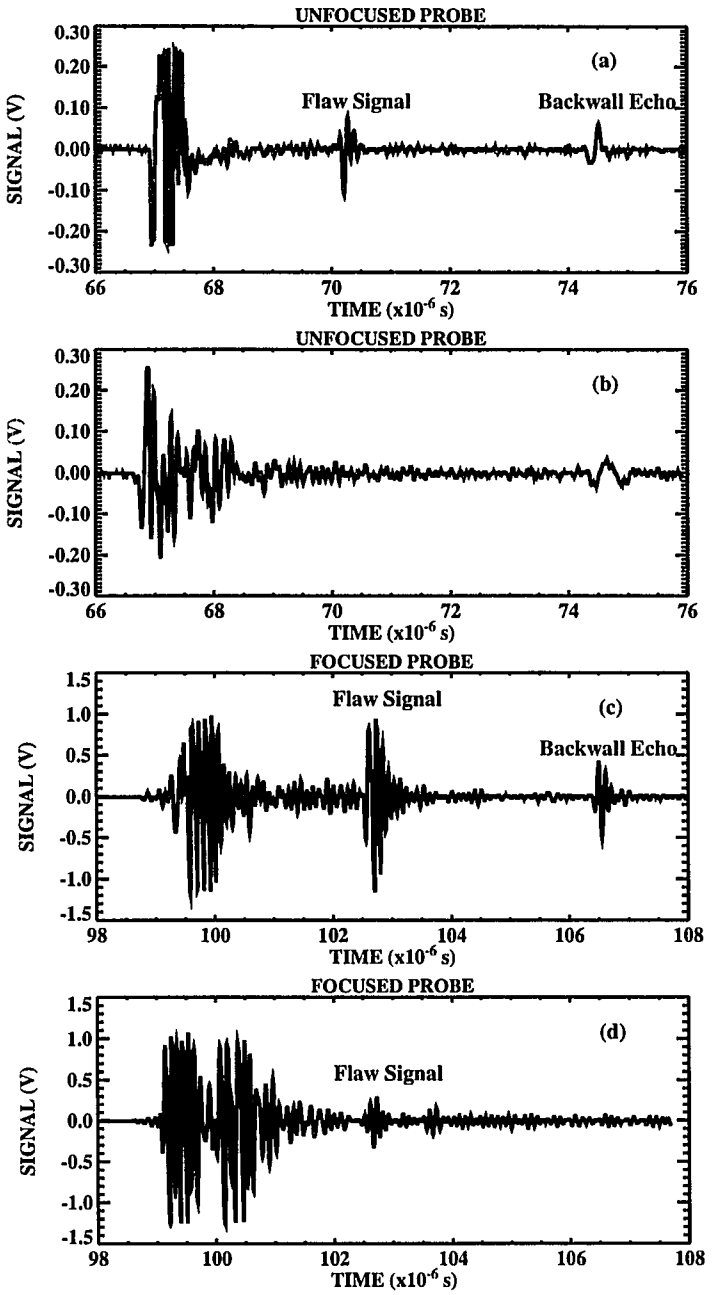

Figure 2. (a) Signal received through the smooth surface for unfocused probe, and (b) Signal received through the rough surface for unfocused probe, and (c) Signal received through the smooth surface for focused probe, and (d) Signal received through the rough surface for focused probe.

concerning the solid. The assumptions can be summarized as follows; 1) the ultrasonic longitudinal wave is modeled by a scalar wave propagation in a constant-density fluid, shear wave propagation is neglected, 2) the size of the microstructures is much smaller than the wavelength, and 3) no attenuation is induced by the microstructure. The approximations are the Born approximation [1] (i.e. the scattering from the microstructure is weak), the phase-screen approximation and the Fresnel approximation [2]. The phase-screen approximation is used to model the reflection or transmission of waves through rough surfaces. In this approximation, the surface roughness changes the phase, but not the amplitude, of the reflected or transmitted wave. The Fresnel approximation simplifies the plane wave expansion in wave propagation. The phase-screen approximation and the Fresnel approximation are tested using the integral equation method for the parameter range of ultrasonic inspection, and found to be reasonably accurate for small rms height and large correlation length. Under the aforementioned assumptions and approximations, Auld's reciprocity formula [3] is the tool employed to estimate the scattering induced signals at the investigating probe. The above model establishes a theoretical basis for the dissertation by providing simple engineering formulas which can be implemented in practice easily. Based on this model, some major findings presented in this dissertation are 1) the observation of a near surface dead-zone for the flaw signal (due to substantially increased attenuation for near-surface flaws), 2) a substantial reduction in roughness-induced noise for focused probes 3) and a consequent improvement in the signal-to-noise ratio, 4) characterization of randomly rough surfaces (the determination of surface statistics from ultrasonic reflections) and 5) comparison of the theoretical results with the available experimental measurements.

Inspection problems involving rough surfaces occur ubiquitously in other physical applications. Examples are the sea surface or a foliage canopy, which can present rough interfaces for microwave imaging or remote sensing [4]. The surface finish of industrial parts affects their nondestructive evaluation using microwaves or eddy currents. In

geophysics, the use of ground penetrating radar for the detection of archeological sites and the detection of ores is impacted by the surface roughness. Optical inspection of defects in semiconductors is affected by the surface properties of the substrates [5]. In biological sciences, the ultrasonic measurements of the contractility in myocardium, the characterization of skin burns and laser light interaction with the tissue cells are also influenced by the surface roughness of the media.

A considerable literature concerning the reflection of waves by the rough surfaces appeared in the past [6-15]. Kirchoff approximation and the perturbation theory are the two common approaches developed to calculate the interaction of waves with the rough surfaces and are reviewed by Ogilvy [16]. Substantially less is known about the transmission of waves through the rough surfaces. Recently, there has been interest in the effects of surface roughness on wave transmission [17] as well as on ultrasonic inspection [18-20]. Nagy and Adler [18] studied the surface roughness induced attenuation of the coherent (average) part of the transmitted wave. They modeled the wave propagation through the rough surface via the phase-screen approximation. With their model, they reached good agreements with the experimentally measured attenuation values of coherent signal and applied their predictions to the detection and characterization of porosity in as-cast aluminum. Nagy and Rose [19] extended the theory of the phase-screen approximation for transducers radiating an angled incidence beam. For the unfocused probes, they experimentally observed the significant attenuation of the flaw signal by the surface roughness while there was only a small change in the material noise signal.

The physics of waves reflected in randomly inhomogeneous media has been reviewed by Kravtsov and Saichev [21]. This review was primarily concerned with the effects of randomly inhomogeneous media on the diffuse scattering of electromagnetic waves. They showed that the average intensity of the backscattered diffuse wave is enhanced by double passage through the random media. Enhanced backscatter from heterogeneous materials and

rough surfaces has been discussed by many authors. Most relevantly, Jakeman [22] has considered double-transmission through a rough surface and calculated the change in the backscattered diffuse waves. He modeled a planar mirror placed behind a smoothly varying deep phase-screen and analyzed the far field intensity distribution of the diffusely scattered wave. Jakeman observed that the backscattered intensity was enhanced with the gain largest when the mirror was positioned near the "so-called" focusing plane of the phase-screen.

Organization of the Dissertation

The main body of this dissertation is organized in five papers. The first three papers address the effects of randomly rough surfaces on material noise, the fourth paper deals with the effects of randomly rough surfaces on flaw signals and the last paper is about the inversion of surface statistics from the ultrasonic surface reflections. These papers have been/are being submitted for publication to journals. The general conclusion is provided following the papers to highlight the results. A bibliography of the literature cited in the general introduction is then listed. Each paper is self sufficient and the figures, tables and references given are numbered sequentially from 1. Following are brief descriptions of each part of this dissertation.

The work of the author was primarily theoretical, although he did carry out the measurements shown in Fig. (2). Other more detailed experimental measurements reported in the thesis were carried out by his valued collaborator Dr. P. B. Nagy of the Welding Engineering Department at Ohio State University.

Paper I. Rough Surface Effects On Incoherent Scattering From Random Volumetric Scatterers: Analytic Solution

Material noise in structural materials with smooth surfaces has been studied extensively in the past and is still an important problem in inspecting material as well as

characterizing its properties, such as grain size in metals and viscosity in curing composites. This paper focuses on surface roughness induced changes in material noise. It calculates the material noise received through randomly rough surfaces analytically using the phase-screen approximation and Fresnel approximation. The surface roughness is described by either Gaussian or an exponential correlation function. The major results are the prediction of an initial enhancement of the material noise followed by a reduction of the backscatter at late times, and a substantial reduction of noise for focused probes.

Paper II. The Effects Of Rough Surfaces On Ultrasonic Backscatter: Comparison Of Phase-Screen Approximation and Integral Equation Method

The phase-screen approximation, although simple and fairly accurate in many circumstances, is uncontrolled and does not provide a systematic means of determining the resulting errors. This paper uses the integral equation method which provides arbitrarily precise answers at the cost of increasingly large numerical calculations, to calculate the material noise. The calculations show that the noise predictions by these two methods differ only by an overall constant of proportionality (nearly one) for a range frequencies, correlation lengths and rms heights. Consequently, the phase-screen approximation, after correction by the constant of proportionality, can be used to accurately calculate the effects of surface roughness on the material noise.

Paper III. Ultrasonic Inspection, Material Noise And Surface Roughness

The predicted enhancement of the material noise in Paper I was observed experimentally and is reported in this paper. This prediction indicates that the phase-screen approximation is fairly robust. Some numerical simulations contained in this paper are also presented in more detail in the second paper.

Paper IV. Doubly-Coherent Transmission at Rough Surfaces And Its Implications For Ultrasonic Inspection

This paper studies the detection of subsurface flaws through randomly rough surfaces. It calculates and examines the flaw signal. It combines the material noise of the first paper and estimates the effects of surface roughness on signal-to-noise ratio. Major findings of the paper are the observation (1) of a near-surface dead-zone for the attenuated flaw signal (due to substantially increased attenuation for near-surface flaw) and (2) an improved signal-to-noise ratio for focused probes compared to unfocused probes.

Paper V. Acoustic Double-Reflection And Transmission At A Rough Water-Solid Interface

This paper studies the double reflection and transmission of ultrasound at rough water-solid interfaces using the phase screen approximation. It experimentally observes coherent double reflection from a rough water-solid interface and relates the changes in the averaged specular reflection to the phenomenon of enhanced backscatter. It also proposes a method of inverting surface statistics from ultrasonic reflections.

PAPER I.

ROUGH SURFACE EFFECTS ON INCOHERENT SCATTERING FROM RANDOM VOLUMETRIC SCATTERERS: ANALYTIC SOLUTION

ABSTRACT

Rough surfaces can greatly alter the signal-to-noise ratio for the ultrasonic detection of subsurface scatterers. In this paper, we discuss the effects of rough surfaces on the "material noise", i.e., the more-or-less random signals generated by backscatter from subsurface, densely-distributed volumetric scatterers such as cells or microcrystallites. A statistical approach is used to analyze the variance of the signal generated by scatterers at a fixed depth below the surface for finite-sized phase-coherent focused transducers. The problem is formulated using the scalar-wave approximation and the reciprocity theorem. The interaction of ultrasound with the volumetric scatterers is modeled in the Born approximation and in the long wavelength limit. Transmission through the rough surface is modeled using the phase-screen approximation. Gaussian and exponential autocorrelation functions model the surface height distribution. The main result is a solution in series form (as well as simple approximating expressions) for the variance of the backscattered signal from scatterers at a fixed depth. Analysis of the solution indicates that (a) the "early-time" variance in the signal, obtained from the scatterers close to the surface, is independent of the transducer type and its radius after normalization, (b) focusing reduces the variance in the signal due to scatterers in the focal zone, in some cases by more than an order of magnitude compared to unfocused probes, (c) the variance generated by scatterers lying beyond the focal zone may be increased or decreased by surface roughness depending on the relative size of the focal spot and the surface correlation length of the roughness. More generally, we find that focusing substantially reduces the surface roughness-induced degradation in the signal-to-noise ratio, and improves the detection of large defects in a background of small volumetric scatterers.

I. INTRODUCTION

Surface roughness can greatly alter the inspection of samples by phase-sensitive transmitters and receivers, such as those used in radar, sonar and ultrasound applications. Signal-to-noise ratios can be reduced by orders of magnitude in unfavorable cases. We will study roughness-induced changes in the (material) noise[1,2] generated by backscattering from the material's microstructure. It will be shown that such noise can be either increased or decreased by surface roughness depending on the depth of the scatterers below the surface and on the degree of focusing of the probe.

We are motivated by experimental results of Bilgen, Rose and Nagy[3], who examined how rough surfaces degrade the detection of discrete subsurface scatterers in polycrystalline solids. They measured the ultrasound reflected from a drill hole in a roughened brass sample in the presence of material noise due to the polyscrytalline nature of the sample. They showed that rough surfaces can significantly reduce the signal-to-noise ratio for both focused and unfocused probes for this type of sample, although the focused probe had a better signal-to-noise than the unfocused probe. In this paper, our theoretical analysis will show that this result is typical; focusing improves the signal-to-noise ratio for the detection of subsurface scatterers that are small compared to the transducer radius.

Rough surfaces occur ubiquitously in inspection problems. Examples are the sea surface or a foliage canopy, which can present rough interfaces for microwave imaging or remote sensing.[4] Similarly, the surface finish of industrial parts affects their nondestructive evaluation using ultrasound, microwaves or eddy-currents. In geophysics, the use of ground penetrating radar for the detection of archeological sites and the detection of ores is impacted by surface roughness. Optical inspection of defects in semiconductors is also affected by the surface properties of the substrates.[5]

A considerable literature, which has been reviewed recently by Ogilvy,[6] exists for the reflection of waves by rough surfaces.[7-20] Substantially less is known about the transmission of waves through rough surfaces. Recently, there has been interest in the effects of surface roughness on ultrasonic inspection. Nagy and Adler[21] considered the effects of surface roughness on the coherent propagation of ultrasound and particularly its effect on the attenuation of the coherent (average) wave. They developed corrections based on the phase-screen approximation and applied these corrections to the ultrasonic detection and characterization of porosity in as-cast aluminum. Nagy and Rose[22] have considered the effects of surface roughness on ultrasonic inspection in a more general context. They observed, for unfocused transducers, that the signal from large discrete flaws could be reduced by orders of magnitude, while the material noise was nearly unaltered and that consequently the signal-to-noise ratio could be seriously degraded. They explained their observations using a model based on the phase-screen approximation. In preliminary reports,[23,24] the backscattered signal has been examined for unfocused probes using both numerically exact Boundary Integral Element calculations and the phase-screen approximation. It was predicted that (1) the signal due to near-surface volumetric scatterers was increased slightly, and (2) that the signal from volumetric scatterers far from the surface was reduced.[23] In a separate experimental report, Bilgen et. al.[24] observed an increase in backscatter from the near-surface region.

In this paper, we develop a theoretical model for the depth-dependence of the material noise, i.e. for the variance of signals backscattered from distributed volumetric scatterers. Our purpose is to develop simple engineering formulas that describe the effects of surface roughness on the ultrasonic inspections of parts immersed in water. The results apply to two problems. First, distributed volumetric scatterers mask the ultrasonic detection of cracks, voids and inclusions, and surface roughness increases the degree of masking. Second,

roughness alters the backscattered signal used to characterize material properties, such as grain size in metals, viscosity in curing composites or contractility in myocardium. Typical frequencies range from 1 to 50 MHz, with wavelength ranging from 30 μm to 6 mm. Transducer radii are on the order of centimeters as are the various path lengths in the problem. Typical volumetric scatterers range from 10 μm to 1 mm in radius. The rms height of the roughness typically varies between 1 and 500 μm, while the surface correlation length varies from 100 μm to several millimeters.

The paper's structure is as follows. Section II contains a description of the problem, its geometry and physical interpretation. Section III reviews a variety of theoretical preliminaries and the approximations needed for analytic calculations. The key results are derived in Section IV. These results include a series solution for the variance, as well as limiting and approximating formulas. The results are described and presented graphically in Section V. The different effects of rough surfaces on focused and unfocused transducers are emphasized. Finally, the paper is concluded with a summary and discussion.

II. GEOMETRY AND PROBLEM DEFINITION

The geometry analyzed in this paper and typical of ultrasonic immersion inspections is shown in Fig. 1. A phase-sensitive transducer is immersed in water and oriented normally to the surface of a rough solid plate sample at a set-off, z_0, of several centimeters. A broadband pressure pulse is excited in water and propagates to the plate's surface. There it interacts with the rough surface, is transmitted into the sample, and scatters from distributed volumetric scatterers. The resulting reflected waves then retransmit through the rough surface and are detected by the same transducer.

The surface is chosen to be randomly rough, planar on the average at z=0. The surface's height variation, h(**r**), is governed by a spatially-uniform, zero-mean Gaussian random-process, and the autocorrelation function, Γ. The coordinate parallel to the surface is denoted by **r** , while the general three dimensional coordinate is **x**=(**r**, z). The assumption of spatial uniformity (translational invariance) implies that the autocorrelation function can be written in the form

$$\Gamma(\mathbf{r}-\mathbf{r}') \equiv \frac{\langle h(\mathbf{r})h(\mathbf{r}')\rangle}{h^2}, \tag{1}$$

where $h^2 = \langle h^2(\mathbf{r})\rangle$. The angular brackets denote an ensemble average. We assume that spatially stationary statistical processes and ensemble averages are equivalent. The autocorrelation function will be represented by either a Gaussian, $\Gamma = \exp(|\mathbf{r}-\mathbf{r}'|^2 / L^2)$, or an exponential $\exp(|\mathbf{r}-\mathbf{r}'| / L)$. Here, L defines the surface correlation length.

We define wave propagation in our study by the scalar wave equation

$$\nabla^2 u(\omega,\mathbf{r},z) + \frac{\omega^2}{c^2(\mathbf{x})} u(\omega,\mathbf{r},z) = 0 \tag{2}$$

where u is the wavefield, and ω is the angular frequency. The boundary conditions are the continuity of the wavefield and its normal derivative at the water-solid interface. The wavefield, u, can be written as $u(\omega,\mathbf{r},z)=\langle u(\omega,\mathbf{r},z)\rangle+\delta u(\omega,\mathbf{r},z)$. The average wavefield, <u>, is called the coherent wave, while the fluctuation δu is called the incoherent wave. Spatial averages can be obtained in practice by translating the transducer parallel to the surface of the plate.

The scattering from volumetric defects (in the scalar approximation) is supposed to result from spatial variations in the sound velocity. These variations are represented by

$$\delta v(\mathbf{x})\equiv\frac{1}{c^2(\mathbf{x})}-\frac{1}{c_s^2}, \tag{3}$$

where c(**x**) is the sound velocity and $1/c_s^2\equiv\langle 1/c^2(\mathbf{x})\rangle$. The velocity deviation, δv, is assumed to arise from a spatially-uniform random-process of zero mean that is characterized by the autocorrelation function

$$K(\mathbf{x}-\mathbf{x}')\equiv\frac{\langle\delta v(\mathbf{x})\delta v(\mathbf{x}')\rangle}{\langle\delta v^2\rangle}, \tag{4}$$

where <δv2> denotes the variance of the velocity deviation. In this paper, we assume that the size of the volumetric scatterers is much smaller than the wavelength (or any other length scale in the problem). Hence, we evaluate the scattering in the long wavelength limit where it is appropriate to describe the velocity deviations by $K(\mathbf{x}-\mathbf{x}')=\delta^3(\mathbf{x}-\mathbf{x}')$.

III. THEORY AND APPROXIMATIONS

The variance in the transducer's voltage will be derived using Auld's reciprocity formula for elastodynamics.[26] Auld's formula determines the voltage change due to a particular scatterer given the wavefields in the presence and in the absence of that scatterer. However, in the weak scattering limit (Born approximation), Auld's formula can be evaluated solely in terms of the wavefield in the absence of the scatterer. Our strategy will use the phase-screen approximation to construct an approximate wavefield that includes the effects of the rough surface but which neglects the effects of the volumetric scatterers. The volumetric scatterers will then be included using the reciprocity formula and the weak scattering approximation.

The most important approximations in this paper are: (1) the use of the scalar wave equation, (2) the Born approximation for volumetric scatterers (3) the Fresnel approximation for wave propagation in a uniform medium and (4) the phase-screen approximation for surface roughness. These approximations will be discussed in order.

By using the scalar wave approximation for the longitudinal modes alone, we neglect some features characteristic of solids such as transverse modes, Rayleigh waves and the fact that volumetric scattering arises from deviations in the elastic constants and density as well as velocity deviations. We base our neglect of these quantities on the following facts. We are using well collimated transducers that are oriented normal to the surface, and it is well known that there is zero conversion into transverse or Rayleigh waves for a perfectly collimated beam normally incident on a smooth surface. Any transverse or Rayleigh waves would only arise either from the divergence of the finite beam (which is small) or from the interaction of the beam with the rough surface. However, we are also assuming that the aspect ratio of the roughness is small, $h / L \ll 1$ (see the discussion of the phase-screen approximation below), which ensures that the generation of both surface and transverse waves is small.

Auld's electro-mechanical reciprocity formula relates the signal change of a piezoelectric transducer for a given scatterer to the wave fields in the presence and absence of the scatterer. In the Appendix, we rewrote this relation in a volume formulation (rather than the original surface form) and simplified it for constant density fluids (the scalar wave approximation). The resulting scalar formulation of the signal change as a function of depth is derived from Eq. (A5) in the Appendix.

$$\delta S(\omega,z)=\frac{i\omega^3}{4\rho P_E(\omega)}\int d^3\mathbf{x}\delta v(\mathbf{x})u_I(\omega,\mathbf{x})u_S(\omega,\mathbf{x})\delta(z-\hat{z}\cdot\mathbf{x}) \tag{5}$$

where $P_E(\omega)$ is the electrical power input to the transducer, ρ is the density of the solid. The integral is over the x-y plane at a depth z. The field u_I denotes the wavefield induced in the sample as transmitted through the rough surface, but in the absence of volumetric scatterers at depth z, while u_S denotes the wavefield generated as transmitted through the rough surface in the presence of the volumetric scatterers at depth z.

The volumetric scattering was evaluated using the Born approximation. Consider a field u that is transmitted through the rough surface in the absence of all volumetric scatterers, not just those at depth z. This field, u, is a good approximation to both u_I and u_S when the scattering from the volumetric flaws is sufficiently weak. Upon substituting u for both u_I and u_S and evaluating the delta function, Eq. (5) can be written as a function of distance z within the sample as

$$\delta S(\omega,z)=\frac{i\omega^3}{4\rho P_E(\omega)}\int d^2\mathbf{r}\delta v(\mathbf{r},z)u^2(\omega,\mathbf{r},z) \tag{6}$$

where the integral is over the **r** plane at a depth z.

The signal change is zero on the average in the Born approximation, i.e. $<\delta S(\omega,z)> = 0$, since $<\delta v> = 0$ and u is independent of δv by construction. The variance of the signal, BP(z), is the first non-trivial average quantity that describes the backscattered power received from the densely-distributed volumetric scatterers located at depth z

$$BP(z) = \langle \delta S(\omega,z)\delta S^*(\omega,z)\rangle. \tag{7}$$

Equation (7) can be evaluated by substituting Eq.(6) and using the assumed delta function nature of the correlation function for the volumetric scatterers. We find that BP(z) is proportional to

$$P(z) \equiv \int d^2\mathbf{r}\langle |u(\omega,\mathbf{r},z|^4\rangle. \tag{8}$$

The calculation of this equation is the basic technical problem addressed in this article.

So far, a frequency domain picture has been used. However, we can relate our results to the time-domain by assuming that the beam is well-collimated and that only single scattering events are important. We imagine a pulse that travels from the transducer to the scattering site and back in a time $t = 2\,z / c_s + 2\,z_o / c_w$. Here z is the depth of the scatterer beneath the water-solid interface, while z_o denotes the off-set of the transducer in water. The time-domain variance can then be related to $P(c_s\,t / 2 - z_o\,c_s / c_w)$. This picture can be elaborated by introducing the idea of windowed Fourier transforms and tone-bursts.

The calculation of the variance requires $u(\omega, \mathbf{r}, z)$, the wavefield obtained in the presence of the rough surface but in the absence of the volumetric scatterers. The determination of u can be approximately divided into three parts: (1) propagation of the wave in water from transducer to the solid; (2) transmission through the rough water-solid

interface; and (3) propagation in the uniform "average" solid. The beam propagation is modeled by the Fresnel approximation[27], which neglects evanescent waves. The transmission through the surface is accomplished via the phase-screen approximation. Below, we first discuss the Fresenel approximation. Then we conclude the section by discussing the phase screen approximation.

Consider a wave propagating along the positive z-axis in a uniform space. If we know the wavefield on the $z=0^-$ plane, we can compute the wavefield everywhere above or below that plane using the plane wave expansion method, and find explicitly,

$$u(\omega,\mathbf{r},z)=\int d^2\mathbf{q}f(\mathbf{q})\exp(i\mathbf{q}\cdot\mathbf{r})\exp(i\sqrt{k^2-q^2}z). \tag{9}$$

Here, k is the wave number of the medium (solid) and f(**q**) is the spatial Fourier transform of the wavefield u on the plane defined by z=0,

$$f(\mathbf{q})\equiv\frac{1}{(2\pi)^2}\int d^2\mathbf{r}u(\omega,\mathbf{r},z=0)\exp(-i\mathbf{q}\cdot\mathbf{r}). \tag{10}$$

The fact that we are interested in well collimated beams simplifies Eq.(9) since f(**q**) is thus concentrated around zero, and consequently the equation can be accurately approximated by expanding the square root

$$\sqrt{k^2-q^2}\approx k-\frac{q^2}{2k}. \tag{11}$$

Equations (9-11) can then be evaluated to give the Fresnel formula for the wave propagation

$$u(\omega,\mathbf{r},z)=\frac{-ik}{2\pi z}e^{ikz}\int d^2\mathbf{r}'u(\omega,\mathbf{r}',z=0)e^{\frac{ik}{2z}|\mathbf{r}-\mathbf{r}'|^2}. \tag{12}$$

The phase screen approximation is often employed in radio astronomy to understand interplanetary scintillation of radio sources.[28-31] The density fluctuations in the solar wind or ionosphere are assumed to introduce phase fluctuations in the electromagnetic wave and as a result intensity fluctuations form as the wave propagates . We use the phase-screen approximation to model the transmission of the beam through the rough surface. The transducer radiates in water and the resulting wavefield is propagated to the surface using Eq.(12). The wavefield immediately above the surface ($z = 0^-$) is denoted by $u(\omega, \mathbf{r}, 0^-)$. The phase-screen approximates the wavefield at $z = 0^+$ via

$$u(\omega,\mathbf{r},z=0^+) = T_o u(\omega,\mathbf{r},z=0^-)\exp(i\phi(\mathbf{r})). \tag{13}$$

Here T_0 denotes the transmission coefficient for a normally-incident plane wave on a smooth surface. That is, the roughness does not affect the amplitude of the transmitted wave in the phase-screen approximation. The phase $\phi(\mathbf{x})$ of the wave is changed at each point of the surface by

$$\phi(\mathbf{r}) = k(1-\frac{c_s}{c_w})h(\mathbf{r}). \tag{14}$$

This is just the phase change that would occur in the geometrical acoustics limit. The phase screen approximation is a limiting expression of the Kirchhoff approximation and becomes rigorous if $h << \lambda_s << L$, where λ_s is the wavelength in the solid.[6-8] The r.m.s. value of the phase, σ, is determined from Eq. (14) in terms of the r.m.s. height, h. Explicitly

$$\sigma = k\left|1-\frac{c_s}{c_w}\right|h. \tag{15}$$

The phase screen approximation provides an estimate for the wavefield at $z = 0^+$. We propagate the field to the interior of the solid using the Fresnel propagation formula Eq.(12).

Focused beams are one of our major interests. For a transducer, slightly above the water-solid interface, we approximate the incident field by

$$u(\omega, \mathbf{r}, 0^-) = e^{-(\frac{1}{R^2} + i\frac{k}{2F})r^2} \tag{16}$$

Here, R defines the radius of the beam, and F describes the focal length of the spherically focused transducer. The unfocused case is evaluated by setting F to infinity.

IV. ANALYTICAL RESULTS

This section consists of two parts. First, in Sec. IV.A., we give exact and approximate solutions for the variance in the signal as a function of depth. In Sec. IV.B. we give asymptotic results of the variance for small and large depths, large radius as well as small σ.

A.Exact and Approximate Formulas for Variance as a Function of Depth

The variance in the signal due to scatterers at a depth z is estimated in this section. We concentrate entirely on evaluating P(z), which we reproduce for convenience

$$P(z) \equiv \int d^2\mathbf{r} \left\langle |u(\omega, \mathbf{r}, z)|^4 \right\rangle \quad . \tag{17}$$

We will provide analytic formulas for a variety of cases. As discussed earlier, P(z) approximates the power backscattered from distributed volumetric flaws (to within an overall constant). P(z) depends both on the coherent and incoherent parts of the wavefield as can be seen by substituting u = <u> + δu in Eq.(17). In the limit of large roughness, <u> is nearly zero, and P(z) measures (the planar average of) fluctuations in the intensity.

P(z) depends on several different parameters; our notation is shorthand for P(h, z,L, R, F, ω). We will often be interested in how much the roughness has changed P(z) compared to the result for a smooth surface. Consequently, we define the normalized backscatter as

$$Q(h, z, \ldots) \equiv \frac{P(h, z, L, \ldots.)}{P(h = 0, z, \ldots.)} \tag{18}$$

We first derive exact series solutions for P(z) and Q(z) for Gaussian autocorrelation functions. Next, we report simple approximations for Q(z) for both Gaussian or exponential autocorrelation functions. These approximations are accurate for each of the following cases independently: (1) z << 1, (2) small roughness, σ << 1, (3) near the focus and (4) in the far-field of the transducer.

It is convenient to scale the variables as follows

$$\tilde{\mathbf{r}} = \frac{\mathbf{r}}{L},\ \tilde{z} = \frac{z}{kL^2},\ \tilde{R} = \frac{R}{L},\ \tilde{F} = \frac{F}{kL^2} \tag{19}$$

where ~ denotes scaled variables. Substituting Eqs.(12-16,19) into Eq.(17) results in

$$P(z) = \frac{L^2|T_o|^4}{(2\pi\tilde{z})^4}\int d^2\tilde{\mathbf{r}}\iiint d^2\tilde{\mathbf{r}}_1 d^2\tilde{\mathbf{r}}_2 d^2\tilde{\mathbf{r}}_3 d^2\tilde{\mathbf{r}}_4 e^{-(\frac{1}{\tilde{R}^2}+i\frac{1}{2\tilde{F}})(\tilde{r}_1^2+\tilde{r}_2^2)} e^{-(\frac{1}{\tilde{R}^2}-i\frac{1}{2\tilde{F}})(\tilde{r}_3^2+\tilde{r}_4^2)} e^{\frac{i}{2\tilde{z}}(|\tilde{\mathbf{r}}_1-\tilde{\mathbf{r}}|^2+|\tilde{\mathbf{r}}_2-\tilde{\mathbf{r}}|^2-|\tilde{\mathbf{r}}_3-\tilde{\mathbf{r}}|^2-|\tilde{\mathbf{r}}_4-\tilde{\mathbf{r}}|^2} \left\langle e^{i(\phi(\tilde{\mathbf{r}}_1)+\phi(\tilde{\mathbf{r}}_2)-\phi(\tilde{\mathbf{r}}_3)-\phi(\tilde{\mathbf{r}}_4))} \right\rangle \tag{20}$$

We have previously assumed that the surface height distribution h(**r**) is described by a spatially-uniform zero-mean Gaussian random process. This assumption allows us to evaluate the expectation value < exp(i(ϕ....> in Eq.(20). We define $q = \phi(\tilde{\mathbf{r}}_1)+\phi(\tilde{\mathbf{r}}_2)-\phi(\tilde{\mathbf{r}}_3)-\phi(\tilde{\mathbf{r}}_4)$ and note that q is a sum of random variables each of which is normally distributed; therefore q is also normally distributed. The characteristic function of q is $\langle e^{iq}\rangle = \exp(-\langle q^2\rangle/2)$. Thus,

$$\langle e^{i(\phi(\tilde{\mathbf{r}}_1)+\phi(\tilde{\mathbf{r}}_2)-\phi(\tilde{\mathbf{r}}_3)-\phi(\tilde{\mathbf{r}}_4))}\rangle = e^{-\sigma^2 H(\tilde{\mathbf{r}}_1,\tilde{\mathbf{r}}_2,\tilde{\mathbf{r}}_3,\tilde{\mathbf{r}}_4)}, \tag{21}$$

where H is defined by

$$H(\tilde{\mathbf{r}}_1,\tilde{\mathbf{r}}_2,\tilde{\mathbf{r}}_3,\tilde{\mathbf{r}}_4) \equiv 2+\Gamma(\tilde{\mathbf{r}}_1-\tilde{\mathbf{r}}_2)+\Gamma(\tilde{\mathbf{r}}_3-\tilde{\mathbf{r}}_4)-\Gamma(\tilde{\mathbf{r}}_1-\tilde{\mathbf{r}}_3) \\ -\Gamma(\tilde{\mathbf{r}}_1-\tilde{\mathbf{r}}_4)-\Gamma(\tilde{\mathbf{r}}_2-\tilde{\mathbf{r}}_3)-\Gamma(\tilde{\mathbf{r}}_2-\tilde{\mathbf{r}}_4)\ , \tag{22}$$

and Γ denotes the surface autocorrelation function. We substitute (21 and 22) into (20) and make the coordinate transformations

$$\begin{aligned}
\tilde{\mathbf{r}}_1 &= (\mathbf{p}_1+\mathbf{p}_2+\mathbf{p}_3+\mathbf{p}_4)/2 \\
\tilde{\mathbf{r}}_2 &= (-\mathbf{p}_1-\mathbf{p}_2+\mathbf{p}_3+\mathbf{p}_4)/2 \\
\tilde{\mathbf{r}}_3 &= (\mathbf{p}_1-\mathbf{p}_2-\mathbf{p}_3+\mathbf{p}_4)/2 \\
\tilde{\mathbf{r}}_4 &= (-\mathbf{p}_1+\mathbf{p}_2-\mathbf{p}_3+\mathbf{p}_4)/2
\end{aligned} \tag{23}$$

We integrate, first over $\tilde{\mathbf{r}}$, then $\mathbf{p}_3$ and $\mathbf{p}_4$, and obtain

$$P(z) = \frac{R^2|T_o|^4}{16\pi\tilde{z}^2}\int\int d\mathbf{p}_1 d\mathbf{p}_2 e^{-\frac{p_1^2+p_2^2}{\tilde{R}^2}-i\beta\mathbf{p}_1\cdot\mathbf{p}_2-\sigma^2 G(\mathbf{p}_1,\mathbf{p}_2)} \tag{24}$$

where

$$\beta = \frac{1}{\tilde{z}}-\frac{1}{\tilde{F}}, \tag{25}$$

and

$$G(\mathbf{p}_1,\mathbf{p}_2) = 2+\Gamma(\mathbf{p}_1-\mathbf{p}_2)+\Gamma(\mathbf{p}_1+\mathbf{p}_2)-2\Gamma(\mathbf{p}_1)-2\Gamma(\mathbf{p}_2). \tag{26}$$

Jakeman and McWhirter[32] studied Eq.(24), in the context of light scattering, for the unfocused and plane wave case after assuming that the surface was very rough, $\sigma >> 1$. Their calculation corresponded to evaluating the fluctuations in the intensity. Jakeman and McWhirter treated Gaussian, truncated parabolic, and truncated linear surface autocorrelation

functions. We, on the other hand, calculated P(z) for much smoother surfaces (σ on the order of one or less) and included both focusing and the finite size of the beam.

We evaluate Eq.(24) for Gaussian and exponential autocorrelation functions. The integral can be completed analytically as an infinite series for Gaussian autocorrelation functions. The "Gaussian" solution procedure can be briefly summarized as follows: (1) expand the exponential $e^{-\sigma^2 G(\mathbf{p}_1,\mathbf{p}_2)}$ in Taylor series, 2) change the order of the resulting summations and integration, 3) evaluate the resulting integrals. After some algebra, the resulting backscattered power can be written as

$$P(z)=\frac{\pi R^2 e^{-2\sigma^2}|T_o|^4}{16}\sum_{a,b,c,d=0}^{\infty}\frac{(2\sigma^2)^{a+b}(-\sigma^2)^{c+d}}{a!b!c!d!}\frac{1}{(\frac{1}{\tilde{R}^2}+a+c+d)(\frac{1}{\tilde{R}^2}+b+c+d)-(\frac{i\beta}{2}+(d-c))^2}. \quad (27)$$

Note that the dependence on $\tilde{z}$ (or z) enters via β. An expression for Q follows from its definition Eq.(18) and Eq.(27). One obtains

$$Q(z)=e^{-2\sigma^2}\sum_{a,b,c,d=0}^{\infty}\frac{(2\sigma^2)^{a+b}(-\sigma^2)^{c+d}}{a!b!c!d!}\frac{\frac{1}{\tilde{R}^4}+\frac{\beta^2}{4}}{(\frac{1}{\tilde{R}^2}+a+c+d)(\frac{1}{\tilde{R}^2}+b+c+d)-(\frac{i\beta}{2}+(d-c))^2}. \quad (28)$$

The series solutions (Eqs. (27,28)) can be used to evaluate $P(z)$ and $Q(z)$ for Gaussian autocorrelation functions. The series converges rapidly for moderate and small values of σ, on the order of 1, in the range suitable for ultrasonic inspection. In the numerical calculations, 8 terms (in each variable) for the 25 μm (σ=0.798) and 10 terms for the 50 μm (σ=1.596) roughness are needed to ensure convergence of the sum. For large values of σ

(e.g. $\sigma > 3$) that may be encountered in other problems, the series solution is not a good way to evaluate these quantities and the reader is referred to the work of Jakeman and McWhirter.

Simpler but less accurate formulas for $P(z)$ and Q(z) can be obtained by approximating the integrand of Eq.(24). Numerical studies showed that the following approximation,

$$e^{-\sigma^2 G(\mathbf{p}_1,\mathbf{p}_2)} \approx e^{-2\sigma^2}\{e^{2\sigma^2 e^{-p_1^2}} + e^{2\sigma^2 e^{-p_2^2}} + e^{-\sigma^2 e^{-|\mathbf{p}_1-\mathbf{p}_2|^2}} + e^{-\sigma^2 e^{-|\mathbf{p}_1+\mathbf{p}_2|^2}} - 3\}, \\ -e^{-2\sigma^2(p_1^2+p_2^2)}(1+2e^{-3\sigma^2}-3e^{-2\sigma^2}) \tag{29}$$

can be used to accurately simulate the integrand in each of the following independent limits: (1) small σ, (2) small z, (3) far-field and (4) in the focal zone. Upon substitution of the above approximation in Eq.(24) one finds

$$Q(z) \approx \varepsilon^2[e^{-2\sigma^2}[\frac{2\gamma(\varepsilon^2,-2\sigma^2)}{(-2\sigma^2)^{\varepsilon^2}} + \mathrm{Re}\{\frac{\gamma(\eta^2,\sigma^2)}{2\tilde{R}^2\eta^{2*}(\sigma^2)^{\eta^2}}\} - 3] - \frac{(1+2e^{-3\sigma^2}-3e^{-2\sigma^2})}{4R^2|\eta^2+\sigma^2|^2}] \tag{30}$$

where

$$\varepsilon^2 = \frac{1}{\tilde{R}^2} + \frac{\tilde{R}^2\beta^2}{4}, \tag{31}$$

$$\eta^2 = \frac{1}{2\tilde{R}^2} + i\frac{\beta}{4} \tag{32}$$

and $\gamma(.,.)$ is the incomplete gamma function as defined in Gradsteyn and Ryzhik.[35] Re{.} denotes the real part of the expression within the curly bracket. In the next section, we compare this relatively simple approximation for $Q(z)$ with the results obtained from the series solution Eq.(28).

Our solutions are not as complete for exponential autocorrelation functions. First, we have been unable to obtain an exact solution of $Q(z)$, although we present a solution for small σ. Second, the approximate method results in a more complex expression, which involves an infinite series.

The derivation of the approximate expression for $Q(z)$ for the exponential correlation function is wholly similar to that given previously for the "Gaussian" case. Namely, we approximate the integrand of Eq.(24) by

$$\begin{aligned} e^{-\sigma^2 G(\mathbf{p}_1,\mathbf{p}_2)} &\approx e^{-2\sigma^2}\{e^{2\sigma^2 e^{-|\mathbf{p}_1|}} + e^{2\sigma^2 e^{-|\mathbf{p}_2|}} + e^{-\sigma^2 e^{-|\mathbf{p}_1-\mathbf{p}_2|}} + e^{-\sigma^2 e^{-|\mathbf{p}_1+\mathbf{p}_2|}} - 3\} \\ &-e^{-2\sigma^2(|\mathbf{p}_1|+|\mathbf{p}_2|)}(1+2e^{-3\sigma^2}-3e^{-2\sigma^2}) \end{aligned} \tag{33}$$

The resulting approximation for $Q(z)$ is

$$\begin{aligned} Q(z) = 2 - 3e^{-2\sigma^2} + 2e^{-3\sigma^2} - \frac{(1+2e^{-3\sigma^2}-3e^{-2\sigma^2})\varepsilon^2}{4\tilde{R}^2|\eta|^4}\left|1-\frac{\sqrt{\pi}\sigma^2}{2\eta}e^{\frac{\sigma^4}{4\eta^2}}Erfc\{\frac{\sigma^2}{2\eta}\}\right|^2 \\ -\sqrt{\pi}e^{-2\sigma^2}\sum_{n=1}^{\infty}[\frac{(-\sigma^2)^n}{(n-1)!}\mathrm{Re}\{\frac{e^{\frac{n^2}{4\eta^2}}}{\eta}Erfc\{\frac{n}{2\eta}\}\}+\frac{(2\sigma^2)^n}{\varepsilon(n-1)!}e^{\frac{n^2}{4\varepsilon^2}}Erfc\{\frac{n}{2\varepsilon}\}] \end{aligned} \tag{34}$$

where Erfc{.} is the complementary Error function.

B. Asymptotics of the Normalized Variance Q(z)

In this subsection, we give asymptotic expressions for Q. First, we express Q in the limit of small roughness $\sigma << 1$. Then we present asymptotic expressions for Q in the small z, small β and large R limits.

1- Small σ Asymptote (either small k or small h)

For both Gaussian and exponential autocorrelation functions, one calculates Q(z) by expanding $e^{-\sigma^2 G(\mathbf{p}_1,\mathbf{p}_2)}$ in Eq.(24) to second order in σ. The resulting integrals can be evaluated analytically . For the "Gaussian" case Q(z) is given by

$$Q(z) = 1 - 2\sigma^2 - 2\sigma^2 \,\mathrm{Re}\{\frac{\frac{1}{\tilde{R}^4} + \frac{\beta^2}{4}}{(\frac{1}{\tilde{R}^2}+1)^2 - (\frac{i\beta}{2}+1)^2}\} + 4\sigma^2 \frac{\frac{1}{\tilde{R}^4} + \frac{\beta^2}{4}}{\frac{1}{\tilde{R}^2}(\frac{1}{\tilde{R}^2}+1) - \frac{\beta^2}{4}}. \qquad (35)$$

For the "exponential" case Q(z) is given by

$$Q(\tilde{z}) = 1 + \sigma^2\sqrt{\pi}[\mathrm{Re}\{\frac{e^{\frac{1}{4\eta^2}}}{\eta} Erfc\{\frac{1}{2\eta}\}\} - \frac{2e^{\frac{1}{4\varepsilon^2}}}{\varepsilon} Erfc\{\frac{1}{2\varepsilon}\}] \qquad (36)$$

Note that Eq.(35) can also be obtained by expanding the series solution for Q(z), Eq.(28), or the approximate expression, Eq.(30), to second order in σ. Similarly, Eq.(36) is the second-order small σ asymptote of Eq.(34). Therefore, we conclude that the approximations introduced above for Q are valid in the small σ limit.

In obtaining the normalized variance in small σ limit Eq. (35), we first expanded $e^{-\sigma^2 G(\mathbf{p}_1,\mathbf{p}_2)}$ to second order in σ and then evaluated the resulting integrals. The integrals explicitly involved $\Gamma(\mathbf{p}_1)$, $\Gamma(\mathbf{p}_2)$, $\Gamma(\mathbf{p}_1 - \mathbf{p}_2)$ and $\Gamma(\mathbf{p}_1 + \mathbf{p}_2)$. The integrals involving $\Gamma(\mathbf{p}_1 - \mathbf{p}_2)$ and $\Gamma(\mathbf{p}_1 + \mathbf{p}_2)$ gave rise to the term

$$-2\sigma^2 \mathrm{Re}\{\frac{\frac{1}{\tilde{R}^4}+\frac{\beta^2}{4}}{(\frac{1}{\tilde{R}^2}+1)^2-(\frac{i\beta}{2}+1)^2}\} \tag{37}$$

and the integrals involving $\Gamma(\mathbf{p}_1)$ and $\Gamma(\mathbf{p}_2)$ resulted in the term

$$4\sigma^2 \frac{\frac{1}{\tilde{R}^4}+\frac{\beta^2}{4}}{\frac{1}{\tilde{R}^2}(\frac{1}{\tilde{R}^2}+1)-\frac{\beta^2}{4}}. \tag{38}$$

In Fig. 2, we show the dependence of the above expressions on depth for both focused and unfocused probes. The sound velocities are given in the next section. The curves obtained from Eq.(37) start at around -0.2 and increase for smaller z, and finally stay almost constant for distances greater than 0.9. On the other hand, the curve for (38) starts at 0.4 and decreases monotonically for the unfocused probe, while it attains its minimum at the focal depth for the focused probe. The results in Fig. 2 clearly indicate that expression (37) determines small z variation in Q, while Eq.(38) determines the large z behavior.

2- Small z asymptote (z->0)

The value of Q is evaluated for small depths (β -> kL^2/z and z->0). First we expand Eq.(28)

$$Q(z) \approx e^{-2\sigma^2} \sum_{a,b,c,d=0}^{\infty} \frac{(2\sigma^2)^{a+b}(-\sigma^2)^{c+d}}{a!b!c!d!}$$
$$\left[1-i4(c-d)\tilde{z}-4\left(4(c^2-cd+d^2)+ab+ac+ad+bc+bd+\frac{a+b+2c+2d}{\tilde{R}^2}\right)\tilde{z}^2+\ldots\right]. \tag{39}$$

Then we use the identities

$$xe^x = \sum_{n=0}^{\infty} \frac{nx^n}{n!} \tag{40}$$

and

$$(x^2 + x)e^x = \sum_{n=0}^{\infty} \frac{n^2 x^n}{n!} \tag{41}$$

to write

$$\begin{aligned} Q(z) &\approx 1 + 32\sigma^2 (\frac{z}{kL^2})^2 + O\left((\frac{z}{kL^2})^3\right) \\ &\approx 1 + 8\frac{z^2}{L_R^2} + O(z^3) \end{aligned} \tag{42}$$

where $L_R = L^2/2(c_s / c_w - 1)h$ is the "roughening distance".[3] Equation (42) shows that Q(z) is independent of transducer radius and focal distance to second order in z.

3- Farfield and large R asymptotes (β -> 0, then R ->large)

The farfield value of Q is obtained by setting β = 0. For unfocused transducers this corresponds to large z and for focused transducers it corresponds to z = F. When β = 0, the expression for Q, Eq.(28), reduces to

$$Q(\beta = 0) = e^{-2\sigma^2} \sum_{a,b,c,d=0}^{\infty} \frac{(2\sigma^2)^{a+b}(-\sigma^2)^{c+d}}{a!b!c!d!} \frac{\frac{1}{\tilde{R}^4}}{(\frac{1}{\tilde{R}^2} + a + c + d)(\frac{1}{\tilde{R}^2} + b + c + d) - (d - c)^2}. \tag{43}$$

Rather surprisingly, the value of Q(β = 0) is independent of the focal length, see Fig. 8 in the next section.

In the large radius limit, any term in the series with either a, b, c, d not equal to zero vanishes, and in the limit, Q is $e^{-2\sigma^2}$. Furthermore, by noticing the terms with either a is nonzero and b, c, d are zero or b is nonzero and a, c, d are zero or c is nonzero and a, b, d are zero or d is nonzero and a, b,c are zero, we can write

$$Q(\beta=0)\approx e^{-2\sigma^2}\left[1+\left(\sum_{n=1}^{\infty}\frac{\sigma^{2n}}{n.n!}(2^{n+1}+(-1)^n)\right)\frac{1}{\tilde{R}^2}+O(\frac{1}{\tilde{R}^4})\right]. \tag{44}$$

Using the identity [35]

$$Ei(x)=C+\ln(|x|)+\sum_{n=1}^{\infty}\frac{x^n}{n.n!} \tag{45}$$

we obtain

$$Q(\beta=0)\approx e^{-2\sigma^2}\left[1+\left(2Ei\{2\sigma^2\}+Ei\{-\sigma^2\}-\ln(4\sigma^6)-3C\right)\frac{1}{\tilde{R}^2}+O(\frac{1}{\tilde{R}^4})\right] \tag{46}$$

where Ei{.} is the exponential integral and C=.577215 is Euler's constant. The leading order term is just the result we would find if the backscatter was entirely due to the coherent part of the wave. The correction term includes part of the signal due to the incoherent field.

4- Plane waves, the large R and z limit (R ->∞, then z-> large)

We evaluate the far-field value of Q for unfocused transducers $\beta = 1/\tilde{z}$ with large radii (i.e. for incident plane waves). From Eq.(28) one finds upon taking the limit that R -> ∞

$$Q(\tilde{z}) \approx e^{-2\sigma^2} \sum_{a,b,c,d=0}^{\infty} \frac{(2\sigma^2)^{a+b}(-\sigma^2)^{c+d}}{a!b!c!d!} \frac{\frac{1}{4\tilde{z}^2}}{ab+(a+b)(c+d)+4cd+\frac{1}{4\tilde{z}^2}+\frac{i}{2\tilde{z}}(c-d)} \tag{47}$$

In the large z limit, any term with c or d not equal to zero will be zero. Hence

$$Q(\tilde{z}) \to e^{-2\sigma^2} \sum_{a,b=0}^{\infty} \frac{(2\sigma^2)^{a+b}}{a!b!} \frac{\frac{1}{4\tilde{z}^2}}{ab+\frac{1}{4\tilde{z}^2}}. \tag{48}$$

Likewise, either a or b must equal zero, otherwise that term vanishes in the limit. Finally, we find

$$Q(z \to \infty) \approx 2 - e^{-2\sigma^2}. \tag{49}$$

By isolating the terms a and b zero but c and d nonzero, a and c zero but b and d nonzero, b and d zero but a and c nonzero, and c and d nonzero but a and b nonzero we can write Q to the next order in the large z limit as

$$\begin{aligned} Q(z) \approx 2 - e^{-2\sigma^2} + e^{-2\sigma^2}\Bigg[& \frac{1}{2}(Ei\{2\sigma^2\} - \ln(2\sigma^2) - C)(Ei\{-\sigma^2\} - \ln(\sigma^2) - C) + \\ & \frac{1}{4}(Ei\{2\sigma^2\} - \ln(2\sigma^2) - C)^2 + \frac{1}{16}(Ei\{-\sigma^2\} - \ln(\sigma^2) - C)^2 \Bigg] \left(\frac{kL^2}{z}\right)^2 + O\left((\frac{kL^2}{z})^3\right). \end{aligned} \tag{50}$$

This value establishes the asymptote of Q for unfocused large radii transducers at large depths.

V. RESULTS

The formulas for P(z) and Q(z), which approximately determine the variance in the backscattered power, will be evaluated and presented graphically in this section. Our intention is to illustrate the dependence of the variance on the problem's physical parameters, such as the r.m.s. height, the correlation length, the transducer size, focal length, and frequency. Most of the results shown for P(z) and Q(z) were calculated using the series solutions, Eqs.(27 and 28), for the Gaussian autocorrelation function. Limited results will be shown for surfaces with exponential autocorrelation functions. We remind the reader that P(z) is roughly proportional to the backscattered power as a function of depth (or time).

Typical "Gaussian" results are shown in Figs. 3a-f for the following parameters (L= 0.15 cm, f= 10 MHz and R= 1 cm). Please note that the vertical scale varies substantially from figure to figure. The sound velocities are $c_w = 1.5\ 10^3$ cm/s and $c_s = 6.3\ 10^3$ cm/s. Figures 3a-c were calculated for a probe with a focal length of 4 cm, while Figs. 3d-f were computed for an unfocused probe . Smooth surface (solid line) and rough surface (dotted line) results for P(z)/P(z=0) are shown in Figs. 3a and 8d. P(z) for the focused probe peaks near the focal depth, but is nearly constant for unfocused transducers. The rough-surface P(z) for focused probes is similar in shape to the smooth surface result. However, the overall size of the peak is reduced by roughly 40%, and there is some increase in signal for smaller z. The rough surface P(z)/P(z=0) behaves quite differently for unfocused probes. Initially, P(z) increases, has a peak at approximately 0.90 cm, and then decreases monotonically with increasing depth.

Differences in the r.m.s. surface height can result in dramatically different results, especially for focused transducers. P(z) calculated for h = 50 μm roughness is shown in Fig. 3b. P(z) for a smooth surface is illustrated in Fig. 3e. The 50 μm rough-surface P(z) still has

a peak at the focal depth, but this peak is much reduced in size compared to the result for h = 25 μm.

The general features of the normalized variance, Q(z), is shown in Figs. 3c and 3f. The first thing to note is that Q(z) for rough surfaces and smooth surfaces are more similar than the P(z). Q(z) for the focused probe varies from 0.30 to 1.70, while Q(z) for the unfocused probe varies from 0.70 to 1.70. P(z), on the other hand, differs by more than a factor of 50 between the focused and unfocused cases. For both focused and unfocused probes, Q(z) initially rises in the same fashion and reaches a peak value of approximately 1.70. This similarity for small z is not an accident. Asymptotic analysis of Q(z) for small z shows that the initial rise is independent of the focal length.

The behavior of Q(z) for the focused case is illustrated by Fig. 3c. There is a rise for small z, a maximum at a characteristic distance, a minimum near the focal length and then a gradual increase for larger z. These results can be understood on a qualitative basis by considering the behavior of the wavefield as a function of depth. In Reference [3], the wavefields generated by focused and unfocused probes are calculated at four different depths; close to the surface, between the surface and the focal distance, at the focal depth and beyond focal distance. For z=0, the magnitude of the wavefield is smooth and Q(z) = 1. The roughness in the wavefield was observed to increase for larger z because the various parts of the wave begin to interfere with each other. This increased roughness with depth is reflected in the rise in Q(z) for small z. However, the wavefield calculations showed that at the focus the wavefield again has a large coherent contribution, the central lobe, which is similar in shape but smaller in magnitude than the wave transmitted through a smooth surface. This coherent central lobe dominates the integral over $|u|^4$. The fact that the coherent part of the field is attenuated by surface roughness accounts for the dip in Q(z) near the focal depth. For larger depths the incoherent component of u becomes increasingly important and Q(z) rises again.

The general features of Q(z) for the unfocused case are illustrated in Fig. 3f. There is an initial rise for small z, a peak at some characteristic distance and then a gradual decrease for larger z. These general features can also be understood by referring to the wavefield calculations.

The dependence of Q(z) on the r.m.s. roughness, correlation length, frequency, focal length and transducer radius will now be discussed. Figures 4a and 4b show Q's dependence on *h*. The signal for both focused and unfocused probes shows a very similar initial rise and peak. The peak is larger and occurs at smaller z for larger roughness. The location of the peak is determined by the enhanced diffraction of the beam due to the roughness.[3] Larger roughness leads to larger signals, increased diffraction, and consequently the peak shifts to smaller depths. Q(z) for the focused probe, on the other hand, shows a pronounced dip near the focal depth. The depth of the minimum increases with roughness. The signal for the focused probe rises with increasing depth below the surface. Q(z) for the unfocused probe falls off monotonically with depth, the larger the roughness the more rapid the decay.

The correlation length dependence of Q(z) is shown in Figs. 5a and 5b for focused and unfocused transducers. Again both the focused and unfocused results show a very similar rise and peak for small depths. The peak occurs for smaller z if the correlation length is smaller. The peak height is weakly dependent on the correlation length and increases slightly for smaller correlation lengths. The focused beam shows a characteristic minimum near the focal depth. The depth of the minimum is weakly dependent on correlation length, and is lightly deeper for the smallest correlation length. For larger z, Q(z) increases for the focused transducer. The increase is greater for larger correlation lengths. Note that Q(z) exceeds one for L = 2.0 mm at depths exceeding 10 cm. This a characteristic feature and is observed when the focal spot size is less than the correlation length, in which case the coherent part of the beam diverges more rapidly than the incoherent part. Q(z) for the

unfocused probe decays monotonically for greater depths, the fall-off is greater for the smaller correlation lengths because of the consequent increased beam diffraction.

The frequency dependence of Q(z) for focused and unfocused beams is shown in Figs. 6a and 6b. Again the small z behavior is similar for focused and unfocused transducers. The peak's height increases with frequency and the peak's position shifts to somewhat greater depths with frequency. For large z the dependence on frequency is small. The depth of the minimum of Q for the focused probe increases with frequency, but as before its position is near the focal depth of the transducer. The fall-off with depth is monotonic for the unfocused probe.

The dependence of Q(z) on the transducer's radius for focused and unfocused beams is shown in Figs. 7a and 7b. Note that the initial rise in Q(z) is the same, not only for focused and unfocused probes, but for all the transducer radii considered. The small-z asymptotics do not depend on the transducer's radius and could be analyzed equally well for an infinite plane wave. The position of the peak depends weakly on the radius and occurs for smaller z for smaller transducers (again consistent with the increase in diffraction). The results for the focused probe again shows a minimum near the focal length. The depth of the minimum depends weakly on the probe's radius and is slightly deeper for the larger probes. The width of the minimum does depend strongly on transducer size, the minimum being sharper for the larger transducers. Q(z) for the focused probe rises for larger values of z. The fall-off with depth for the unfocused probes is monotonic and most rapid for the smaller radius transducer. In the limit of an infinite-radius unfocused transducer, Q(z) would not decay with depth. Rather, it would rise initially, have possibly a small peak and then give way to a plateau with $Q > 1$ for greater depths.

The dependence of Q(z) on the focal length is shown in Fig. 8. The initial rise of Q for small z is the same for all focal lengths. The height of the peak and the depth of the

minimum depends weakly on the transducer's focal length. In each case, the minimum occurs near the focal depth. The large z value of Q is larger for smaller focal length.

So far in this section, we have been examining the series solution for Gaussian autocorrelation functions. Much simpler approximate formulas were given for Gaussian and exponential autocorrelation functions. Here, we will first compare the approximate "Gaussian" solution with the exact series solution, and then describe the results for the "exponential" case. Figure 9 compares the approximate "Gaussian" solution with the series solution for two different values of h and for focused and unfocused beams. The approximate solution is a good match to the series solution for larger values of z and is accurate at the focal depth. The approximate solution is less accurate for depths that are close to the maxima in the curves. Substantial errors occur for depths less than the depth at which the peak occurs ($z < 2.2$ cm for h=25 μm and $z<1$ cm for h=50 μm).

The approximate solution for the exponential autocorrelation is given in Fig. 10. The curves are similar to those obtained for the Gaussian autocorrelation function. For unfocused beams there is an initial rise, followed by a maximum and then a monotonic fall off. However, in the exponential case the peak in Q occurs at a shallower depth and the fall-off occurs more rapid compared to the Gaussian case. We do not have an exact solution that will enable us to do the benchmark comparison of the approximate "exponential" solution. However, we hope that the approximation will be accurate for depths greater than twice the depth at which the peak occurs (in analogy to the "Gaussian" case). We also expect that the solution will be most accurate in the focal zone and in the far-field.

VI. DISCUSSION AND SUMMARY

This section discusses three questions. (1) "What is the bottom line for the detection of subsurface scatterers ?" (2) "What is the bottom line for materials characterization ?" and (3) "Why does the rough surface increase the early-time variance in the signal ?" After addressing these questions the section is concluded with a summary.

The ability to detect subsurface scatterers in the presence of surface roughness depends on the signal-to-noise ratio. The signal-to-noise ratio for unfocused probes can be greatly reduced by surface roughness.[3] The loss of signal-to-noise results since surface roughness can reduce the signal from localized flaws by orders of magnitude, while the material noise is changed by much smaller amounts.

The signal-to-noise ratio for focused probes is degraded much less. As with unfocused probes, the signal can be reduced substantially (roughly $\exp(-2\,\sigma^2)$ for localized scatterers). However, the material noise originating from the focal region has also been shown to reduced by roughly the same large factor Eq.(46). Consequently, for moderate amounts of roughness ($\sigma \approx 1$) the signal-to-noise ratio for focused probes is nearly unchanged by surface roughness. This result can be explained as follows. Crudely, only the coherent part of the field participates in focusing. The incoherent part of the field radiates into, more or less, the whole field of view depending on the spatial frequencies of the roughness. For strong focusing, the coherent part of the wavefield at the focus dominates the backscattered power, and both the signal and the material noise are nearly proportional to the square of the coherent field. Thus, in the focal region, the signal-to-noise ratio is relatively unaffected by surface roughness (when compared to the case of unfocused transducers) since the signal and the noise are altered in the same way. However, for sufficient roughness, the coherent part of the beam becomes negligible even in the focal zone and a loss in the signal-to-noise ratio results.

The bottom line is that the signal-to-noise ratio for the detection of localized subsurface scatterers by focused probes will be significantly less degraded than for unfocused probes. The signal-to-noise ratio will be best for probes with tighter focuses and larger radii. Quantitative predictions for the noise in the focal zone can be obtained from Eq.(43).

The backscattered signal can also be used for materials characterization. As discussed in this article, the backscattered signal of unfocused probes is changed relatively little by surface roughness. Consequently, material characterization using unfocused probes will be relatively insensitive to surface roughness and great care need not to be exercised in the construction and interpretation of the experiment. By contrast, the backscattered signal for focused probes, see e.g. Fig. 3, depends strongly on surface roughness and the probe characteristics. The formulas developed in this paper, esp., Eq.(28), can be used to interpret and optimize the strength of the backscattered signal. The bottom line is as follows. Focusing changes the backscattered signal dramatically and consequently care must be exercised in constructing the experiment and interpreting the signal.

Next, we address the fact that an initial increase in the normalized backscattered power as a function of depth is characteristic of all of the calculations reported in this paper. This enhancement of the backscattered power has been observed experimentally using a specially prepared sample.[24]

One may ask, "Why is the backscattered power increased for early time?" Rather surprisingly the answer involves the double-scattering phenomenon known as "weak localization" or enhanced backscatter.[36,37] The basic idea of "weak localization" can be seen by crudely modeling wave propagation in the geometrical acoustics limit. Consider a sound ray that enters the solid through some particular bump in the rough surface, consequently suffers a phase change, ϕ_1, propagates some distance into the solid, is reflected by a volumetric scatterer and then is retransmitted through the surface. If the ray retransmits

through the same bump, the resulting phase change on the way out, ϕ_2, is the same as for the incident ray, $\phi_2 = \phi_1$. Consequently, $<(\phi_1 + \phi_2)^2> = 4<\phi^2>$. However, if the ray propagates back out through a different bump, then ϕ_1 and ϕ_2 are statistically independent and $<(\phi_1 + \phi_2)^2> = 2<\phi^2>$. Thus, the phase is randomized more (in the mean-square sense) if the ray backscatters through the same bump (correlation region) , than if it backscatters through a different bump (correlation region). The scattered wave is more likely to reflect through the same correlation region if the scatterer is near the surface, i.e. within the "roughening length", L_R.[3] The reflected field is randomized more and hence has a larger incoherent signal for reflections from near-surface scatterers.

We connected the initial increase in the normalized backscattered power and the consequent peak in Q(z) with "weak localization" by performing two calculations. First, we hypothesized a system such that the phase changes for the incident and backscattered waves are statistically independent; that is, the incident wave sees one phase screen, but the reflected wave sees a different phase screen. By construction there is no correlation between the phase of the incident and the backscattered waves. We then repeated the calculations of Sec. IV using this hypothesis. We found that the normalized backscattered power of this hypothetical system does not increase with depth and never exceeds one. That is, no peak exists for this hypothetical system in the Q(z) and backscattering is not enhanced. The normalized backscatter for this hypothetical system decayed monotonically with depth for all the examples studied. Second, we considered bistatic scattering, where one transducer serves as the transmitter and a different transducer as the receiver. These transducers were oriented so as to insonify the surface at nearly normal incidence, one at a polar angle θ and the other at a polar angle $-\theta$. A brief consideration of the geometry shows the probability of a ray transmitting through a given bump is greatest if $\theta = 0$. For non zero θ, the signal is reduced for a scatterer at some fixed depth below the surface. We expected and found that the peak in the backscattered power vanished very rapidly as θ increased from zero. The

peak vanished for θ on the order of 1^{o} or less for depths of 1 cm for the parameters typically used in this paper. The two calculations just discussed clearly show that the origin of the peak in the normalized backscattered power. It is the result of the enhanced randomization of the wavefield due to "weak localization".

In summary, we have derived a model for the effects of random-rough surfaces on the backscattered power from distributed volumetric scatterers. These results are relevant for two problems: (1) predicting the signal to noise ratio for subsurface scatterers, and (2) for materials characterization. The signal-to-noise ratio for the detection of subsurface scatterers can be greatly reduced for unfocused probes. The same signal-to-noise ratio is reduced much less for focused probes. Measurements of the backscattered noise for materials evaluation is little affected by surface roughness for unfocused probes. By contrast the backscattered material noise for focused probes depends sensitively on the roughness.

VII. ACKNOWLEDGEMENT

We thank Dr. Peter Nagy for his many insights and useful discussions. We, also, thank Dr. R. Roberts for his useful comments and the use of his laboratory. This work was supported by the National Science Foundation (Grant No. ECO-9008272) and the FAA-Center for Aviation Systems Reliability, operated by the Ames Laboratory, USDOE, for the Federal Aviation Administration under Contract No. W-7405-ENG-with Iowa State University.

VIII. APPENDIX

The voltage at a transducer due to the backscatter of ultrasound from a sample with a rough surface and densely-distributed volumetric scatterers is derived from Auld's electromechanical reciprocity formula in this appendix. Auld considered a two transducer (bistatic) measurement model. The electrical signal change at the receiver due to a scatterer in a homogeneous elastic background is given by

$$\delta S_E(\omega) = \frac{1}{4P_E(\omega)} \int_{S_F} (\mathbf{V}^1 \cdot \underline{\underline{\mathbf{T}}}^2 - \mathbf{V}^2 \cdot \underline{\underline{\mathbf{T}}}^1) \cdot \hat{\mathbf{n}} dS \qquad \text{(A1)}$$

Here $\mathbf{V}$ is the particle velocity, $\underline{\underline{\mathbf{T}}}$ is the stress tensor, P_E is the electric power input to the transducer, $\hat{n}$ is the inward directed normal to the surface and defines the S_F that contains the scatterer. Superscript 1 describes the measurement (1) in the absence of the scatterer and (2) where A is the transmitter and B is the receiver. Superscript 2 describes the measurement (1) in the presence of the scatterer and (2) B is the transmitter and A is the receiver. The surface integral in Eq.(A1) can be converted to a volume integral via Green's theorem. After some algebra, one finds

$$\delta S_E(\omega) = \frac{i\omega}{4P_E(\omega)} \int_{\Omega} d^3\mathbf{x} [\delta c_{ijkl}(\mathbf{x}) \psi^1_{i,j}(\omega,\mathbf{x}) \psi^2_{k,l}(\omega,\mathbf{x}) + \omega^2 \delta\rho(\mathbf{x}) \psi^1_i(\omega,\mathbf{x}) \psi^2_i(\omega,\mathbf{x})]. \qquad \text{(A2)}$$

Here, Ω is the volume of the scatterer, while $\delta\rho$ and δC_{ijkl} denote the deviation of the density and elastic constants of the scatterer from their average values. Finally, ψ_i denotes the displacement field in the solid and related to the velocity components by

$$V_l = -i\omega\psi_l \quad \text{for } l = 1, 2, 3. \qquad \text{(A3)}$$

The reciprocity equation (A2) can be reduced to scalar form by assuming that the only non-zero elastic constant is given by the Lame parameter λ ($\delta C_{ijkl} = \delta\lambda\, \delta_{ij}\, \delta_{kl}$) and setting the density deviation, $\delta\rho = 0$. After defining $u_j = \psi^j_{i,i}$ we obtain

$$\delta S_E(\omega) = \frac{i\omega}{4P_E(\omega)} \int_V d^3\mathbf{x}\left[\left(\frac{1}{\lambda(\mathbf{x})} - \frac{1}{\lambda_s}\right) u_1(\omega,\mathbf{x}) u_2(\omega,\mathbf{x})\right] \tag{A4}$$

The simplifications concerning the density and elastic moduli have been made for simplicity, and cannot be rigorously supported by physical arguments. Nonetheless, scalar wave calculations have often been found to elucidate key elements of wave phenomena in both electrodynamics and elastodynamics.

Equation (A4) can be further recast in terms of the velocity deviation, δv,

$$\delta S_E(\omega) = \frac{i\omega^3}{4\rho P_E(\omega)} \int_V d^3\mathbf{x}\, \delta v(\mathbf{x}) u_1(\omega,\mathbf{x}) u_2(\omega,\mathbf{x}). \tag{A5}$$

Here, we have used the equality $c^2(\mathbf{x}) = \lambda(\mathbf{x})/\rho$ and Eq.(A4). Equation (A5) establishes the relationship between the velocity variation within the scatterer and the consequent voltage change at the receiving transducer for a general transmitter and receiver configuration.

IX. REFERENCES

[1]J. H. Rose, "Ultrasonic backscatter from microstructure," in Review of Progress in Quantitative Nondestructive Evaluation, edited by D. O. Thompson and D. E. Chimenti (Plenum, NY, 1992), Vol. 11B, pp. 1677-1684.

[2]M. D. Russell, S. P. Neal and E. J. Boote, "Experimental estimation of the longitudinal-wave backscatter coefficients for ultrasonic interrogation of weak scattering materials," J. Acoust. Soc. Am. 93, 1267-1276 (1993).

[3]M. Bilgen, J. H. Rose and P. B. Nagy, "Rough surface effects on incoherent scattering from random volumetric scatterers: Experiment,"

[4]J. A. Kong, L. Tsang and R. Shin, Theory of Microwave Remote Sensing, (Wiley Interscience, New York, 1985).

[5]J. C. Stover, Optical Scattering: Measurement and Analysis (McGraw-Hill, New York, 1990).

[6]J. A. Ogilvy, Theory of Wave Scattering from Random Rough Surfaces (Adam Hilger, Bristol, 1991).

[7]C. Eckart, "The scattering of sound from the sea surface," J. Acoust. Soc. Am. 25, 566-570 (1953).

[8]P. Beckmann and A. Spizzichino, The Scattering of Electromagnetic Waves from Rough Surfaces, (Pergamon, Oxford, 1963).

[9]M. L. Boyd and R. L. Deavenport, "Forward and specular scattering from a rough surface: theory and experiment," J. Acoust. Soc. Am. 53, 791-801 (1973).

[10]P. J. Welton, "The potential-method formulation of acoustic-wave scattering by rough surfaces," J. Acoust. Soc. Am. 54, 66-73 (1973).

[11]F. G. Bass and I. M. Fuks, Wave Scattering from Statistically Rough Surfaces (Pergamon, Oxford, 1979).

[12]J. Shen and A. A. Maradudin, "Multiple scattering of waves from random rough surfaces," Phys. Rev. B 22, 4234-4240 (1980).

[13]M. deBilly and G. Quentin, "Backscattering of acoustic waves by randomly rough surfaces of elastic solids immersed in water," J. Acoust. Soc. Am. 86, 591-601 (1982).

[14]J. G. Watson and J. B. Keller, "Reflection, scattering, and absorption of acoustic waves by rough surfaces," J. Acoust. Soc. Am. 74, 1887-1894 (1983).

[15]D. H. Berman and J. S. Perkins, "The Kirchhoff approximation and first order perturbation theory for rough surface scattering," J. Acoust. Soc. Am. 78, 1045-1051 (1985).

[16]E. I. Thorsos, "The validity of the Kirchhoff approximation for rough surface scattering using a Gaussian roughness spectrum," J. Acoust. Soc. Am. 83, 78-92 (1988).

[17]D. K. Dacol and D. H. Berman, "Sound scattering from a randomly rough fluid-solid interface," J. Acoust. Soc. Am. 84, 292-302 (1988).

[18]E. I. Thorsos and D. R. Jackson, "The validity of the perturbation approximation for rough surface scattering using a Gaussian roughness spectrum," J. Acoust. Soc. Am. 86, 261-277 (1989).

[19]W. A. Kuperman and H. Schmidt, "Self-consistent perturbation approach to rough surface scattering in stratified elastic media," J. Acoust. Soc. Am. 86, 1511-1522 (1989).

[20]Ö. Bozma and R. Kuc, "Characterizing pulses reflected from rough surfaces using ultrasound," J. Acoust. Soc. Am. 89, 2519-2531 (1991).

[21]P. B. Nagy and L. Adler, "Surface roughness induced attenuation of reflected and transmitted ultrasonic waves," J. Acoust. Soc. Am. 82, 193-197 (1987).

[22]P. B. Nagy and J. H. Rose, "Surface roughness and the ultrasonic detection of subsurface scatterers," J. Appl. Phys. 73, 566-580 (1993).

[23]J. H. Rose, M. Bilgen, P. B. Nagy, and L. Adler, "Effects of surface roughness on ultrasonic backscatter," in Review of Progress in Quantitative Nondestructive Evaluation,

edited by D. O. Thompson and D. E. Chimenti (Plenum, New York, 1992), Vol. 11B, pp. 1693-1700.

[24]M. Bilgen, J. H. Rose and P. B. Nagy, "Ultrasonic inspection, material noise and surface roughness," in Review of Progress in Quantitative Nondestructive Evaluation, edited by D. O. Thompson and D. E. Chimenti (Plenum, New York, 1993), Vol. 12B, pp. 1767-1774.

[25]P. B. Nagy, L. Adler and J. H. Rose, "Effects of acoustic scattering at rough surfaces on the sensitivity of ultrasonic inspection," in Review of Progress in Quantitative Nondestructive Evaluation, edited by D. O. Thompson and D. E. Chimenti (Plenum, New York, 1993), Vol. 12B, pp. 1775-1782.

[26]B. A. Auld, "General electromechanical reciprocity relations applied to the calculation of elastic wave scattering coefficients," Wave Motion 1, 3-10 (1979).

[27]J. W. Goodman, Introduction to Fourier Optics (McGraw-Hill, New York, 1969).

[28]R. P. Mercier, "Diffraction by a screen causing large random phase fluctuations," Proc. Camb. Phil. Soc, A 58, 382-400 (1962).

[29]E. E. Salpeter, "Interplanetary scintillations. I. Theory," Astrophys. J. 147, 433-448 (1967).

[30]R. Buckley, "Diffraction by a random phase screen with very large r.m.s. phase deviation," Aust. J. Phys., 24, 351 (1971).

[31]H. A. Whale, "Near-field statistics for the field diffracted by a thin one-dimensional random phase screen," J. Atmos. Terr. Phys. 36, 1045-1056 (1974).

[32]E. Jakeman and J. G. McWhirter, "Correlation function dependence of the scintillation behind a deep random phase screen, "J. Phys. A: Math. Gen. 10, 1599-1643 (1977).

[33]B. J. Uscinski and C. Macaskill, "Intensity fluctuations due to a deeply modulated phase screen -I. Theory," J. Atmos. Terr. Phys. 45, 595-605 (1983).

[34]C. Macaskil and B. J. Uscinski, "Intensity fluctuations due to a deeply modulated phase screen -II. Results," J. Atmos. Terr. Phys. 45, 607-615 (1983).

[35]I. S. Gradshteyn and I. M. Ryzhik, Tables of Integrals, Series, and Products (Academic, New York,1980).

[36]M. P. van Albada and A. Lagendijk, "Observation of weak localization of light in a random medium," Phys. Rev. Lett. 55, 2692-2695 (1985).

[37] E. Jakeman, "Enhanced backscattering through a deep random phase screen," J. Opt. Soc. Am. A 5, 1638-1648 (1988).

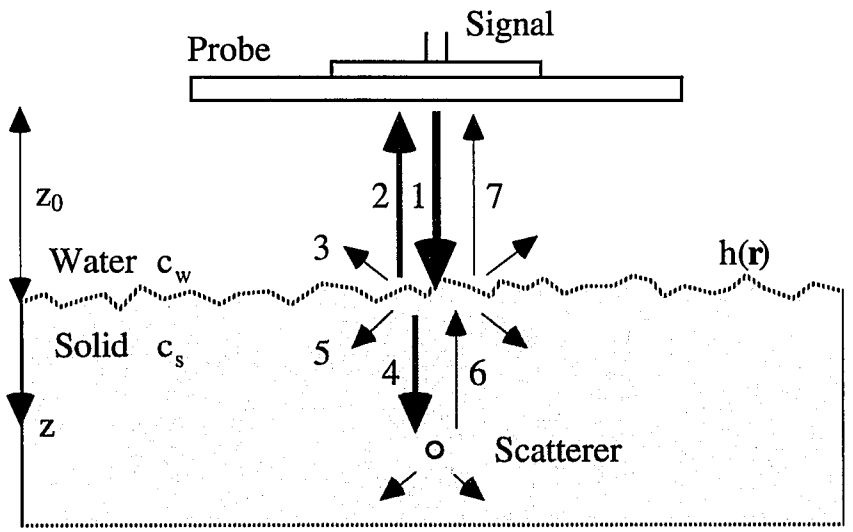

1-Incident Wave; 2-Coherent Reflection; 3-Incoherent Reflection; 4-Coherent Transmission; 5-Incoherent Transmission; 6,7-Backscattering

Figure 1. Schematic geometry of hypothetical ultrasonic inspection. Shows various scattering events for the detection of a subsurface defects below a rough surface.

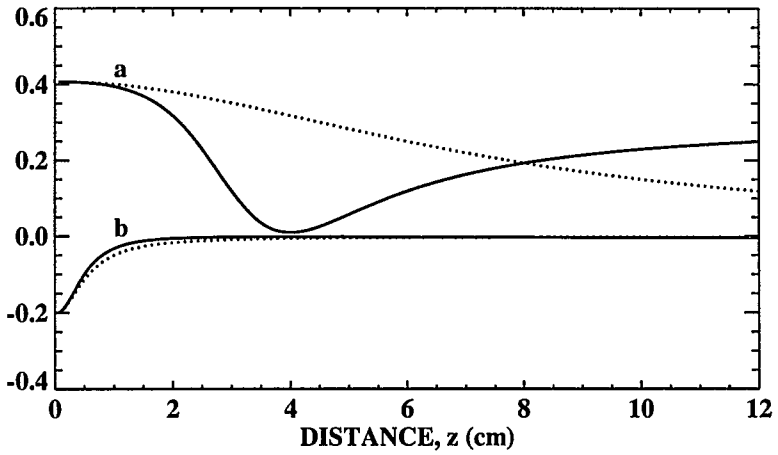

Figure 2. Shows two components of Q(z) as a function of depth for a focused (solid line) and an unfocused (dotted line) transducer. The parameters are f=10 MHz, R=1 cm, h = 10 μm, L=1.5 mm and F=4 cm ('a' is the result of Eq.(45) and 'b' is result of Eq.(44)).

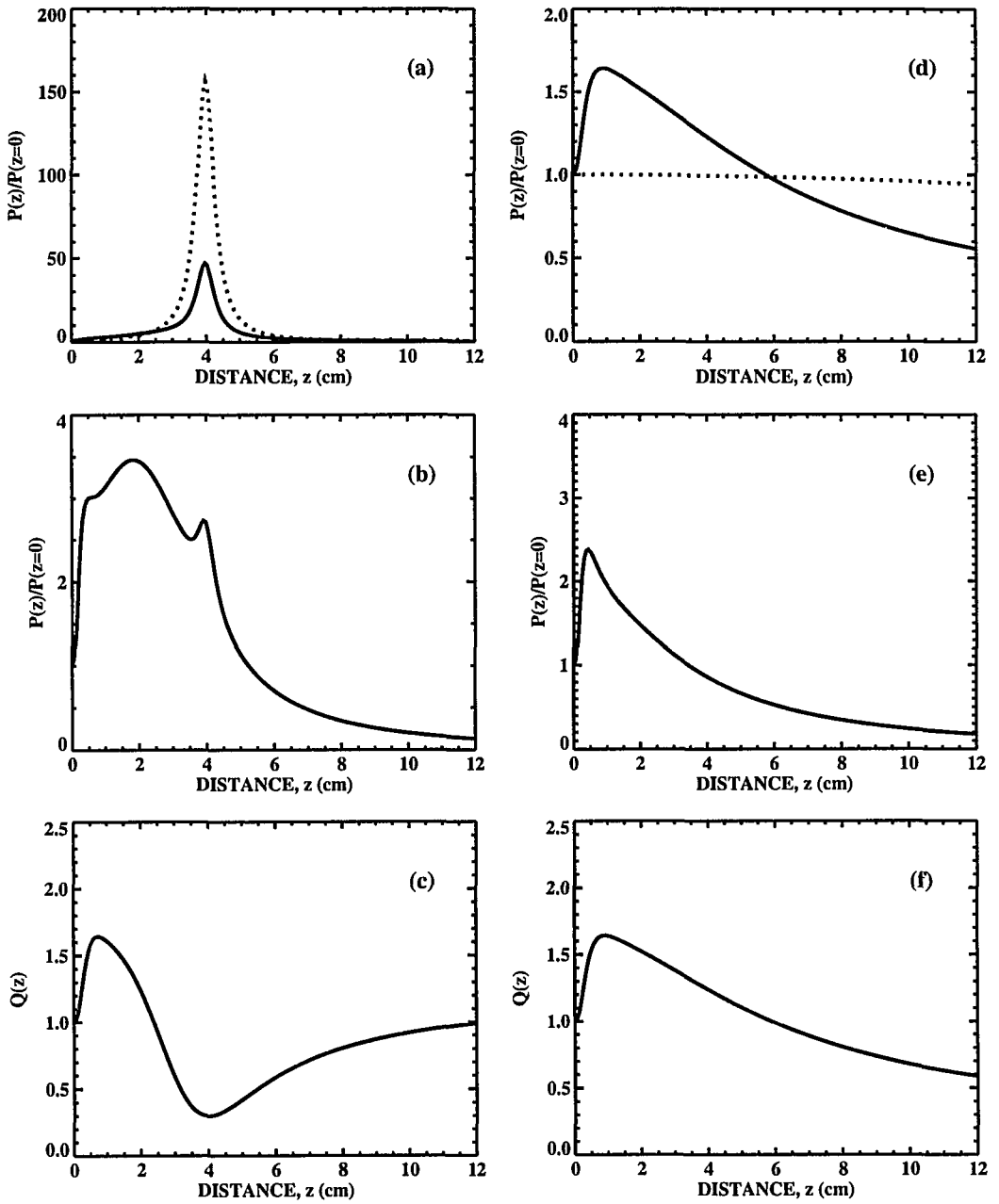

Figure 3. Variance P(z) and the normalized variance Q(z) of the signal versus the distance from the surface. (a) and (d) show P(z) for smooth and rough surfaces with h=25 μm, and (b) and (e) show P(z) for rough surface with h=50 μm, and (c) and (f) show Q(z) with h = 25 μm.

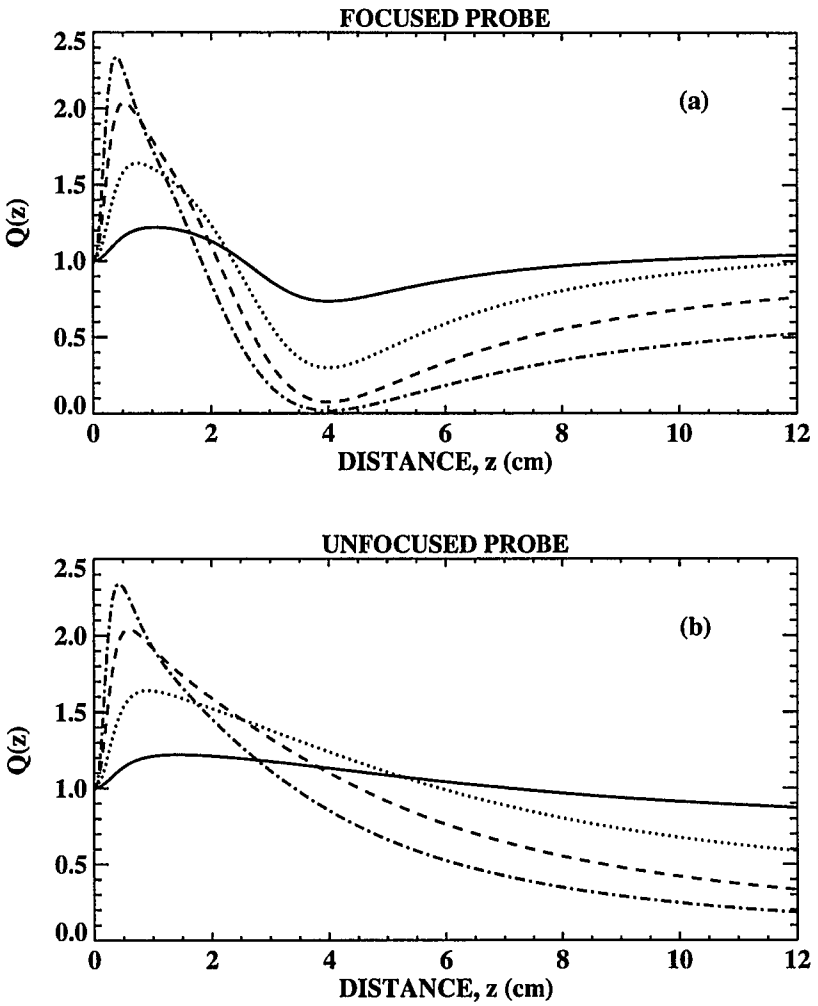

Figure 4. Comparison of the normalized variance Q(z) of the signal for four different r.m.s heights: solid line 12.5 μm, dotted line 25 μm, dashed line 37.5 μm and dash-dotted line 50 μm. The other parameters were f=10 MHz, R=1 cm, L=1.5 mm and F=4 cm.

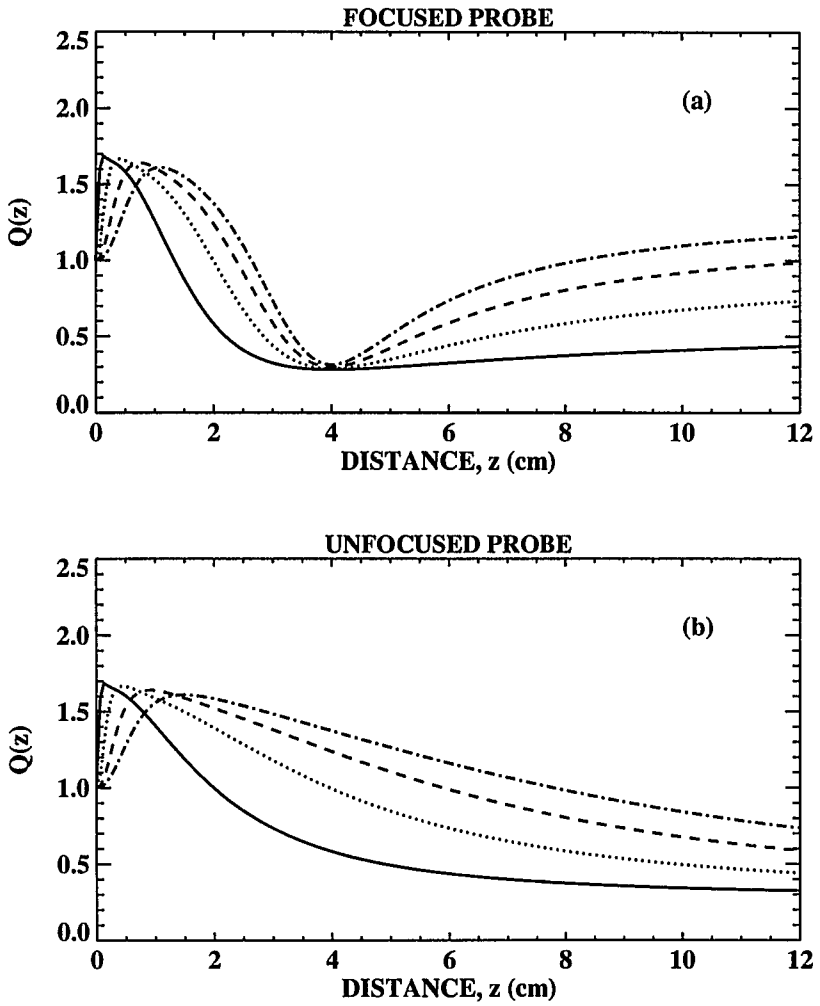

Figure 5. Comparison of the normalized variance of the signal Q(z) for four different correlation lengths. solid line 0.5 mm, dotted line 1.0 mm, dashed line 1.5 μm, and the dash-dotted line 2 mm. The other parameters were f=10 MHz, R=1 cm, h = 25 μm, and F=4 cm.

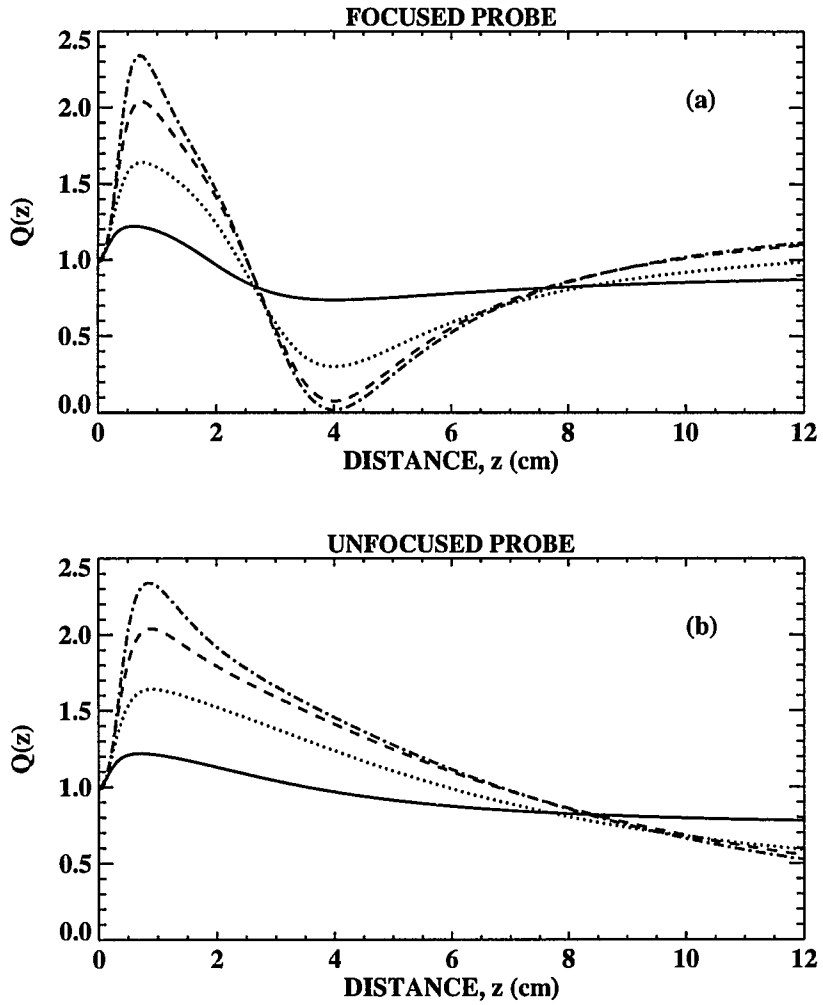

Figure 6. Comparison of the normalized variance of the signal Q(z) for four different frequencies. The solid line 5 MHz, dotted line 10 MHz, dashed line 15 MHz and dash dottted line 20 MHz). The other parameters were L = 1.5 mm, R=1 cm, h = 25 μm, and F=4 cm.

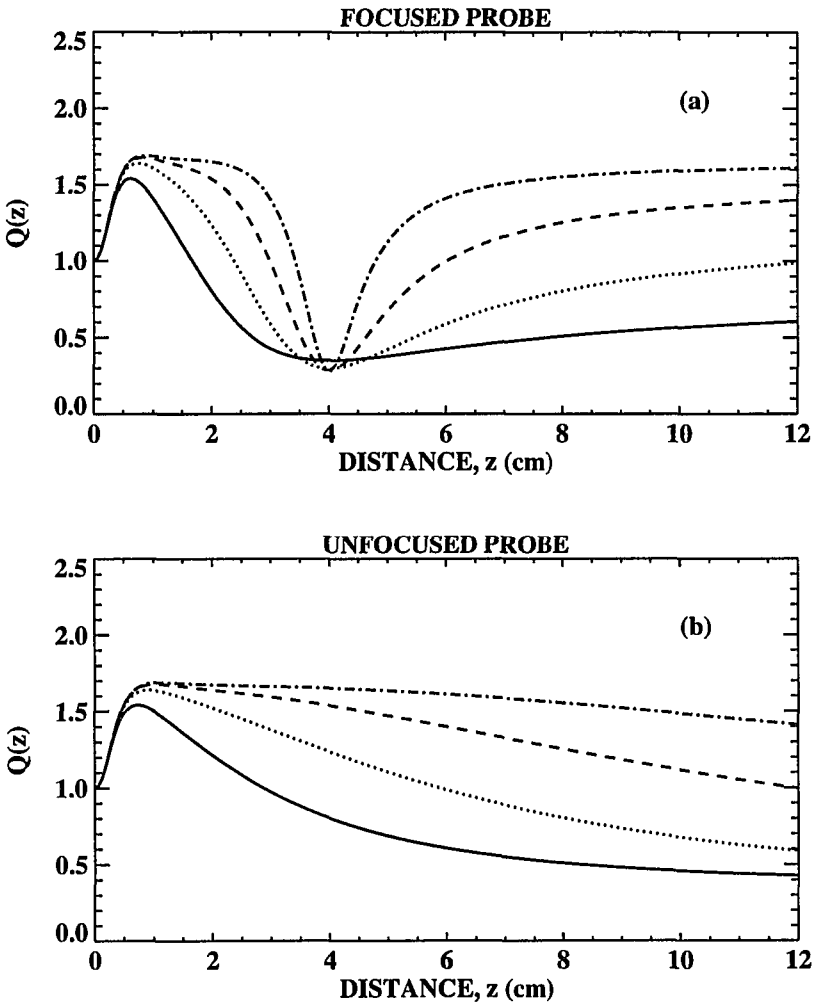

Figure 7. Comparison of the normalized variance of the signal Q(z) for four different radii. The solid line 0.5 cm, dotted line 1 cm, dashed line 1.5 cm and dash dotted line 2 cm). The other parameters were L = 1.5 mm, f = 10 MHz, h = 25 μm, and F=4 cm.

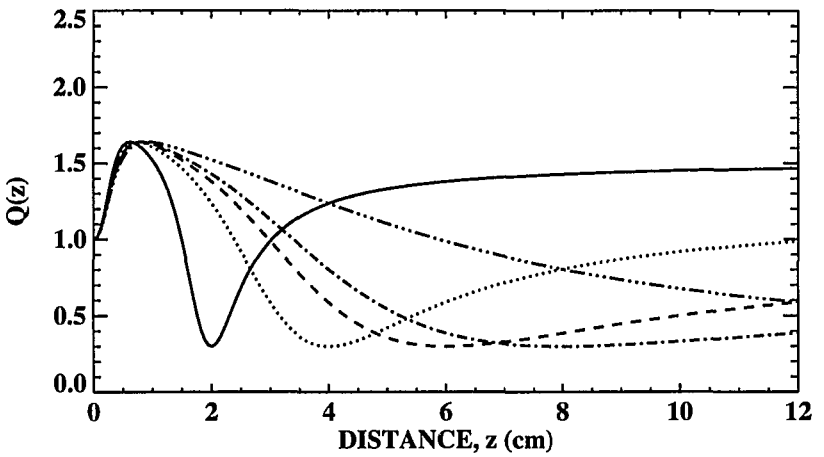

Figure 8. Comparison of the normalized variance of the signal Q(z) for five different focal lengths: solid line 2 cm, dotted line 4 cm, dashed line 6 cm, dash dotted 8 cm and dash-dot-dot-dot unfocused). The other parameters were L = 1.5 mm, f = 10 MHz, h = 25 μm, and R = 1 cm.

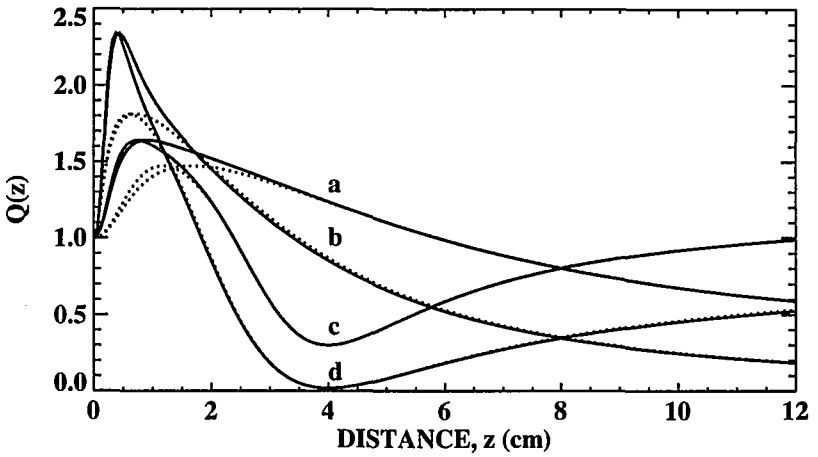

Figure 9. Comparison of approximate solution and series solution of Q(z) for two different r.m.s. heights: 'a' and 'c' have h = 25 μm, while 'b' and 'd' have h=50 μm. 'a' and 'b' are for unfocused probes, 'c' and 'd' are for focused probes. The other parameters are f=10 MHz, R=1 cm, L=1.5 mm, and F=4 cm.

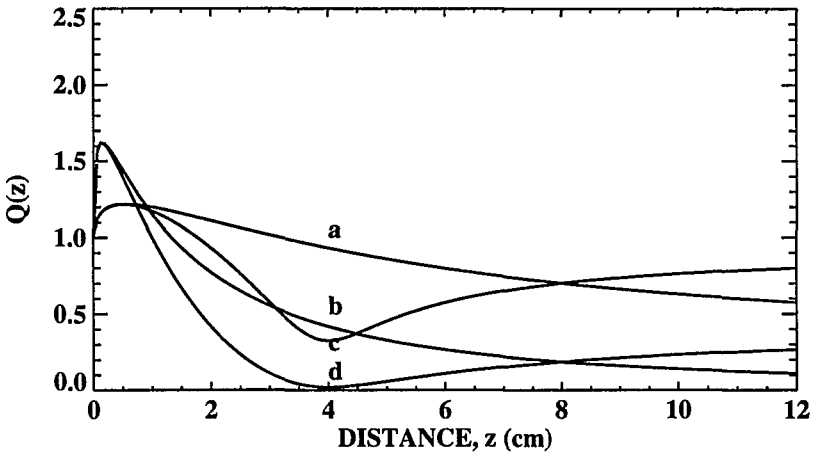

Figure 10. Normalized variance of signal, Q(z), for exponential autocorrelation function for two different r.m.s. heights: 'a' and 'c' have h = 25 μm, while 'b' and 'd' have h=50 μm. 'a' and 'b' are for unfocused probes, 'c' and 'd' are for focused probes. The other parameters are f=10 MHz, R=1 cm, L=1.5 mm, and F=4 cm.

PAPER II.

THE EFFECTS OF ROUGH SURFACE ON ULTRASONIC BACKSCATTER: COMPARISON OF PHASE-SCREEN APPROXIMATION AND INTEGRAL EQUATION METHOD

ABSTRACT

The phase-screen approximation and the boundary integral element (BIE) method are used to calculate, in a simple approximate model, the ultrasonic backscatter (material noise) generated by the interaction of an incident ultrasonic beam with the microstructure of a half-space with a randomly rough surface. The phase-screen approximation, although simple and fairly accurate in many circumstances, is uncontrolled and does not provide a systematic means of determining the resulting errors. In contrast, the boundary integral (BIE) equation method can provide arbitrarily precise answers at the cost of increasingly large numerical calculations. The normalized backscattered noise, calculated by these two methods, is shown to differ only by an overall constant of proportionality (nearly one) for a range of frequencies, correlation lengths and rms heights. Consequently, in our model the phase-screen approximation, after correction by the constant of proportionality, can be used to accurately calculate the effects of surface roughness on the material noise.

I. INTRODUCTION

The phase-screen approximation has long been used to compute the *reflection* of waves including ultrasound from randomly rough surfaces and, in recent years, it has been used to interpret experiments involving the *transmission* of ultrasound through rough water-solid interfaces. For example, transmission coefficients for singly-transmitted fields have been measured as a function of angle and frequency and shown to be well predicted except in the vicinity of the critical angles. Double transmission (and double reflection) at rough surfaces has also been accurately modeled by the phase screen approximation. Moreover, the phase-screen approximation has been used to interpret measurements of ultrasonic backscatter from microstructure in roughened aluminum plates. The phase-screen approximation agreement with experiment in this case indicates that it is fairly robust. However, it is an uncontrolled approximation, and the remaining errors are unknown.

In this paper, we test the utility of the phase-screen approximation for calculating the ultrasonic backscatter (from microstructure). The physical model for microstructural scattering beneath rough surfaces is considerably simplified, e.g. we use a fluid-fluid model and assume that the density is constant everywhere. We also assume that microstructure scatters ultrasound weakly and that its characteristic size is much less than the wavelength of ultrasound. Finally, we assume that the surface roughness varies in only one-dimension (i.e. the surface is rippled). We think that these assumptions, although severe, preserve the essential physics of the problem. The resulting model is simple enough that wave transmission through the rough interface can be quickly and accurately calculated using the Boundary Integral Element (BIE) method. The BIE results are used to explicitly test two approximate solutions (1) the phase-screen approximation as calculated numerically without further assumptions and (2) an analytic formula obtained by further making the Fresnel approximation.

The problem we are considering is important for practical reasons concerning ultrasonic inspection of industrial parts and explores a previously unexamined physical regime. Consider a solid plate with rough surfaces immersed in water and insonified by a phase-coherent transducer in the pulse-echo mode. The transducer insonifies the sample with a broadband pulse. The received signal includes the reflection from the plate's front surface, incoherent backscatter from densely-distributed random volumetric scatterers, such as microcrystallites, as well as reflection from a discrete subsurface scatterer, such as voids, cracks or inclusions within the sample. The incoherent backscatter from the microstructure produces a more-or-less random signal, "material noise" which is weakly modified by the surface roughness. On the other hand, reflections from any discrete subsurface flaw can be greatly attenuated by the surface roughness. Consequently, the noise, which is weakly affected by surface roughness, can mask the attenuated flaw signal completely.

Material noise in structural materials with smooth surfaces has been studied extensively in the past and is still an important problem in material inspection.[1-3] In this study, we focus on the changes in the material noise induced by the rough surfaces (particularly corrugated surface finish, e. g. machine marks). In a preliminary report[4], the backscatter through rough surfaces characterized by Gaussian correlation function was calculated using the phase-screen approximation for unfocused transducers. Initially unexpected, the phase-screen calculation predicted an initial enhancement of the material noise followed by a reduction of the backscatter at late times. The predicted enhancement of the material noise was subsequently observed experimentally using a specially-prepared sample.[5] In another context, Rose et. al.[6] experimentally observed coherent double reflection from a rough water-solid interface and related the changes in the averaged specular reflection to the phenomenon of enhanced backscatter[7], previously observed for diffuse scattering. The phase screen approximation was used to analyze the data and provided

quantitative agreement. Consequently, it is of considerable interest to determine the conditions under which the phase-screen appproximation provides accurate answers.

We will show that a numerical evaluation using the phase-screen approximation overestimates the backscatter by very nearly an overall constant. The same result holds for the analytic solution that employs both the phase-screen and the Fresnel approximation. The constant is shown to be nearly independent of the radius of the transducer and the degree of focusing. It is also shown that the constant depends systematically on the statistics of the surface profile as well as the frequency, rms height and correlation length of the surface.

Ogilvy in Ref. (8) has provided a comprehensive review of the literature associated essentially with the reflection of waves from the rough surfaces. However, much less work concerning the transmission of the waves through the rough surfaces has appeared in the literature. Recently, some research has been conducted to determine the effects of surface roughness on the ultrasonic inspection.[9-11] Nagy and Adler[9] studied the surface roughness induced attenuation of the coherent (average) part of the transmitted wave. They modeled the wave propagation through the rough surface via the phase-screen approximation. With their model, they reached good agreements with the experimentally measured attenuation values of coherent signal and applied their predictions to the detection and characterization of porosity in as-cast aluminum. Nagy and Rose[11] extended the theory of the phase-screen approximation for the transducers radiating an angled incidence beam. For the unfocused probes, they experimentally observed the significant attenuation of the flaw signal by the surface roughness while observing a small change in the material noise signal. For focused transducers, Bilgen and Rose[12] theoretically analyzed the characteristics of the flaw signal as a function of the flaw's distance from the surface with Gaussian and exponential correlation functions. They predicted increased attenuation of the flaw signal from the near-surface flaw and less attenuated signal from a flaw at larger distances to the surface. They explained this feature of the flaw signal via the double-coherent and -incoherent transmission at rough

surfaces. More interestingly, they demonstrated that the focusing substantially reduces the effects of surface roughness and improves the signal-to-noise ratio.

This paper is organized as follows. Section II describes the problem of incoherent scattering from densely-distributed volumetric scatterers below rough surfaces and introduces our simplified model. Section III briefly outlines the BIE and the phase-screen approximation. An analytic solution for Gaussian beams and Gaussian correlation functions is given. Section IV contains calculations of the normalized backscatter. The dependence of the constant-of-proportionality on the frequency, rms height and correlation length is reported in this section. Finally, we end the paper with a discussion and conclusion.

II. GEOMETRY, ASSUMPTIONS AND SIMPLIFIED MODEL

The geometry of the problem addressed in this paper is shown in Fig. 1. A phase-sensitive transducer is immersed in water and oriented normally to the surface of a rough solid plate sample at a set-off, z_0, of several centimeters. A broadband pressure pulse is excited in water and propagates to the plate's surface. There it interacts with the rough surface, is transmitted into the sample, and scatters from the distributed volumetric scatterers, e. g. microcrystallites or grains. The resulting reflected waves then back propagates through the rough surface and are detected by the same transducer. The reflection is time-gated and the signal received at time t is related to the scattering from the microstructure in the sample at depth z.

The surface roughness is assumed to be one-dimensional and spatially uniform. That is, the surface is randomly rippled; the height variation of the surface is described by a function h(x) that depends only on the x-coordinate. It is assumed that the surface height at a point x is described by a Gaussian random process with zero-mean. Further, the variation of the roughness along the surface is described to second-order by an autocorrelation function, which due to spatial uniformity can be written as

$$\Gamma(x-x') \equiv \frac{\langle h(x)h(x')\rangle}{h^2}. \tag{1}$$

Here $h = \sqrt{\langle h^2(x)\rangle}$ and <.> denotes an ensemble average which is assumed to be equal to the result obtained by spatially averaging over a large surface (the ergodic hypothesis). The autocorrelation function is represented by either a Gaussian,

$$\Gamma(x-x') = e^{-\frac{(x-x')^2}{L^2}}, \tag{2}$$

or an exponential

$$\Gamma(x-x') = e^{-\frac{|x-x'|}{L}} \tag{3}$$

where L defines the surface correlation length.

In order to obtain our simple model we make the following assumptions concerning the solid; 1) the ultrasonic longitudinal wave is modeled by a scalar wave propagation in a constant-density fluid, shear wave propagation is neglected, 2) the size of the microstructures is much smaller than the wavelength, 3) no attenuation is induced by the microstructure, 4) the scattering from the microstructure is weak. Under these assumptions (using Auld's reciprocity formula[13] and the Born approximation) it can be shown that the backscatter is proportional to

$$P(h,z,L,R,F,\omega) \equiv \int dx |u(\omega,x,z|^4. \tag{4}$$

Here z denotes the coordinate normal to the surface, while x denotes the coordinate parallel to the surface. The use of Born approximation implies a single-scattering theory. Consequently, the material noise generated at a depth z can be roughly associated with the backscattered noise at time $t = 2\, z_o / c_s$, where z_o denotes the distance beneath the surface and c_s denotes the velocity in the fluid that represents the solid. Also, F denotes the focal length, while R denotes the radius of a transducer . The integration is taken over the plane parallel to the surface, and u(w,x,z) is the wavefield obtained in the presence of the rough surface but in the absence of the volumetric scatterers.

The determination of u can be approximately divided into three parts: (1) propagation of the wave in water from transducer to the solid; (2) transmission through the rough water-solid interface; and (3) propagation in the uniform "average" solid. The beam propagation in water is modeled by the integral equation method. The transmission through the rough surface is accomplished via the integral equation method and the phase-screen approximation. The wave in the uniform solid is propagated by the integral equation method and the plane wave expansion method. Analytic solutions are obtained using the Fresnel approximation[14] which is employed to propagate the wave in the solid.

We are interested in the changes introduced into the material noise by the presence of a rough surface. Consequently, we define the normalized backscatter,

$$Q(h,z,L,R,F,\omega)=\frac{\langle P(h,z,L,R,F,\omega)\rangle}{P(h=0,z,L,R,F,\omega)}, \tag{5}$$

which is obtained by dividing the backscatter in the presence of roughness by the backscatter measured through a smooth surface. Equation (5) is the basis for the rest of this paper.

III. WAVE PROPAGATION AND APPROXIMATIONS

Equation (5) indicates that the numerical calculation of the normalized backscatter requires the transmitted wavefields obtained in the uniform solid. The wavefields can be determined in three steps: (1) the wave in water is propagated from transducer to the solid; (2) the wave is transmitted through the rough or smooth water-solid interface; and (3) the wave is propagated in the uniform "average" solid.

For the first step, we approximate the transducer's radiation by

$$u(\omega, x, z_0) = e^{-(\frac{1}{R^2}+i\frac{k_w}{2F})r^2} \tag{6}$$

where k_W denotes the wave number in water, R defines the radius of the beam, and F describes the focal length of the cylindrically focused transducer. The unfocused case is evaluated by setting F to infinity. The field in water is propagated from the transducer to the solid using integral representation.

The transmission through the rough surface is accomplished via the integral equation method and the phase-screen approximation. The wavefield is propagated within the solid using the integral equation representation and the plane wave expansion method. For analytical solutions, we approximated the plane wave expansion by the Fresnel approximation.

A. Integral Equation Method

Integral equations are very often employed to solve partial differential equations with defined boundary conditions. Many alternative forms of integral equations have been

proposed to provide different computational advantages and an extended list of literature can be found in Ref.(15). In the following we briefly review the integral equation method since it serves as a benchmark calculation by providing numerically exact backscatter.

The approach for the problem of wave propagation through rough surfaces can be summarized as follows. The integral representations of wavefields in water and in solid are first written. The representation integral in water includes the incident field radiated by the transducer. The Greens function is $G(x,x') = \frac{i}{4} H_0^{(1)}(k|x-x'|)$ the zero order Hankel function of the first kind. The parameter k denotes the wavenumber of the medium. By letting the fields in water and the sample approach to the surface, we obtain two coupled integral equations. These equations involve four unknowns which are the wavefields in water, in the sample, and their normal derivatives. The acoustical boundary conditions at the surface are the continuity of the pressure field and the continuity of the velocity field.

For randomly rough surfaces, analytical solutions for the unknowns are not tractable and the problem is either solved approximately or computed numerically. The numerical calculation is achieved by converting the resulting coupled integral equations into a matrix equation by partitioning the surface into N subintervals (boundary elements). Ogilvy[8] describes the numerical generation of rough surfaces with Gaussian or exponential autocorrelation functions. In this work, the rough surface is defined by the discrete coordinates $\mathbf{r}_i' = \left(x_i', h(x_i')\right)$. The discretization length along the x-axis is chosen to be $(x_{i+1}' - x_i') = \lambda_s / 8$. for i=1,..N+1 where λ_S is the wavelength in the solid. The boundary element S_i lies between the end points $\mathbf{r}_i'$ and $\mathbf{r}_{i+1}'$. We adopt the pulse base function which assumes the wavefield over each boundary element be constant. By point matching at the mid-point $\bar{\mathbf{r}}'$ of each boundary element and using the boundary conditions along the surface S a matrix-vector equation is written

$$\mathbf{AU} = \mathbf{U}^{\mathrm{inc}} \tag{7}$$

where the unknown vector is the transmitted wavefield $\mathbf{U}_i = u(\bar{\mathbf{r}}_i')$ and its normal derivative $\mathbf{U}_{i+N} = \partial u(\bar{\mathbf{r}}_i')/\partial \mathbf{n}$ on the surface. The elements of the vector on the right hand side are $\mathbf{U}_i^{\mathrm{inc}} = u^{inc}(\bar{\mathbf{r}}_i')$ and $\mathbf{U}_{i+N}^{\mathrm{i}} = 0$ for i=1,...,N. The incident field $u^{inc}(\bar{\mathbf{r}}_i')$ is induced by transducer at the mid-point of the i-th segment of the surface.

The vector-matrix equation is solved for the unknown vector **U**. Then the wavefield at any point (x,z) within the sample is calculated using

$$u(x,z) = \mathbf{BU}. \tag{8}$$

The elements of matrices **A** and **B** are found in Ref. (15). The integrals associated with the elements of the matrices **A** and **B** over the boundary elements are computed using the 8-point Gaussian quadrature integration rule.

B. Phase-screen Approximation

Phase-screen approximation assumes that the only effect of the roughness is to change the phase of the transmitted wave. The amplitude of the transmitted wave is assumed to be unchanged. When the wavefield immediately above the $z=0^-$ plane is known, the transmitted wavefield at $z = 0^+$ is given by

$$u(\omega, x, z = 0^+) = T_o u(\omega, x, z = 0^-)\exp(i\phi(x)) \tag{9}$$

where T_0 denotes the transmission coefficient for a normally-incident plane wave on a smooth surface. At each point of the surface, the phase change f(x) is predicted on the basis of geometrical acoustics limit and expressed by

$$\phi(x) = k_s(1 - \frac{c_s}{c_w})h(x). \tag{10}$$

The r.m.s. value of the phase, σ, is determined from Eq. (10) in terms of the r.m.s. height, *h*. Explicitly

$$\sigma = k\left|1 - \frac{c_s}{c_w}\right|h. \tag{11}$$

The wave field was propagated into the sample using the modal expansion of plane waves once the value at the surface ($z=0^+$) was calculated.[7] Explicitly, the field at a depth z was calculated via

$$u(\omega, x, z) = \int dq\, f(q) e^{iqx + i\sqrt{k_s^2 - q^2}z}, \tag{12-a}$$

where k_S denotes the wave number in a uniform medium below the rough surface and

$$f(q) \equiv \frac{1}{2\pi}\int dx\, u(\omega, x, z = 0)e^{-iqx}. \tag{12-b}$$

We evaluate Eq.(12) numerically using the fast Fourier transform which provides a simple and convenient method for beam propagation studies.

When the transducer radiates well collimated beams, Eq.(12-a) can be accurately approximated by expanding the square root

$$\sqrt{k_s^2 - q^2} \approx k_s - \frac{q^2}{2k_s}. \tag{13}$$

This expansion neglects the evanescent waves. Equations (12-a) and (12-b) can then be evaluated to give the Fresnel formula for the wave propagation in interior of the sample

$$u(\omega, x, z) = \sqrt{\frac{-ik_s}{2\pi z}} e^{ik_s z} \int dx'\, u(\omega, x', z = 0) e^{\frac{ik_s}{2z}(x - x')^2}. \tag{14}$$

We also derive the normalized variance expression analytically in series form for the corrugated surfaces with Gaussian autocorrelation functions. We first represent the wavefield in water but just above the surface by

$$u(\omega, x, 0^-) = Ue^{-(\frac{1}{R_1^2} + i\frac{k_s}{2F_1})r^2} \tag{15}$$

where U, R_1 and F_1 are the estimated amplitude, radius and focal depth, respectively. Then we evaluate the normalized backscatter using the phase-screen model Eq.(9) and Fresnel approximation Eq. (14). The approach is similar the one outlined in the paper by Bilgen and Rose[3] for randomly rough isotropic surfaces. The normalized backscatter can be given by

$$Q(z) = \sum_{a,b,c,d=0}^{\infty} \frac{(2\sigma^2)^{a+b}(-\sigma^2)^{c+d}}{a!b!c!d!} \frac{\sqrt{\frac{L^2}{R_1^2} + \frac{\beta^2}{4}}}{\sqrt{(\frac{L^2}{R_1^2} + a + c + d)(\frac{L^2}{R_1^2} + b + c + d) - (\frac{i\beta}{2} + (d - c))^2}} \tag{16}$$

where

$$\beta = k_s L^2 \left(\frac{1}{z} - \frac{1}{F_1} \right). \tag{17}$$

IV. NORMALIZED BACKSCATTER CALCULATIONS

In this section, we calculate the normalized backscatter Q as a function of the miscrostructure's distance from the surface. We consider both focused and unfocused transducers. The transducers are assumed to have radii of R=0.5 cm and to be positioned at z_0 = 2.54 cm standoff distance in water. The focal length of the focused transducer is assumed to be at 2 cm within the sample. The sound velocity of the solid was chosen to be that of aluminum, c_S=6.3 10^5 cm/s. while the sound velocity of water is c_W=1.5 10^5 cm/s.

The numerical calculations proceeded as follows. The propagation of the incident beam in water is straightforward for both methods and can be accomplished by either the BIE or by the expansion-in-planewaves method. In fact, the BIE was used to determine the field incident on the rough surface. Next, we separately used the BIE and the phase-screen approximation to calculate two approximations to the transmitted wavefield u . The wavefields were propagated in the solid (the second fluid) using either the BIE or the expansion-in-plane waves method. Finally, the normalized backscatter was determined from Eq. (5) for both the BIE and the phase-screen approximation.

Figure 2 shows three calculations for the normalized backscatter as a function of depth at 10 MHz. First, the solid line shows the result for the BIE. Second, the dotted line shows the result for the numerical computation of the phase-screen approximation including evanescent waves. Finally, the dashed line shows the result of Eq.(17), the analytic series solution for the phase-screen approximation (requires a Gaussian correlation length, a Gaussian beam and the Fresnel approximation). For these calculations the surfaces are described by a fairly large rms height, h=50 μm., and a Gaussian autocorrelation function with L=787.5 μm. Ten different surface profiles were generated, the backscatter was calculated for each profile, the results were averaged and finally normalized by the smooth surface result. Figures 2a and 2b show the results for unfocused and focused probes.

The dependence on depth (or equivalently time) is nearly the same for each calculation shown. First, there is an initial enhancement of the backscattered noise. Second, the normalized backscatter decreases with depth. In the case of the unfocused probe this decrease is continuous and the smallest value is obtained in the far-field limit. For the focused probe the backscatter decreases more rapidly and reaches a minimum near the focal depth of 2 cm. It then increases slightly for greater depths. It is everywhere true that the backscatter computed by the BIE is less than the value computed numerically using the full phase-screen approximation, which is in turn less than the analytic result given in Eq.(17) that employed the Fresnel approximation. Figure 2 is typical of the many calculations carried out for the various parameters of the problem and which are summarized below in Figs. 4 and 5.

The results presented in Fig. 2 reveal that BIE and phase-screen calculations have nearly the same dependence on depth and consequently very nearly differ only by a constant. The dotted-dashed line in Fig. 2 represents the constant curve that was obtained by dividing the phase-screen results by the BIE results. Similar constants were obtained for a wide variety of surface profiles and also for surfaces with exponential autocorrelation function. The simple phase-screen predictions differ from the exact results by a constant of proportionality (a difference in the transmission coefficient) and are otherwise nearly identical. The analytical results overestimate the normalized variance calculations because the Fresnel approximation ignores the evanescent waves.

The close agreement between the integral equation and the phase-screen approximation results suggests that examination of their differences may lead to an improved understanding of the phase-screen approximation and a method for correcting it. We performed a series of parametric studies on the constant of proportionality between the integral equation and the phase-screen approximation with plane wave representation results.

We changed the parameters h, L and frequency and related the changes to the variation in the constant of proportionality. We found that the constant of proportionality, C, can be empirically fit by

$$C = 1 + 16(h / L)^2 \{\cos(.6) - \exp(-.5k_s L)\cos(.75k_s L + .6)\} \tag{20}$$

for the Gaussian autocorrelation function and similar fit can be found for the exponential autocorrelation function.

Figures (3), (4) and (5) show the dependence of the constant of proportionality on the frequency, rms height and correlation length for both Gaussian and exponential statistics. Results are given by the symbols for focused probes and unfocused probes. The effects of focusing are negligible over almost the entire range. The discrepancies between the phase-screen and BIE are more pronounced for surfaces described by exponential correlation functions. They are much less pronounced for Gaussian autocorrelation functions. The discrepancies increase with increasing frequency or rms height and decrease with increasing correlation length. The solid line shows the results of the empirical formula, which was constructed to agree with the symbols for the case of Gaussian correlation function. Figure 3 shows the nearly quadratric dependence of the constant on the r.m.s. height. Figure 4 illustrates the inverse dependence of the constant on the correlation length. These results indicate that the phase-screen approximation predicts the backscatter accurately for smaller rms height and larger correlation length. Fig. 5 shows the frequency dependence of the constant for unfocused probes and for two different correlation lengths for which the curves approach to two different constants at high frequencies.

Clearly, the phase-screen approximation describes the variation in the backscatter as a function of depth. Its major error appears as an overall constant that is independent of the transducer type and depends primarily on the rms height, the correlation length L and the

frequency. Presumably, this error arises since the phase screen approximation ignores the roughness-induced changes in the amplitude of the transmitted wave (it only corrects for the phase variation). Consequently, progress in improving the phase-screen will most probably be made by focusing on an appropriate correction for the amplitude of the beam.

V. DISCUSSION AND CONCLUSION

Rough surfaces affect focused and unfocused beams differently as the beam propagates in a uniform sample. In turn, these effects determine the characteristic behavior of the backscatter observed in the last section. In this section, we present BIE and phase-screen calculations and then use them to explain some of the characteristic features predicted in the last section.

Figure 6 shows a rough surface profile obtained from a single realization of a zero-mean Gaussian random-process with h=25 mm and L=1.5 mm . An incident Gaussian beam (with radius 0.635 cm) is transmitted through this surface and propagated to a depth of 2 cm. The amplitudes of the wavefields, generated by focused (F = 2 cm) and unfocused probes, are plotted in Fig. 7. The solid lines represent the wavefields obtained using the BIE while the others are the phase screen approximation results. The dotted curve is obtained from the plane-wave expansion Eq.(12a,b) and the broken curve is calculated from the Fresnel approximation Eq.(14). The wavefields transmitted through planar interface are also given for reference. Figure 7 indicates close agreement between the BIE and phase-screen result for this particular rough surface. . The Fresnel approximation (for the unfocused probe) estimates the beam shape near the center of the beam correctly but breaks down for the side lobes, as expected.

Figure 7 can be analyzed as follows. Both focused and unfocused beams are randomized because of the interference introduced by the rough interface. However in the focused case, the division of the beam into coherent and incoherent parts is more readily apparent. There, aside from an overall attenuation, the (coherent) wavefield is remarkably similar to that produced by a smooth surface. The incoherent part of the field produces random appearing side lobes. This occurrence of the coherent central lobe in the region of the focus is important for moderately rough surfaces, since, aside from an overall attenuation,

this lobe is nearly independent of small-scale roughness. This feature dominates the backscatter from the microstructure at the focal region. The other parts of the wavefield depend in detail on the surface profile and vary with different statistical realizations. Hence, their contribution to the backscatter tend to be averaged out compared to the coherent central lobe. Similar calculation with the same parameters for the two dimensional surface profile would produce a focused beam at the focal depth with thinner central lobe, larger peak and lower side lobes.

The phase-screen model is in general a good approximation and yields correct answers when the correlation length is much longer than the wavelength and both are much larger than the r.m.s. height. When these conditions are violated the quality of approximation becomes poorer. The phase-screen approximation is much simpler, less computationally demanding and identifies the basic physics of wave transmission through rough surfaces. The Fresnel approximation brings simplicity to the analytical calculations. Consequently, the phase-screen approximation can, after suitable correction, be evaluated for problems that are too numerically demanding for the integral equation method.

VI. ACKNOWLEDGMENT

This material is based upon work performed by the FAA-Center for Aviation Systems Reliability, operated by the Iowa State University and supported by the Federal Aviation Administration under Contract No.93-G-029.

VII. REFERENCES

[1]M. D. Russell, S. P. Neal and E. J. Boote, "Experimental estimation of the longitudinal-wave backscatter coefficients for ultrasonic interrogation of weak scattering materials," J. Acoust. Soc. Am. 93, 1267-1276 (1993).

[2]J. H. Rose, "Ultrasonic backscatter from microstructure," in Review of Progress in Quantitative Nondestructive Evaluation, edited by D. O. Thompson and D. E. Chimenti (Plenum, New York, 1992), Vol. 11B, pp. 1677-1684.

[3]M. Bilgen and J. H. Rose, "Rough surface effects on incoherent scattering from random volumetric scatterers: Analytic Solution," to be published.

[4]J. H. Rose, M. Bilgen, P. B. Nagy, and L. Adler, "Effects of surface roughness on ultrasonic backscatter," in Review of Progress in Quantitative Nondestructive Evaluation, edited by D. O. Thompson and D. E. Chimenti (Plenum, New York, 1992), Vol. 11B, pp. 1693-1700.

[5]M. Bilgen, J. H. Rose and P. B. Nagy, "Ultrasonic inspection, material noise and surface roughness," in Review of Progress in Quantitative Nondestructive Evaluation, edited by D. O. Thompson and D. E. Chimenti (Plenum, New York, 1993), Vol. 12B, pp. 1767-1774.

[6]J. H. Rose, M. Bilgen and P. B. Nagy, "Acoustic double reflection and transmission at a rough water-solid interface," to be published.

[7]E. Jakeman, "Enhanced backscattering through a deep random phase screen," J. Opt. Soc. Am. A 5, 1638-1648 (1988).

[8]J. A. Ogilvy, Theory of Wave Scattering from Random Rough Surfaces (Adam Hilger, Bristol, 1991).

[9]P. B. Nagy and L. Adler, "Surface roughness induced attenuation of reflected and transmitted ultrasonic waves," J. Acoust. Soc. Am. 82, 193-197 (1987).

[10]P. B. Nagy, L. Adler and J. H. Rose, "Effects of acoustic scattering at rough surfaces on the sensitivity of ultrasonic inspection," in Review of Progress in Quantitative Nondestructive Evaluation, edited by D. O. Thompson and D. E. Chimenti (Plenum, New York, 1993), Vol. 12B, pp. 1775-1782.

[11]P. B. Nagy and J. H. Rose, "Surface roughness and the ultrasonic detection of subsurface scatterers," J. Appl. Phys. 73, 566-580 (1993).

[12]M. Bilgen and J. H. Rose, "Doubly-coherent transmission at rough surfaces and its implications for ultrasonic inspection," Review of Progress in Quantitative Nondestructive Evaluation in press.

[13]M. Bilgen and J. H. Rose, "Focused ultrasonic probes and the effects of surface roughness on material noise," Review of Progress in Quantitative Nondestructive Evaluation in press.

[13]B. A. Auld, "General electromechanical reciprocity relations applied to the calculation of elastic wave scattering coefficients," Wave Motion 1, 3-10 (1979).

[14]J. W. Goodman, Introduction to Fourier Optics (McGraw-Hill, New York, 1969).

[15]J. G. T. Schuster and L. C. Smith, "A comparison among four direct boundary integral methods," J. Acoust. Soc. Am. 77, 850-564 (1985).

[17]M. deBilly and G. Quentin, "Backscattering of acoustic waves by randomly rough surfaces of elastic solids immersed in water," J. Acoust. Soc. Am. 86, 591-601 (1982).

[18]E. I. Thorsos, "The validity of the Kirchhoff approximation for rough surface scattering using a Gaussian roughness spectrum," J. Acoust. Soc. Am. 83, 78-92 (1988).

[19]E. I. Thorsos and D. R. Jackson, "The validity of the perturbation approximation for rough surface scattering using a Gaussian roughness spectrum," J. Acoust. Soc. Am. 86, 261-277 (1989).

[20]W. A. Kuperman and H. Schmidt, "Self-consistent perturbation approach to rough surface scattering in stratified elastic media," J. Acoust. Soc. Am. 86, 1511-1522 (1989).

[21] Ö. Bozma and R. Kuc, "Characterizing pulses reflected from rough surfaces using ultrasound," J. Acoust. Soc. Am. 89, 2519-2531 (1991).

[22]M. Blakemore, "Scattering of acoustic waves by the surface of an elastic solid," Ultrasonics 31, 161-174 (1993).

[23]P. Beckmann and A. Spizzichino, The Scattering of Electromagnetic Waves from Rough Surfaces, (Pergamon, Oxford, 1963).

[24]F. G. Bass and I. M. Fuks, Wave Scattering from Statistically Rough Surfaces (Pergamon, Oxford, 1979).

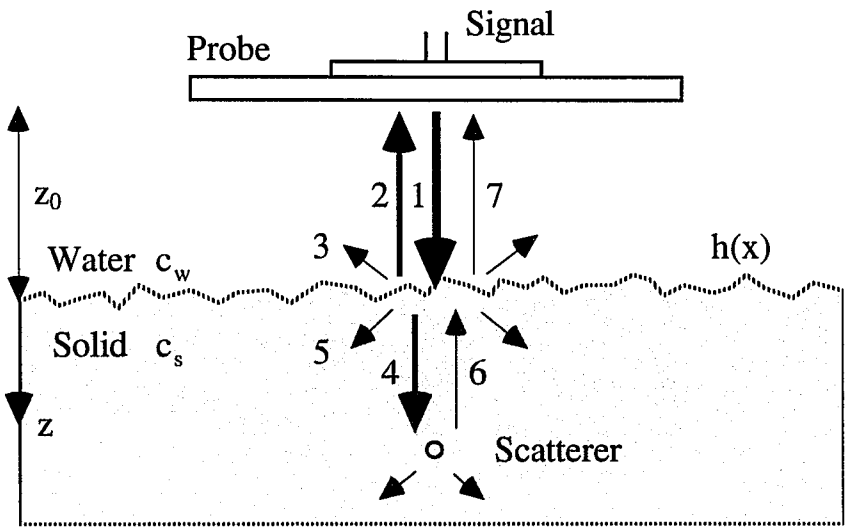

1-Incident Wave; 2-Coherent Reflection; 3-Incoherent Reflection; 4-Coherent Transmission; 5-Incoherent Transmission; 6,7-Backscattering

Figure 1. Schematic geometry of hypothetical ultrasonic inspection. Shows backscattering below a rough surface.

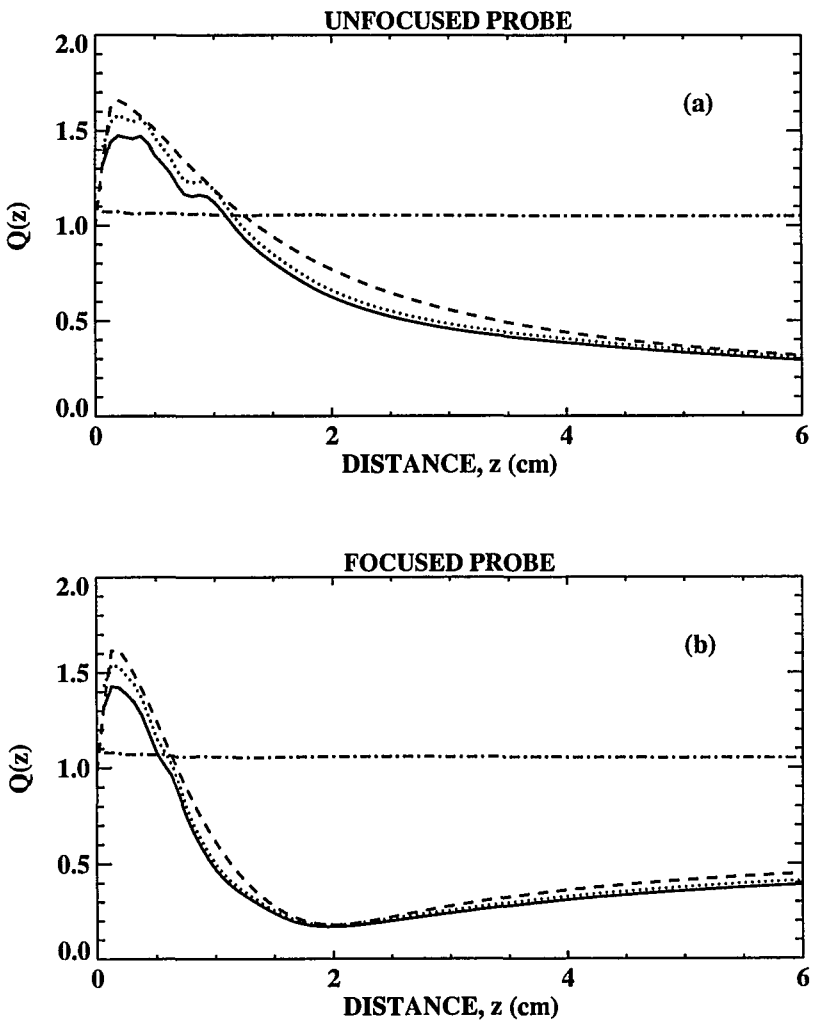

Figure 2. Normalized backscatter. Solid line- BIE result, Dotted line- phase-screen approximation result, Deshed line- analytical solutions and Dashed dotted line- the ratio of phase-screen approximation to BIE.

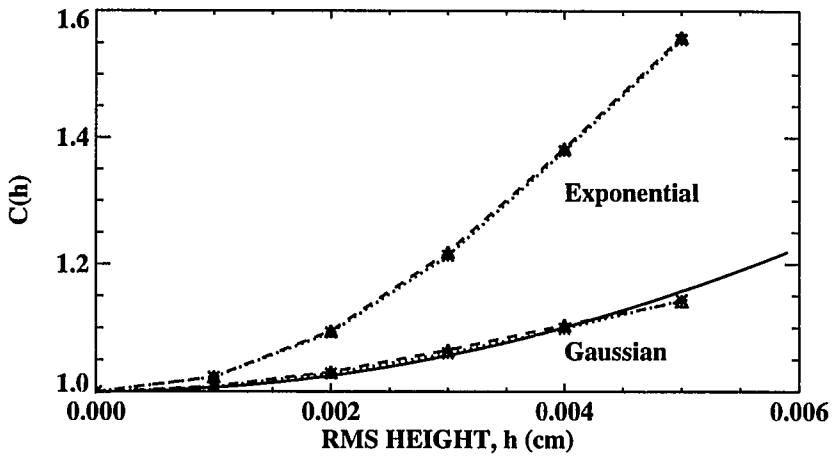

Figure 3. Functional dependence of constant on r.m.s. height for L=472.5 μm and f=10 MHz, Solid line- empirical fit, Δ: focused probe and *: unfocused probe.

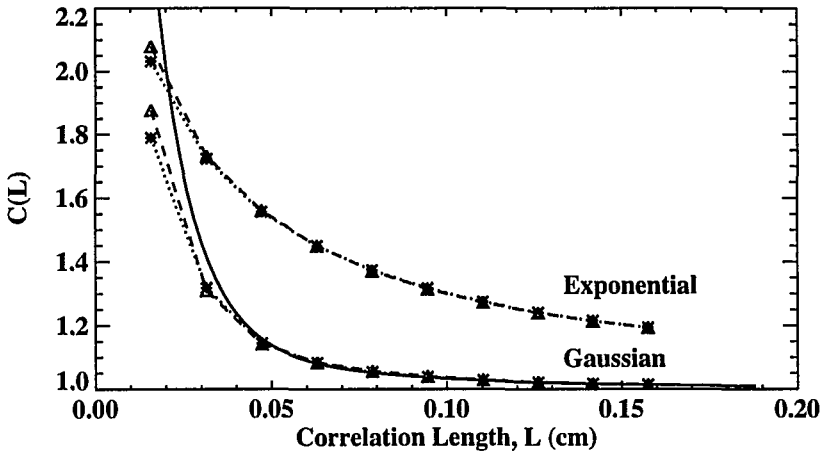

Figure 4. Functional dependence of constant on correlation length for h=50 μm and f=10 MHz, Solid line- empirical fit, Δ: focused probe and *: unfocused probe.

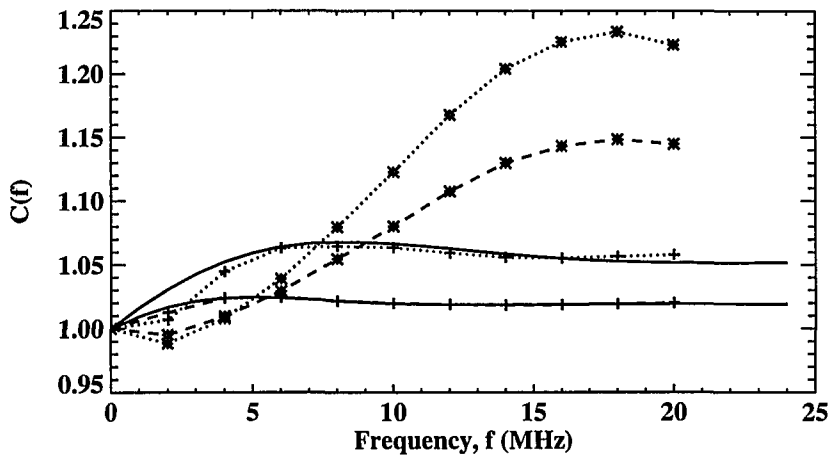

Figure 5. Functional dependence of constant on frequency for unfocused probe and h=20 μm, *: exponential correlation function, +: Gaussian correlation function, Dotted line- L=315 μm and Dashed line- L=525 μm.

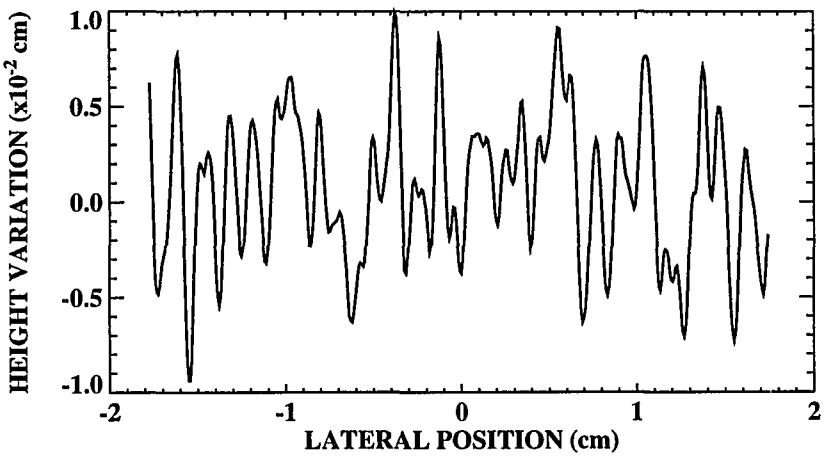

Figure 6. Numerically generated "Gaussian" randomly-rough surface-profile for h=25 μm and L=1.5 mm.

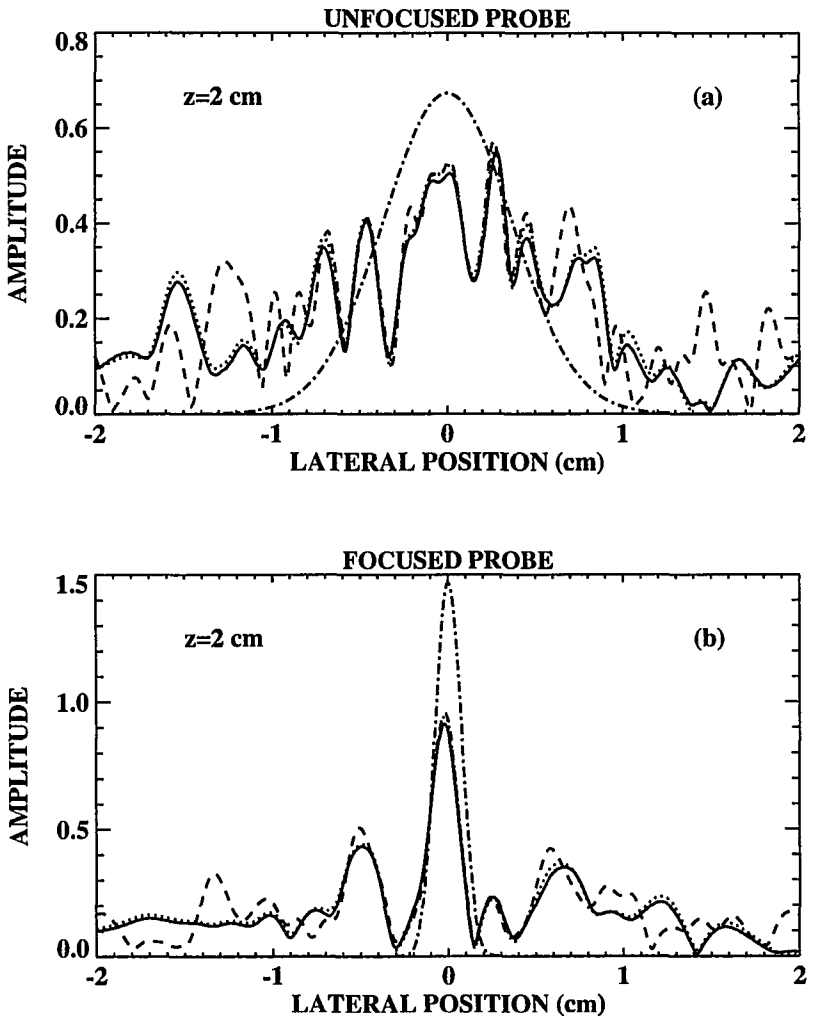

Figure 7. Magnitude of wavefield below the surface. Solid line- BIE result, Dotted line- phase-screen approximation result, Dashed line- Fresnel Approximation and Dashed dotted line- BIE result for smooth interface. Notice the variation in vertical scale for the focused probe results.

PAPER 3:

ULTRASONIC INSPECTION, MATERIAL NOISE AND SURFACE ROUGHNESS

I. INTRODUCTION

The ultrasonic detection of subsurface flaws, such as cracks or voids, may be greatly degraded by the presence of rough surfaces [1,2]. The loss of signal-to-noise arises for three reasons. First, the randomization of the phase of the wave by the roughness may reduce the phase coherent signal from the flaw. Second, additional noise is generated directly by the reflection of the incident beam by the rough surface. Finally, the material noise is modified.

We focus on the changes in the material noise, which for structural metals is generated primarily by the backscatter from the polycrystalline microstructure. Increased roughness tends to randomize the wavefield. Consequently, the phase coherent detection of scattering from surfaces and large flaws is decreased. It might be supposed that the material noise might also be decreased by the randomization of the wavefield. However, this is not the case. The material noise is sometimes increased and at other times decreased by the presence of roughness [1]. The change in the material noise is relatively small for surfaces of interest to NDE (typically several dB).

In this paper we present the following results. First, an experiment shows that the material noise can in fact be enhanced by surface roughness. Second, the Boundary Integral Equation (BIE) method is used to analyze the change in backscatter noise. In previous work, [1], the effects of surface roughness were included via the phase-screen approximation (PSA). Both the BIE and PSA predict the backscattered noise as a function of time (or, roughly the depth into the sample). Third, we find that the BIE and PSA results are very nearly the same to within an overall constant of proportionality. That is, the simple and easy to use phase-screen approximation yields nearly exact results aside from an overall constant.

II. EXPERIMENTAL OBSERVATION OF INCREASED BACKSCATTER

In the experiment, a broadband, immersion transducer with a diameter of 1.27 cm and a center frequency of 15 MHz was oriented normally at 3.2 cm standoff to the surface of a rectangular, flat (10 cm x 10 cm x 5 cm) aluminum plate. One surface of the plate was roughened by shot peening. The surface roughness can be roughly described as resulting from overlapping hemispherical bosses. The r.m.s. roughness, h, of the surface was 25 μm. The autocorrelation function of the surface was measured and found to be nearly isotropic. The correlation length, L, was estimated by fitting a Gaussian function to the autocorrelation function, and L = 2.415 mm.

The signal was recorded when the transducer was facing the roughened side of the sample. It was also recorded when the transducer was facing the smooth surface. Time-gating was employed to remove the echo due to the water-solid interface, and to obtain measurements characteristic of the microstructure of the sample's interior. The signal was filtered to a 1 MHz bandwidth, and recorded for frequencies between 12 and 18 MHz. The square of the filtered signal (at each frequency) was taken. Next, the squared signals were spatially averaged over the 5 cm by 5 cm surface of the sample in order to obtain the backscattered noise.

The averaged material noise measured through the rough surface will be denoted $N_R(t)$, while that measured through the smooth surface will be denoted by $N_S(t)$. The ratio of these two quantities is defined to be the normalized backscatter noise

$$Q(t) = N_R(t) / N_S(t). \tag{1}$$

Q is greater than one if the roughness enhances the material noise and less than one if it decreases the material noise.

Fig. 1 shows Q(t) as measured at 12, 15 and 18 MHz and clearly shows the predicted enhancement of the material noise due to surface roughness. The increased noise is on the order of 2 or 3 dB, and has its maximum at a time 52 μs, which corresponds to a depth d = 2.8 cm below the surface of the aluminum plate after accounting for the travel path in water. To within experimental error the signal is independent of frequency. We note that the maximum in the signal occurs at a time that can be estimated by considering the hemispherical bosses on the surface to be focusing lenses. The focal length, estimated from the radius and the depth of the bosses, is roughly 2.5 cm which is close to the experimental result, 2.8 cm.

III. MODELS FOR THE EFFECTS OF SURFACE ROUGHNESS ON BACKSCATTER

The basic theoretical model will be introduced in this section. The problem can roughly be divided into two parts. First, the wavefield changes as it transmits through the rough surface and propagates into the solid. Second, the beam interacts with the solid's microstructure and acoustic energy is backscattered. We focus our attention almost entirely on the first part, changes due to the transmission and propagation of the beam. The interaction of the beam with the microstructure is modeled in the most trivial way possible. Namely, we assume a scalar model for the longitudinal waves, and approximate the noise via

$$N_{R,S}(t) = \eta \int d^3\vec{r} \left| u^o_{R,S}(\omega, \vec{r}) \right|^4 \delta(t - 2\hat{z} \cdot \vec{r} / c). \tag{2}$$

Here, h denotes the power backscattered per unit volume, while $\hat{z}$ denotes the normal to the surface. The delta-function restricts the integration to the plane defined by $\hat{z} \cdot \vec{r} = d$, where d is the depth below the surface. The subscripts R and S denote the transmission through the rough and through the smooth surfaces. Finally, u^o denotes the wavefield at a point below the surface in the absence of microstructure (i.e. for a completely uniform plate). Equation(2) can be derived from the volumetric form of the reciprocity theorem by assuming small microstructures, weak scattering and no acoustic attenuation. The effects of surface roughness on the material noise is then estimated from normalized backscatter coefficient Q, which is defined in Eq.(1) as the ratio of N_R and N_S.

IV. BIE AND PSA CALCULATIONS OF NORMALIZED BACKSCATTER COEFFICIENT

The normalized backscatter coefficient Q was calculated using the Boundary Integral Equation method [3] and will be reported for a variety of random one-dimensional (i.e. randomly rippled surfaces) surfaces. These BIE calculations will be compared to the normalized backscatter coefficients that were calculated using the phase-screen approximation as reported last year [1]. The results of the two methods are surprisingly similar. Consequently, the PSA can, after suitable correction, be evaluated for problems that are too numerically demanding for the BIE method. In the calculations presented below, the surface profiles are constructed to have a height distribution that is described by Gaussian statistics of zero mean, r.m.s. height h, and a Gaussian autocorrelation function with correlation length L.

The BIE approach was used as a benchmark calculation since it provides numerically exact results (within the scalar model of a uniform rough plate) for the transmitted wavefield at the surface of the sample. The phase-screen approximation (PSA) is, on the other hand, much simpler, less computationally demanding, and identifies the basic physics. The PSA assumes that the only effect of the roughness is to change the phase of the transmitted wave. The amplitude of the transmitted wave is assumed to be unchanged. The phase change is predicted on the basis of geometrical optics and the transmitted wave is given by

$$u_R^o(\omega, x, z = 0^-) = u_S^o(\omega, x, z = 0^+)\exp(-is(x)(k_s - k_w)) \tag{3}$$

Here, s(x) denotes the surface height at x, while k_S and k_W denote the wave vectors in the solid and in water.

The wave field was propagated into the sample using a modal expansion once the value at the surface (z=0) was calculated. Explicitly, the field at a depth z was calculated via

$$u(\omega,x,z)=\frac{1}{2\pi}\int_{-\infty}^{\infty}dq\hat{u}(\omega,q,0^{-})\exp(iqx)\exp(-i\sqrt{k^2-q^2}z), \tag{4}$$

where

$$\hat{u}(\omega,q,0^{-})=\int_{-\infty}^{\infty}dxu(\omega,x,0^{-})\exp(-iqx). \tag{5}$$

Equations (4) and (5) were evaluated using fast Fourier transforms and provide a simple and convenient method for beam propagation studies.

The PSA, as expected, was found to yield correct answers when the correlation length was much longer than the wavelength and both were much larger than the r.m.s. height. We performed a series of studies when these conditions were violated, and compared the PSA with the "exact" results of the BIE. Figure 2 shows calculations of the normalized backscatter power as a function of depth (2 d / c = t, c = 6300 m/s) at 10 MHz for h=50 μm and L=787.5 μm. The dashed line represents the PSA and the solid line is the BIE calculation. As can be seen the two calculations have nearly the same dependence on depth. When the two results are divided it becomes evident that they are very nearly proportional. Similar results to those shown in Fig. 2. were obtained for a wide variety of surface profiles. Thus, the simple phase screen approximation is found to very nearly give the exact result aside from a constant of proportionality (a difference in the transmission coefficient).

The PSA has been shown to describe the most important effects of rough surfaces on the ultrasonic inspection of flat plates [1,2]. However, as currently used, it is an uncontrolled approximation; we have no systematic manner of determining the errors that are introduced, nor do we understand how these errors change for different parts. For example, "Is the PSA

useful if the part has curved surfaces?" The close agreement between the "exact" BIE results and the PSA suggests that examination of their differences may lead to an understanding of the PSA results and a method for correcting them. To this end, we will present a parametric study of the constant of proportionality between the PSA and BIE results. We hope that this study will guide us in developing corrections to the PSA.

The functional dependence of the constant of proportionality on the r.m.s. height, the correlation length and the wavelength were studied numerically by comparing BIE and PSA calculations for randomly rippled surfaces. We found that the constant of proportionality, C, can be empirically fit by

$$C = 1 + 16(h / L)^2 \{\cos(.6) - \exp(-.5k_s L)\cos(.75k_s L + .6)\} \qquad (6)$$

Figures. 3a,b,c compare the empirical formula (solid lines) with the calculated results (symbols) for the constant of proportionality. Fig. 3a. shows the dependence of the constant on the r.m.s. height, while Fig. 3b. shows the inverse dependence on the correlation length. Fig. 3c. shows the frequency dependence of the constant for two different correlation lengths. The location of the peak is proportional to $k_S L$; at high frequency, the curves approach to different constants. As seen from these plots, the above equation captures the essentials of the functional form of the constant. The phase screen approximation ignores roughness-induced changes in the amplitude of the transmitted wave; it only corrects for the phase variation. The next most important correction will be to adjust for the overall amplitude of the transmitted wave, which will be more important for shorter correlation lengths.

V. COMPARISON WITH EXPERIMENT

The experiment mentioned above was simulated and the results are shown in Figs. 4a,b. The PSA was used due to its simplicity, which allowed us to model the two dimensional nature of the sample's surface profile. The two-dimensional surface profile of the sample was measured, and used to compute the phase shifts used in the PSA. We modeled a piston transducer probe, as well as a series of less abrupt profiles (including two with a Gaussian variation). The incident beam is imagined to insonify 10 different locations on the surface and the normalized backscatter power was calculated for each of these locations. Finally, we spatially averaged the result. The dashed lines in Fig. 4a show the theoretical comparison to the experimental data for different transducer radiation profiles shown in Fig. 4b. As can be seen, when the theoretical radiation profile approaches the piston profile, both the theory and the experiment predict that the material noise is enhanced with a peak near 2 or 3 cm respectively. The experimental result is perhaps 50% larger overall than the calculation. However, given the small size of the signal, the approximate nature of the theory and the difficulty of the measurement, we consider the agreement between theory and experiment to be adequate.

VI. SUMMARY

The phase-screen approximation can be used to model the interaction of ultrasound with rough surfaces provided the height variation is small and the correlation length is large compared to the wavelength. The material noise is enhanced for early times and decreased for the late times. The agreement between theory and experiment lends credence to the model for the backscattered power. It was shown that the PSA predicts the normalized backscattered power to within an overall constant of proportionality. An empirical functional form of this constant was presented based on the numerical studies.

The phase-screen approximation can serve as a powerful tool for calculating the transmission of ultrasound through random rough surfaces. As a numerical method it will be most appropriate for complicated problems such as rough curved surfaces, where the BIE is too time-consuming to implement. Also, the PSA can serve as an appropriate starting point for analyzing the physics of transmission through rough surfaces. As we have seen, improvements to the PSA will need to focus on corrections to the amplitude of the transmitted wave. The phase-screen approximation accurately predicts the effects of surface roughness on ultrasonic inspections, and should serve as the basic engineering model for this important problem.

VII. ACKNOWLEDGMENT

This work was supported by the National Science Foundation (Grant No. Eco-9008272) and the Center for NDE at Iowa State University.

VIII. REFERENCES

1. J. H. Rose, M. Bilgen, P. B. Nagy and L. Adler, in Review of Progress in Quantitative Nondestructive Evaluation, Eds. D. O. Thompson and D. E. Chimenti (Plenum, New York, 1992), Vol. 11B, pp. 1693.

2. P. B. Nagy and J. H. Rose, "Surface Roughness and The Ultrasonic Detection of Subsurface Scatterers", J. Appl. Phys. 73, 566-580 (1993).

3. R. P. Shaw, "Boundary Integral Equation Methods Applied to Wave Problems," Chap. 6, Developments in Boundary Element Methods-I, Eds. P. K. Banerjee and R. Butterfield (Elsevier App. Sc. Publisher, London, 1979), pp.121.

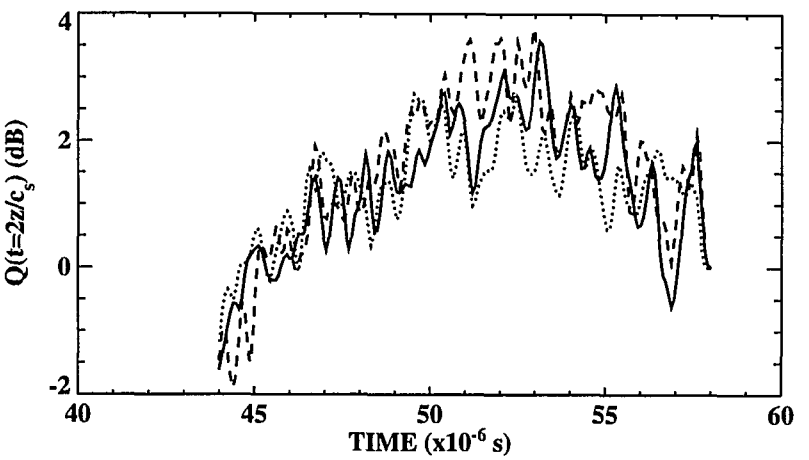

Figure 1. Experimental normalized backscatter power as a function of time. Dotted line - 12 MHz, Solid line - 15 MHz and dashed line - 18 MHz.

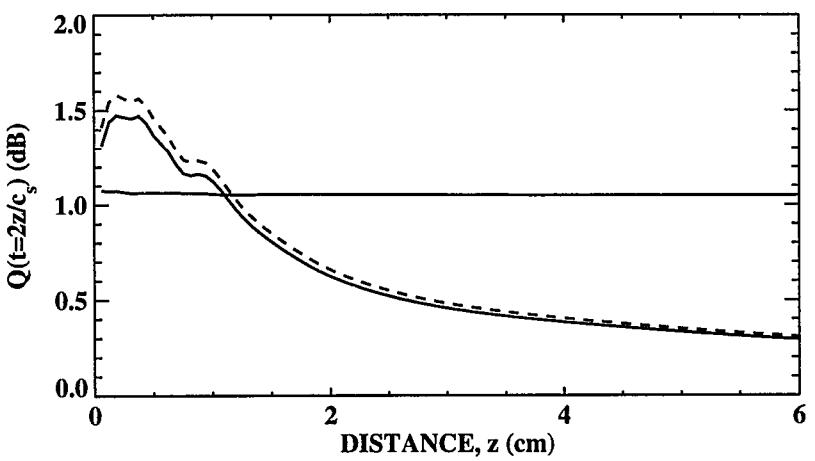

Figure 2. Normalized backscatter power. Solid line - BIE result, Dashed line - PSA result and dot-dashed line - the ratio of BIE to PSA.

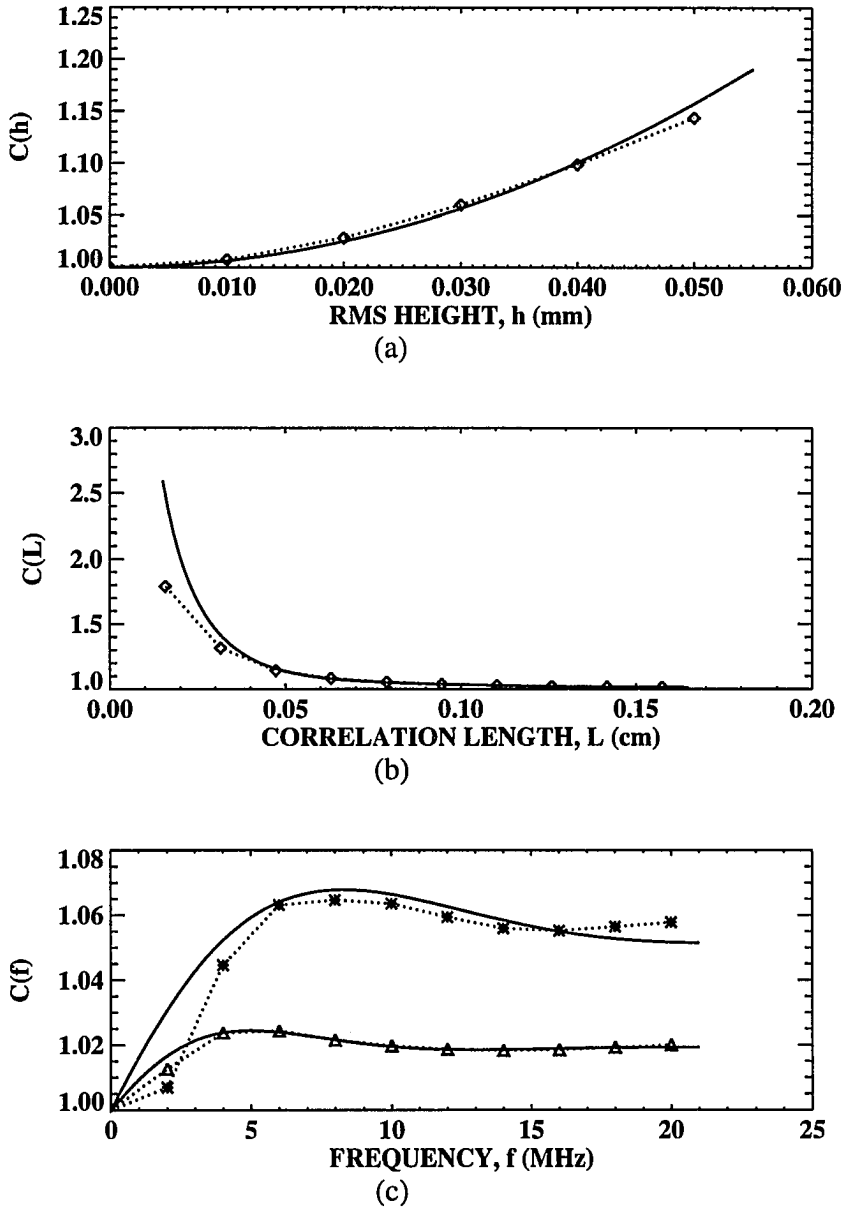

Figure 3. Functional Dependence of the constant on, (a) r.m.s. height, L=472.5 μm, f=10 MHz, (b) Correlation length, h=50 μm, f=10 MHz, (c) Frequency, h=20 μm, D: L=525 μm, *: L=315 μm.

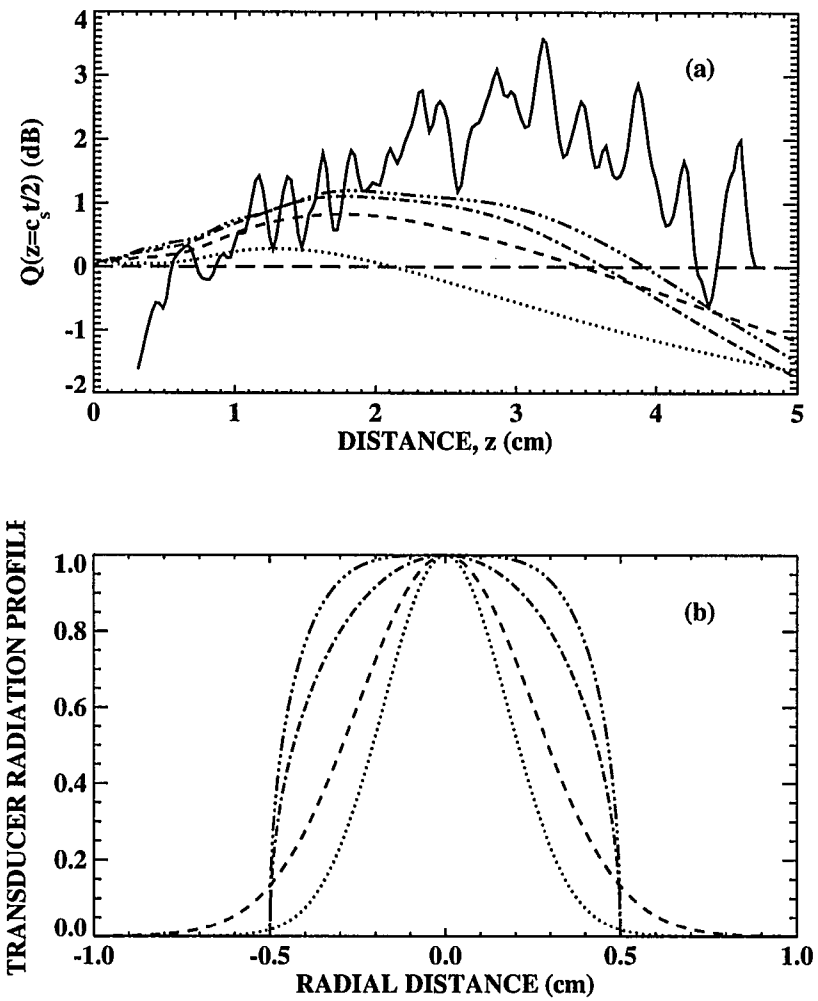

Figure 4. Simulates the experiment for several different transducer profiles. The broken lines used to define the profiles were also used to indicate the backscatter generated from that profile.

PAPER IV.

DOUBLY-COHERENT TRANSMISSION AT ROUGH SURFACES AND ITS IMPLICATIONS FOR ULTRASONIC INSPECTION

I. INTRODUCTION

Ultrasonic immersion inspection for subsurface scatterers such as voids, cracks or inclusions depends critically on the double transmission of sound through the water-solid interface (once when it transmits into the solid, and once when it transmits out). Surface roughness can strongly reduce the average signal. Up to the present time, roughness-induced losses have either been ignored or been modeled by a frequency-dependent transmission coefficient. [1] In this paper, we will show that double-transmission through a rough surface induces a near-surface region (the "dead-zone") of substantially increased loss for pulse-echo measurements. We will further show that the increased loss is due to phase coherence between the entering and exiting sound. The loss depends strongly on the depth of the scatterer beneath the surface. The attenuation in dB can be twice as large for flaws in the dead-zone. [2] Consequently, the effects of roughness cannot be described by a transmission coefficient, but must be incorporated in a depth-dependent transmission function.

The transmission function derived in this paper is appropriate for small defects whose scattering is described by the Born approximation. The same transmission function is obtained when one considers the back-surface echo from a solid plate with a roughened top surface and a smooth, parallel and planar bottom surface. Due to limitations of space, we will phrase the discussion in terms of the plate geometry in the rest of this paper. We imagine that the plate is interrogated by a focused Gaussian-transducer and the time-gated back-surface echo is measured. We analyze this measurement using a statistical approach and give analytical formulas for the ensemble-average scattering induced loss.

The structure of this paper is as follows. First, we describe the theoretical model and list our approximations. Next, we give the analytic formulas for the transmission function for surfaces described by Gaussian or exponential autocorrelation functions. Then we describe the dependence of the loss on the surface parameters such as rms height, and correlation

length, as well as the probe parameters; radius, focal length and frequency. Next, we discuss the implications of the results on the signal-to-noise ratio. Finally, we conclude with a brief summary.

II. THEORETICAL MODEL AND APPROXIMATIONS

In this section, we first review the theoretical model as well as the approximations and assumptions needed to calculate the transducer signal induced by a subsurface flaw. Then, we demonstrate the effects of phase coherence (or its lack) on double-transmission and the flaw signal. Note that the effects of rough surfaces on the detection of subsurface scatterers have been discussed in several recent papers; see [3] for additional references.

Consider ultrasonic immersion inspection of a solid plate of thickness d with a roughened top-surface and flat bottom-surface by a phase-coherent circular transducer. The probe is oriented normal to the rough surface of the plate. A broadband pressure-pulse is excited in water, propagates through the rough surface, and reflects from the bottom surface. This specular reflection is detected by the same probe and the signal is time gated.

We make the following approximations: 1) The ultrasonic longitudinal wave in the plate is modeled by a scalar field, shear wave propagation is neglected and, 2) the microstructure of the plate is ignored, i.e. the plate is assumed uniform. We further assume the water-solid interface is randomly rough and planar on the average at z=0. The surface's profile function $h(\mathbf{r})$ is governed by a spatially-uniform (translationally invariant), zero-mean Gaussian random-process, and the autocorrelation function, Γ. The autocorrelation function will be represented by either a Gaussian or an exponential function. The surface will be described by the rms height h and the correlation length L.

We model the inspection by a focused Gaussian-transducer of radius R at a lift-off distance $z = -z_o$ from the surface. The wavefield emitted by the transducer is described by

$$u(\omega, \mathbf{r}, z = -z_o) = \exp(-\frac{r^2}{a^2}), \tag{1}$$

and

$$a^2 = \left(R^{-2} + ik_w/2F\right)^{-1}, \tag{2}$$

where ω is the angular frequency and k_w denotes the wavenumber in water. F denotes the focal length of the probe. The transducer's signal, S, is assumed to be proportional to the reflected wave field u_R at the transducer's surface integrated over the transducer's aperture, i.e.

$$S(h,z,L,R,F,\omega) = \int d^2\mathbf{r} u_R(\omega,\mathbf{r},z=-z_o)\exp(-r^2/a^2). \tag{3}$$

The signal is estimated as follows, the wave: (1) propagates in water from the transducer to the solid; (2) transmits through the rough water-solid interface; (3) propagates through the plate; (4) reflects from the bottom surface; (5) propagates back to the top surface; (6) transmits through the rough solid-water interface; and (7) propagates in water from the solid to the transducer. The beam propagation is modeled by the Fresnel (paraxial) approximation [4], which neglects evanescent waves. The effects of the rough surface on transmission is modeled using the phase-screen approximation. [1, 2]

For well-collimated beams, such as those described by Eqs.(1) and (2), the wavefield can be accurately calculated using the Fresnel (paraxial) approximation, which allows us to make analytic progress,

$$u(\omega,\mathbf{r},z) \approx -\frac{ik}{2\pi(z-z_1)} e^{ikz} \int d^2\mathbf{s} u(\omega,\mathbf{s},z_1)\exp\left(\frac{ik}{2(z-z_1)}|\mathbf{s}-\mathbf{r}|^2\right). \tag{4}$$

This equation propagates the wavefield from the z_1-plane to the z-plane.

The determination of the signal will now be described in more detail. The phase-screen approximation is used to describe transmission through the rough water-solid interface. The wavefield immediately above the surface ($z = 0^-$) is calculated from Eqs. (1), (2) and (4) and is denoted by $u(\omega, \mathbf{r}, 0^-)$. The phase-screen approximation relates the wavefields on both sides of the rough surface via

$$u(\omega,\mathbf{r},z=0^+) = T_o^{w-s} u(\omega,\mathbf{r},z=0^-)\exp(i\phi(\mathbf{r})). \tag{5}$$

Here T_o^{w-s} denotes the transmission coefficient from water to solid for a normally-incident plane wave on a smooth surface. We assume that the roughness only changes the phase of the wave. Changes in the local amplitude of the transmitted wave are neglected. The phase $\phi(\mathbf{r})$ of the wave is assumed to be changed at each point of the surface by

$$\phi(\mathbf{r}) = (k_s - k_w)h(\mathbf{r}) \tag{6}$$

which is the phase change that would occur in the geometrical acoustics limit.

Equation (4) provides an estimate for the incident wavefield just inside the solid at $z = 0^+$. We take this field and propagate it through the interior of the solid using Eq.(4), the Fresnel propagation formula. The wave is reflected from the bottom of the plate and propagated back to the surface to obtain the reflected wavefield $u_R(\omega, \mathbf{r}, 0^+)$, immediately below the surface. The reflected wavefield is coupled back into the water via the phase-screen approximation

$$u_R(\omega,\mathbf{r},z=0^-) = T_o^{s-w} u_R(\omega,\mathbf{r},z=0^+)\exp(-i\phi(\mathbf{r})). \tag{7}$$

Here T_o^{s-w} denotes the transmission coefficient from solid to water for a normally-incident plane wave on a smooth surface. Finally, the wave is propagated back to the transducer and the output signal is calculated from Eq.(3).

In determining the output signal, we need to evaluate <exp(i $\phi(\mathbf{r})$) exp(i $\phi(\mathbf{r}')$)> . The angular brackets denote the ensemble average, which is assumed to be equivalent to the spatial average. We define $q = \phi(\mathbf{r}) + \phi(\mathbf{r}')$, and note from Eq.(6) that q and $\phi(\mathbf{r})$ are normally distributed random processes since $h(\mathbf{r})$ is. Consequently,

$$\left\langle \exp(i\phi(\mathbf{r})\exp(i\phi(\mathbf{r}')\right\rangle = \exp(-\frac{\left\langle q^2\right\rangle}{2}) = \exp(-\sigma^2)\exp(-\sigma^2\Gamma(\mathbf{r}-\mathbf{r}')), \tag{8}$$

where

$$\sigma^2 \equiv \left\langle \phi(\mathbf{r})^2\right\rangle = \left(k_s - k_w\right)^2 h^2, \tag{9}$$

and Γ is the surface correlation function.

The transmission function is just the ratio of the signal measured through the rough surface divided by the signal through the smooth surface,

$$Transmission \quad Function \equiv \frac{\left\langle S(h,d,L,....)\right\rangle}{S(h=0,d,L,..)}. \tag{10}$$

The roughness induced attenuation is defined by

$$Attenuation = -20\ Log_{10}(Transmission \quad Function). \tag{11}$$

The transmission function can be calculated analytically for Gaussian and exponential surface correlation functions. For a Gaussian autocorrelation function, $\exp(-r^2 / L^2)$, we found the closed-form expression

$$Transmission \quad Function = \beta^2 L^2 \exp(-\sigma^2) \frac{\gamma(\beta^2 L^2, \sigma^2)}{\sigma^{2\beta^2 L^2}}, \tag{12}$$

where $\gamma(.,.)$ is the incomplete gamma function as defined in Gradshteyn and Ryzhik [5], and

$$\beta^2 = \frac{1}{2(a^2 + i2z_0/k_w)} - \frac{ik_s}{4d}. \tag{13}$$

Here d denotes the thickness of the plate and k_s is the wavenumber in the solid. The effects of focusing occur only in the parameter β through the parameter a defined in Eq.(2). For the exponential autocorrelation function, $\exp(- r / L)$, we found an explicit series solution

$$Transmission \quad Function = \exp(-\sigma^2) \sum_{n=0}^{\infty} \frac{(-1)^n \sigma^{2n}}{n!} \left(1 - \frac{n}{2\beta L} \exp(\frac{n^2}{4\beta^2 L^2}) Erfc(\frac{n}{2\beta L}) \right) \tag{14}$$

where Erfc(.) denotes the complementary error function.

III. NORMALIZED SIGNAL CALCULATIONS

The transmission function which is calculated for an aluminum plate is shown in Fig. (1) as a function of the flaw's depth beneath the surface and for transducers of various focal lengths. The characteristic features are as follows. First, the transmission function depends on the distance of the flaw from the surface. For larger distances, the transmission function becomes independent of the depth and the transmission coefficients of Ref. (1) describe this part of the curve well. Second, the dead-zone for the exponential autocorrelation function is more extensive than for the Gaussian autocorrelation function. Third, focusing reduces the depth of the dead-zone. Fourth, the transmission function is largest at the focal depth.

The existence of a dead-zone for pulse-echo measurements can be understood on the basis of ray theory. Consider a ray that enters through the rough surface, scatters from the flaw and is reflected back to the transducer. If the flaw is close to the rough surface, the incident and reflected rays interact with the same region of the surface, the same "bump". Consequently, the change in phase of the incident and reflected rays are coherent ; the average total phase variation is then $\langle(\phi(\mathbf{r}_1)+\phi(\mathbf{r}_1))^2\rangle = 4\,\sigma^2$. The transmission function consequently is given asymptotically (z -> 0) by

$$Transmission \quad Function \approx e^{-2\sigma^2}. \tag{15}$$

On the other hand, if the flaw is far from surface, the incident and reflected rays will transmit through different bumps. In this case the phase changes of the incident and reflected ray are incoherent and the total phase variation is $\langle(\phi(\mathbf{r}_1)+\phi(\mathbf{r}_2))^2\rangle=2\sigma^2$ on the average since $\langle\phi(\mathbf{r}_1)\phi(\mathbf{r}_2)\rangle=0$. Consequently, we find that the normalized signal from flaws located at larger depth is dominated by incoherent double transmission and is given asymptotically (z -> ∞) by

$$Transmission \quad Function \approx e^{-\sigma^2}. \tag{16}$$

Eqs.(15) and (16) also follow immediately from the asymptotic analysis of Eqs.(12) and (14). The transition from one asymptotic regime to the other occurs at approximately the depth z_e for Gaussian autocorrelation functions (i.e. z_e describes the depth of the dead-zone)

$$z_e \approx \frac{k_s L^2 e^{-\sigma^2/5}}{4}. \tag{17}$$

The roughness-induced attenuation as a function of the flaw's distance from the surface and its dependence on h, L, R, F and frequency will be illustrated next. We expect that these results will be useful in the development of experiments and the interpretation of measurements. The dependence of the attenuation on the radius is shown in Fig. (2), the correlation length dependence in Fig. (3) which is followed by the rms height dependence in Fig. (4), and finally the frequency dependence in Fig. (5).

The roughness-induced attenuation depends weakly on the radius of the transducer for both Gaussian and exponential correlation functions. The roughness-induced attenuation is a minimum at the focal depth, which is desirable for ultrasonic inspection. The dead zone is reduced for either shorter focal lengths or shorter correlation lengths.
Figures (4) and (5) show the strong dependence of the roughness-induced attenuation on the rms height and frequency. Special care must be exercised in choosing the frequency.
For surfaces with large roughness, the attenuation can be reduced by using relatively low frequencies However, low frequencies lead to a loss of resolution.

Figure (6) shows the normalized SNR which is obtained by dividing the normalized signal by the square root of the normalized material noise as calculated from Eq.(7) in [3]

(noise generated by direct reflections from the rough surface is neglected). The best signal-to-noise ratio occurs at the focal depth for this example. The normalized SNR is approximately twice as large for the focused probe (compared to the unfocused probe). Further, the SNR for the focused probe at the focal depth is almost as good as the SNR that would have been measured through the smooth surface. The effects of roughness are relatively small for focused probes.

IV. SUMMARY

We have examined the double-transmission of sound through a rough-surface using the phase-screen approximation. Analysis of the solutions indicates that there is a near-surface dead-zone that may extend up to several centimeters into the sample. Finally and more generally , we find that the use of focused probes substantially reduces the effects of the dead-zone and the resulting roughness-induced degradation of the signal-to-noise ratio. The signal-to-noise ratio will be best for probes with tighter focuses and large radii.

V. ACKNOWLEDGEMENT

This work was supported by the FAA-Center for Aviation Systems Reliability, operated by the Ames Laboratory, USDOE, for the Federal Aviation Administration under Contract No. W-7405-ENG with Iowa State University.

VI REFERENCES

1. P. B. Nagy and J. H. Rose, "Surface roughness and the ultrasonic detection of subsurface scatterers," J. Appl. Phys. 73, 566-580 (1993).
2. J. H Rose, M. Bilgen and P. B. Nagy, "Acoustic Double Reflection and Transmission at a Rough Water-Solid Interface", submitted to J. Acoust. Soc. Am.
3. M. Bilgen and J. H. Rose, "Focused ultrasonic probes and the effects of surface roughness on material noise," in Review of Progress in Quantitative Nondestructive Evaluation, edited by D. O. Thompson and D. E. Chimenti (Plenum, New York, 1994).
4. J. W. Goodman, Introduction to Fourier Optics (McGraw-Hill, New York, 1969).
5. I. S. Gradshteyn and I. M. Ryzhik, Tables of Integrals, Series, and Products (Academic, New York, 1980)

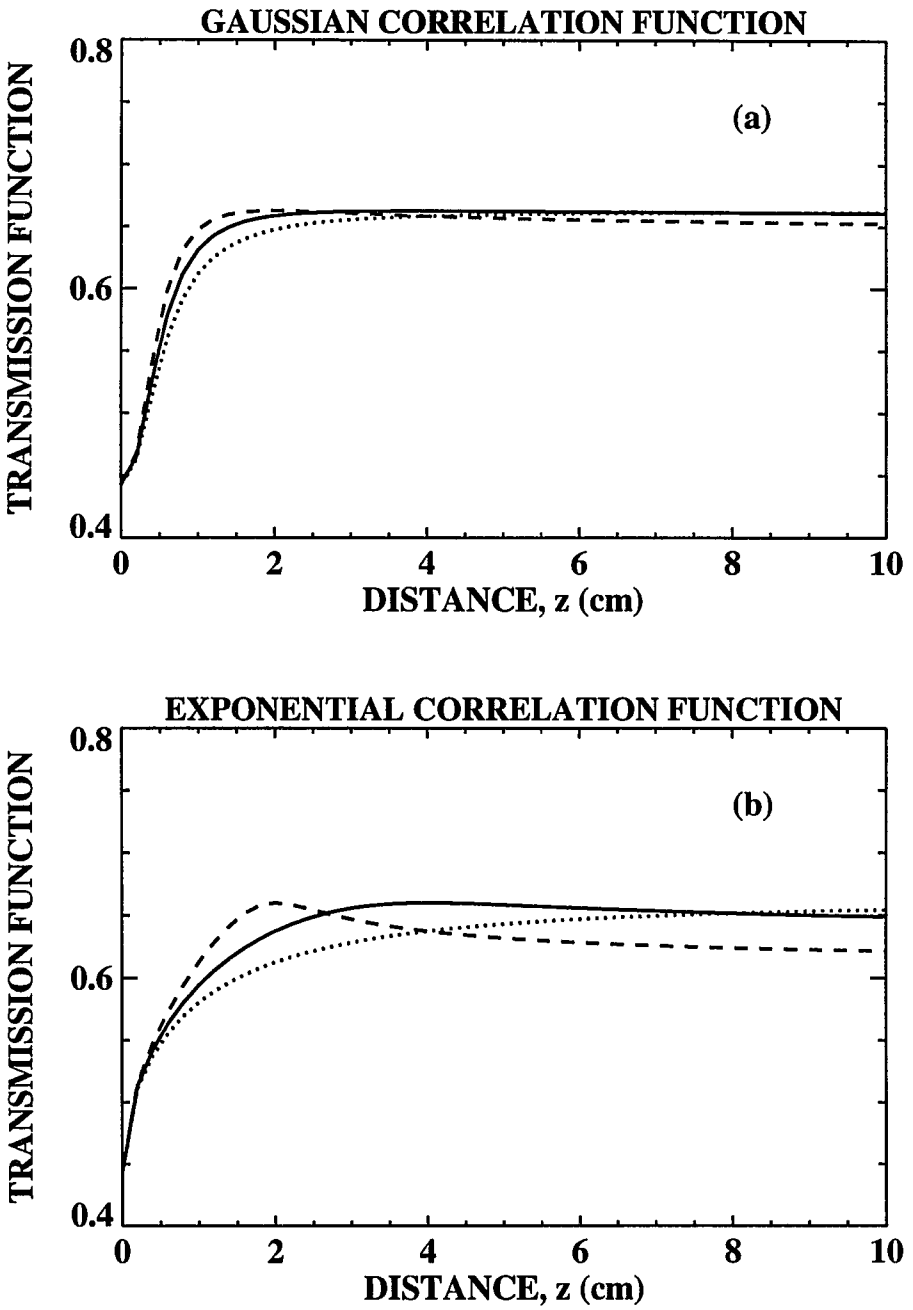

Figure 1. Transmission Function for three different focal lengths: dashed line F=2 cm solid line F=4 cm and dotted line F=∞. The other parameters were L = 1.5 mm, f = 10 MHz, h = 20 μm, and R = 1 cm.

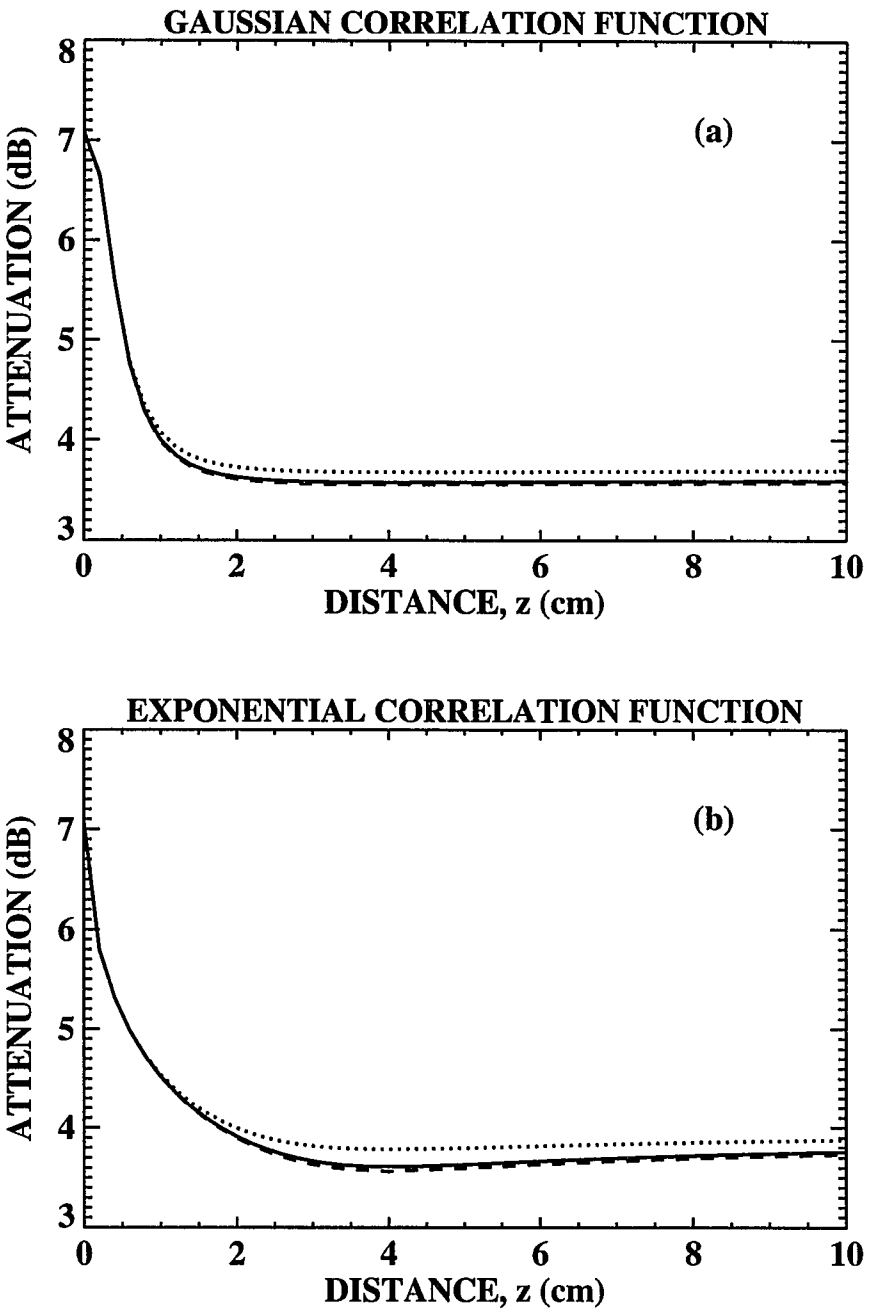

Figure 2. Attenuation for three different radii. The dotted line R=0.5 cm, solid line R=1 cm and dashed line R=1.5 cm. The other parameters were L = 1.5 mm, f = 10 MHz, h = 20 μm, and F=4 cm.

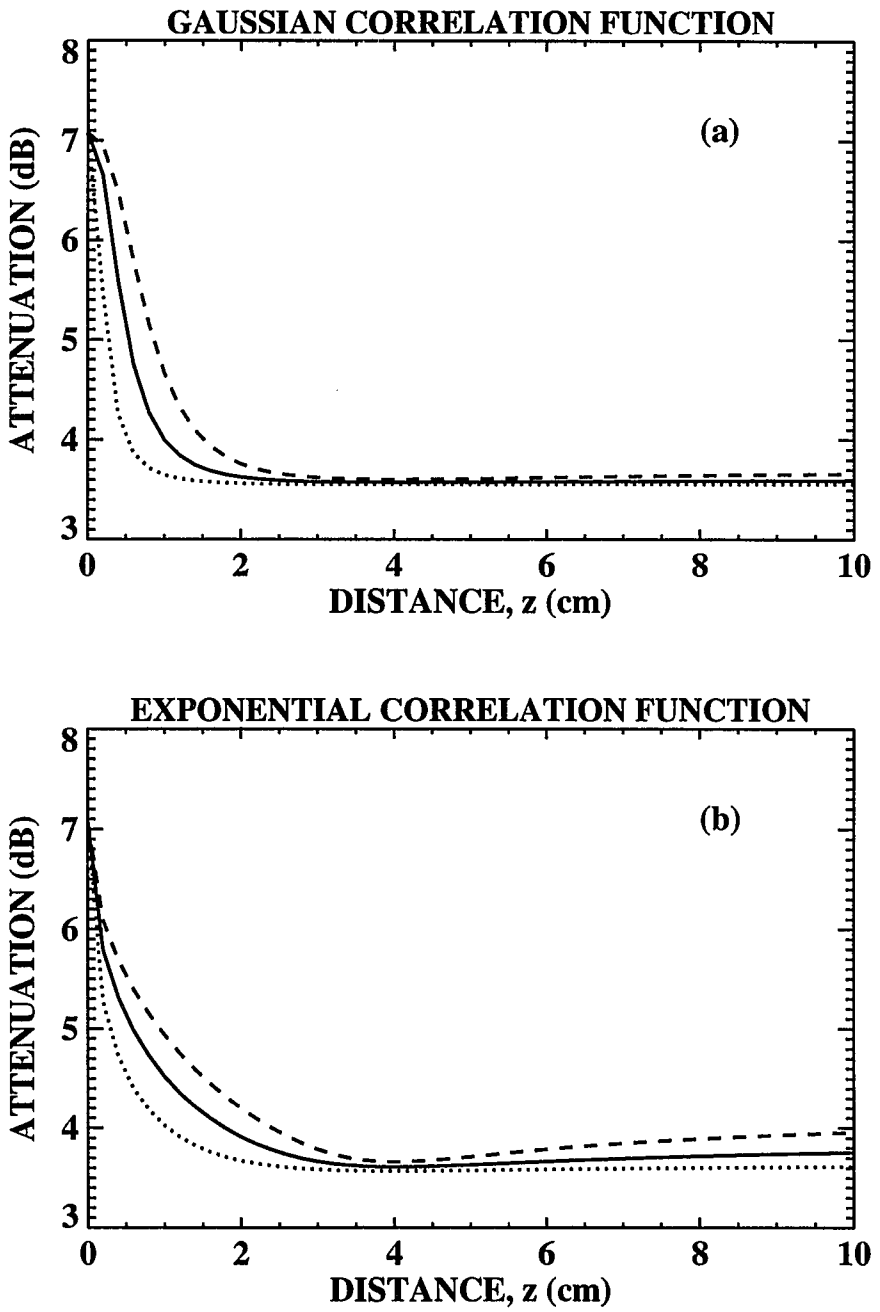

Figure 3. Attenuation for three different correlation lengths. The dotted line L=1.0 mm solid line L=1.5 mm and dashed line L=2 mm. The other parameters were f=10 MHz, R=1 cm, h = 20 μm, and F=4 cm.

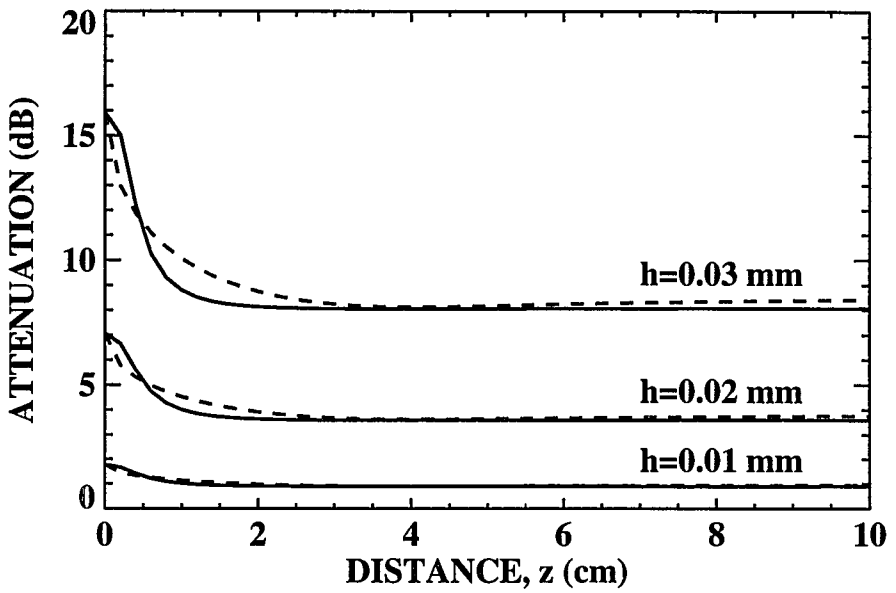

Figure 4. Attenuation for three different r.m.s heights: solid line Gaussian and dashed line exponential correlation function. The parameters were f=10 MHz, R=1 cm, L=1.5 mm and F=4 cm.

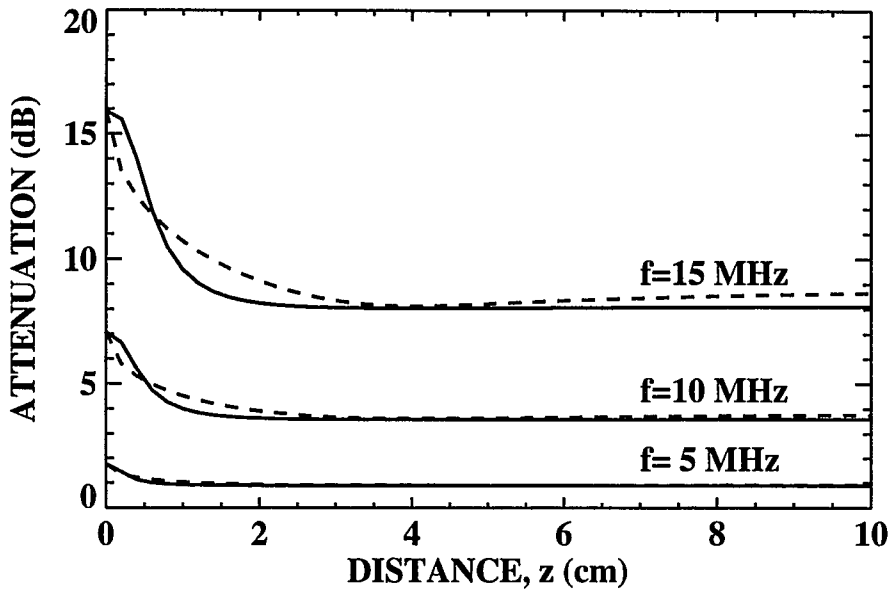

Figure 5. Attenuation for three different frequencies. The solid line Gaussian and dashed line exponential correlation function. The parameters were L = 1.5 mm, R=1 cm, h = 20 μm, and F=4 cm.

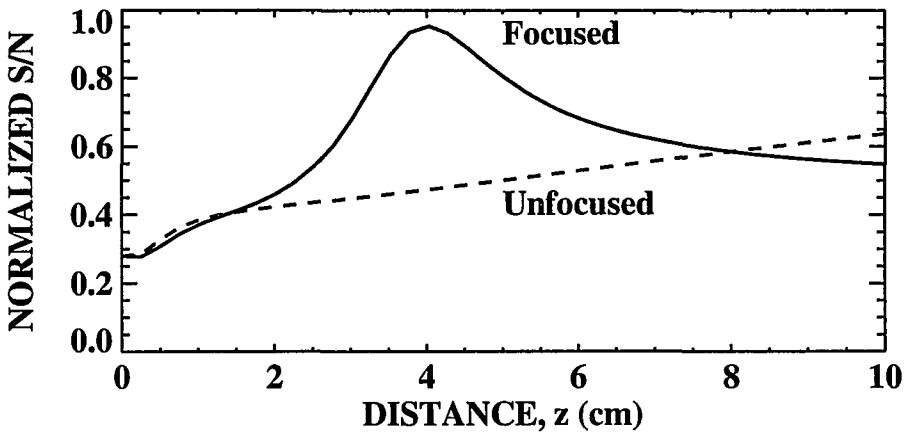

Figure 6. Normalized signal-to-noise ratio; solid line focused probe with focal length 4 cm and dashed line unfocused probe. The parameters were f = 10 MHz, L = 1.5 mm, h = 25 μm, and R = 1 cm.

PAPER V.

ACOUSTIC DOUBLE-REFLECTION AND TRANSMISSION AT A ROUGH WATER-SOLID INTERFACE

ABSTRACT

The double interaction of a wave with a rough interface is important in many acoustic measurements. We consider an acoustic beam that reflects twice from a rough water-solid interface. The second reflection from the rough surface is accomplished after the transducer's buffer rod is used as an acoustic mirror. Changes in the spatially-averaged specular reflection are related to the phenomenon of "enhanced backscatter", previously observed for diffuse scattering. Simple, approximate, closed-form analytic formulas for the strength of the specular double-reflections are given as a function of frequency and the stand-off distance of the transducer. As one application of our analytic results, we propose a method for determining the surface correlation function from the specular double-reflections. The same physics (and appropriately modified analytic formulas) apply to doubly-transmitted waves. We have made experimental measurements of acoustic double-reflection with a normally-oriented broadband piezoelectric transducer near a rough water-solid interface. We measured (1) the wave reflected once from the rough interface, and (2) the wave reflected twice from the rough interface. The strength of the specular reflections was measured as a function of frequency and the transducer's distance from the surface. It was observed that for large distances between the transducer and the rough surface and at low frequencies the scattering-induced loss of the doubly reflected wave was twice the loss of a singly reflected wave. However, for small distances between the transducer and the surface and at high frequencies the scattering-induced loss of the doubly reflected wave was four times the loss of a singly reflected wave.

I. INTRODUCTION

The double interaction of waves with rough surfaces leads to a great deal of interesting physics. Figure (1) shows a schematic of a double-reflection acoustic measurement. The incident wave initially reflects from the rough surface, then reflects off the transducer's face, and finally reflects again from the rough surface. At low frequencies, the beam diffracts a lateral distance that is greater than the surface correlation length. The portion of the beam that reflects from some particular bump on the first pass will reflect from a different bump on the second pass. Consequently, roughness-induced changes in the phase add independently (incoherently). At high frequencies the situation is qualitatively different for surfaces with low relief. In this case ray theory is appropriate and a ray reflects from the same bump on both the first and the second pass. Consequently, roughness-induced changes in the phase add dependently (coherently) at high frequencies.

The incoherence or coherence of the roughness-induced phase change has striking consequences for the strength of doubly-reflected waves. Let the scattering induced attenuation of a plane wave that reflects from the surface once be denoted by l_o. At low frequencies , the scattering-induced attenuation of a doubly reflected wave is twice l_o , as one might naively expect. However, at high frequencies when the phase changes are coherent, it will be shown theoretically and experimentally that the scattering-induced attenuation of the doubly-reflected wave can be much greater, as much as four times l_o. Simple analytic formulas will be derived that describe the frequency and depth dependence of this increased attenuation.

As is well known, the rms height of the surface can be straightforwardly determined from the frequency-dependent attenuation of the first specular reflection[1-3]. However, current acoustic methods for estimating the surface correlation length rely on measurements of the diffuse scattering, which is relatively difficult[4,5] . In this paper, we propose, based on

our theoretical analysis, a new method for estimating the surface autocorrelation function (and the correlation length) from the frequency-dependent attenuation of the first and second specular reflections.

The double transmission of ultrasound through a rough surface also has important consequences. The reflection of ultrasound from scatterers beneath a rough water-solid interface is one of the canonical problems of ultrasonic nondestructive evaluation (NDE), since rough surfaces degrade the detection of subsurface scatterers such as voids, cracks and inclusions[1,6]. The roughness induced phase changes upon first and second passage are coherent at high frequencies and incoherent at low frequencies (again due to diffraction).

We use the phase-screen approximation [7] to study double-reflection from and double-transmission through rough surfaces. This approximation is expected to be valid if the rms height, h, of the surface is much less than the correlation length, L, which describes the lateral variation of the surface profile. Analytic formulas for the change in the average signal result. It is reasonable to ask, "Is the phase-screen approximation suitable for relatively subtle questions concerning correlated versus uncorrelated phases ?" and "Can the analytic results be used to estimate the correlation length ?" According to the phase-screen approximation, the loss of the specular signal is proportional to the square of the variance of the total phase-perturbation, $Loss \approx 1/2\langle\phi^2\rangle$. In the case of double-interaction with a rough surface, the resulting phase variance can be very different depending on whether the first and second perturbations are coherent, in which case $\phi_{double} \approx 2\phi_{single}$, or incoherent, in which case $\phi_{double} \approx \sqrt{2}\phi_{single}$. Therefore, it can be expected that the ratio between the losses of the double- and single-reflected (or transmitted) specular signal increases from two to four as the coherency between the two phase-perturbations increases from zero to 100%. In this paper, we are going to use the phase-screen approximation to predict the main features of this transition from incoherent to coherent double-reflection as the frequency is increased or the propagation distance between the two interactions is decreased.

Experimental measurements were undertaken with an eye towards testing the phase-screen approximation as well as the essential physics exposed by the theoretical analysis. We placed a normally-oriented broadband piezoelectric transducer near a rough water-solid interface and measured (1) the wave reflected once from the rough interface, and (2) the wave reflected twice from the rough interface (using an acoustic mirror). The strength of the specular reflections was measured as a function of frequency and the transducer's distance from the surface. It was observed that for large distances between the transducer and the rough surface and at low frequencies the scattering-induced loss of the doubly reflected wave was twice the loss of a singly reflected wave. However, for small distances between the transducer and the surface and at high frequencies the scattering-induced loss of the doubly reflected wave was four times the loss of a singly reflected wave in accord with our model predictions.

Many studies concerning the reflection of ultrasound from rough water-solid interfaces have appeared in the literature and are reviewed in Ogilvy's[2] recent book. Much less has appeared concerning the transmission of ultrasonic waves through rough surfaces. Within the context of ultrasonic nondestructive evaluation, Nagy and Adler[6] studied the effects of rough interfaces on the measurement of the ultrasonic attenuation. They presented experimental measurements, which they analyzed using the phase-screen approximation to describe transmission at the water-solid interface. An experimental and theoretical study that extended the phase-screen approximation for transmission to non-normal directions of incidence is contained in Ref. (1). References (8-10) contain experimental and theoretical studies of the effects of rough surfaces on the incoherent backscatter of ultrasound from distributed volumetric scatterers (i.e. the effects of surface roughness on material noise).

The physics of waves reflected in randomly inhomogeneous media has been reviewed by Kravtsov and Saichev[11]. This review was primarily concerned with the effects of randomly inhomogeneous media on the diffuse scattering of electromagnetic waves. They

showed that the average intensity of the backscattered diffuse wave is enhanced by double passage through the random media. Enhanced backscatter from heterogeneous materials and rough surfaces has been discussed by many authors. Most relevantly, Jakeman[12] has considered double-transmission through a rough surface and calculated the change in the backscattered diffuse waves (in contrast we consider specular reflections). He modeled a planar mirror placed behind a smoothly varying deep phase-screen and analyzed the far field intensity distribution of the diffusely scattered wave. Jakeman observed that the backscattered intensity was enhanced with the gain largest when the mirror was positioned near the "so-called" focusing plane of the phase-screen.

The structure of this paper is as follows. Section II is devoted to theoretical preliminaries, which include the statement of the problem, its geometry and an introduction of the various approximations used in the derivation. Simple analytic expressions for the roughness-induced changes in double-reflection and double-transmission are given in Sec. III. The characterization of the surface autocorrelation function is the subject of the fourth section. Experimental measurements of acoustic double-reflection are presented in Sec. V. Section VI compares theory and experiment, and concludes with a brief summary.

II. THEORETICAL PRELIMINARIES

The geometry for double-reflection is as shown in Fig. (1). A circular Gaussian transducer of radius a is oriented normal to the water-solid interface at a lift-off distance, z_o, from the surface. A broadband pressure-pulse is excited in the water, reflects from the rough surface, then from the transducer's front where it is detected for the first time, then from the rough surface again and is finally detected a second time. The roughness profile is known statistically. In this paper, we will model the ensemble average of the specularly reflected wave.

The geometry for double transmission is shown in Fig. (2). A solid plate of thickness d is immersed in a water bath. The top surface of the plate is rough, while the back surface is smooth. A broadband pressure-pulse is excited in the water, propagates through the rough water-solid interface, reflects off the back surface and then retransmits through the water-solid interface and is detected by the same transducer.

The randomly rough top-surface is planar on the average at z=0. The surface's height variation, $h(\boldsymbol{r})$, is governed by a spatially-uniform, zero-mean Gaussian random process, and the autocorrelation function, $\Gamma(\mathbf{r})$. The coordinate parallel to the surface is denoted by $\boldsymbol{r}$, while the general three dimensional coordinate is $\boldsymbol{x} = (\boldsymbol{r}, z)$. The assumption of spatial uniformity (translational invariance) implies that the normalized autocorrelation function can be written in the form

$$\Gamma(\mathbf{r}-\mathbf{r}') \equiv \frac{\langle h(\mathbf{r})h(\mathbf{r}')\rangle}{h^2}, \tag{1}$$

here $h = \sqrt{\langle h(\mathbf{r})^2 \rangle}$. The bracket denotes an average over a hypothetical ensemble of samples with different realizations of the surface roughness. We assume that the ensemble average is

identical with a spatial average over the rough surface. When an explicit representation is needed, the normalized autocorrelation function will be represented by either a Gaussian or an exponential function.

Wave propagation in both the solid and the fluid will be modeled, for simplicity, using the following scalar wave equation

$$\nabla^2 u(\omega,\mathbf{r},z)+\frac{\omega^2}{c^2}u(\omega,\mathbf{r},z)=0 \tag{2}$$

where u denotes the wavefield, and ω the angular frequency. The velocity of sound is denoted by c, and in water $c = c_w$, while $c = c_s$ in the solid. The boundary conditions are the continuity of the wavefield and its normal derivative at the water-solid interface. The wavefield, u, can be written as

$$u(\omega,\mathbf{r},z)=\langle u(\omega,\mathbf{r},z)\rangle+\delta u(\omega,\mathbf{r},z). \tag{3}$$

In the literature $<u>$ and δu are sometimes called the coherent and incoherent fields. We will avoid this language, and use coherent and incoherent to describe changes in the phase due to roughness. We will call $<u>$ the specular wave and δu the diffuse wave.

We now discuss wave propagation in the double-reflection geometry. The wavefield is expanded in plane waves and each plane wave propagated independently. We make the Fresnel[13] (paraxial) approximation, and assume that the wave propagation is concentrated in the near-forward direction. The reflection from the rough surface is treated in the phase-screen approximation, which includes the effects of surface roughness as follows

$$u_R(\omega,\mathbf{r},z=0)\approx R_o e^{i\phi(\mathbf{r})}u_I(\omega,\mathbf{r},z=0). \tag{4}$$

Here, u_I and u_R denote the incident and reflected waves. R_O denotes the reflection coefficient for a normally incident plane wave on a smooth interface. Finally, $\phi(\mathbf{r})$ approximates the phase change in the wave front at $\boldsymbol{r}$ in terms of the local roughness by

$$\phi(\mathbf{r}) = 2k_w h(\mathbf{r}). \tag{5}$$

Here, k_w denotes the wavenumber in water.

Given the wavefield on a plane, u can be calculated by the expansion-in-plane-waves method for a region of homogeneous velocity as long as reflections can either be treated exactly or ignored. For well-collimated beams such as those discussed in this paper, the wavefield can be accurately calculated using the Fresnel (paraxial) approximation, which allows us to make further analytic progress,

$$u_R(\omega,\mathbf{r},z) \approx -\frac{ik}{2\pi z} e^{ikz} \int d^2\mathbf{s} u_R(\omega,\mathbf{s},z=0) \exp\left(\frac{ik}{2z}|\mathbf{s}-\mathbf{r}|^2\right). \tag{6}$$

The reflected wavefield can be computed from Eqs. (4) - (6). For the purposes of this paper, we assume a normally-oriented, unfocused Gaussian-transducer of radius a at $z = -z_O$. The field emitted by the transducer is described by

$$u(\omega,\mathbf{r},z=-z_o) = \exp\left(-\frac{r^2}{a^2}\right). \tag{7}$$

The transducer's output signal, S, is assumed to be proportional to the reflected wave field at the transducer's surface integrated over the transducer's aperture , i.e.

$$S(\omega) = \int d^2\mathbf{r} u_R(\omega,\mathbf{r},z=-z_o) \exp(-r^2/a^2). \tag{8}$$

Finally, in determining the average of the specular reflection, we will evaluate <exp(i $\phi(\mathbf{r})$) exp(i $\phi(\mathbf{r}')$)> . We define $q = \phi(\mathbf{r}) + \phi(\mathbf{r}')$, and note from Eq.(5) that q and $\phi(\mathbf{r})$ are normally distributed random processes since $h(\mathbf{r})$ is. Consequently,

$$\left\langle \exp(i\varphi(\mathbf{r}) \exp(i\varphi(\mathbf{r}')\right\rangle = \exp(-\frac{\left\langle q^2 \right\rangle}{2}) = \exp(-\sigma^2) \exp(-\sigma^2 \Gamma(\mathbf{r} - \mathbf{r}')), \tag{9}$$

where

$$\sigma^2 \equiv \left\langle \varphi(\mathbf{r})^2 \right\rangle, \tag{10}$$

and Γ is the correlation function defined by Eq.(1).

III. ANALYTIC RESULTS

We first modeled the double-reflection experiment, Fig.(1). We calculated the roughness-induced attenuation of the average signal, $<S_R>$, that was specularly reflected twice from the rough water-solid interface. The roughness-induced attenuation involves the ratio of $<S_R>$ to S_o, the signal calculated in the absence of surface roughness and is defined by

$$Loss = -20Log_{10}(< S_R > / S_o). \tag{11}$$

The signals S_R and S_o were computed as follows. First, we used the Fresnel approximation to propagate the beam from the transducer to the surface. Second, we used the phase-screen approximation to account for surface roughness in the reflected portion of the beam. Third, we used the Fresnel approximation to propagate the beam to the front of the transducer, where it reflected with reflection coefficient, R_1, for a normally incident plane wave. Fourth, we used the Fresnel approximation to propagate the reflected beam back to the water-solid interface. Fifth, we used the phase-screen approximation to account for the second reflection from the rough water-solid interface. Sixth, the Fresnel approximation was used to propagate the beam back to the transducer. The signal, S_R, was determined from Eq.(8). Finally, the reference signal S_o was obtained by setting the rms roughness to zero.

We find the average specular signal, normalized by the smooth surface result, is given by

$$\frac{\langle S_R \rangle}{S_o} = \exp(-\sigma^2)\beta^2 \int_0^\infty 2pdp \exp(-\beta^2 p^2)\exp(-\sigma^2\Gamma(p)). \tag{12}$$

Here,

$$\beta^2 = \frac{k_w^2}{8z_o^2(\frac{1}{a^2} - \frac{ik_w}{2z_o})} - \frac{ik_w}{2z_o}, \tag{13}$$

and

$$\sigma^2 = 4k_w^2 h^2. \tag{14}$$

Note that due to the normalization, Eq.(11) is independent of the smooth-surface reflection coefficients of the specimen and the mirror.

Analytic results will be presented for Gaussian and exponential autocorrelation functions. For a Gaussian normalized autocorrelation function, $exp(-r^2/L^2)$, we found the analytic, closed-form expression

$$\frac{\langle S_B \rangle}{S_o} = \beta^2 L^2 \exp(-\sigma^2) \frac{\gamma(\beta^2 L^2, \sigma^2)}{\sigma^{2\beta^2 L^2}}, \tag{15}$$

where $\gamma(.,.)$ is the incomplete gamma function as defined in Gradshteyn and Ryzhik[14]. For exponential normalized autocorrelation functions, $exp(-r/L)$, we found

$$\frac{\langle S_B \rangle}{S_o} = \exp(-\sigma^2) \sum_{n=0}^{\infty} \frac{(-1)^n \sigma^{2n}}{n!} (1 - ny \exp(n^2 y^2) Erfc(ny)). \tag{16}$$

Here, *Erfc(.)* denotes the complementary error function, and

$$y = \frac{1}{2L\beta}. \tag{17}$$

The roughness-induced attenuation in the double-transmission experiment can be calculated in an entirely similar way. The model geometry is shown in Fig. (2). The signal was calculated using the Fresnel approximation to propagate the beam and the phase-screen approximation to account for phase changes that are introduced by the roughness. The results are given by Eqs.(11, 12) and (15-17) save that for double-transmission

$$\sigma^2 \equiv \langle \varphi^2 \rangle = (k_w - k_s)^2 h^2, \tag{18}$$

and

$$\beta^2 = \frac{1}{2(a^2 + \frac{2iz_o}{k_w})} - \frac{ik_s}{4d}, \tag{19}$$

where d denotes the thickness of the plate.

IV. INVERSION FOR THE AUTOCORRELATION FUNCTION

In this section, we derive an approximate formal expression for inverting measured data to obtain the autocorrelation function. Different forms of the autocorrelation function lead to distinctly different dependence of the attenuation, *Loss*, on the transducer offset, z_o, and on the frequency. Figure (3) shows the attenuation of the double-reflection measurement as a function of z_o for both a Gaussian and an exponential autocorrelation function. The distinct differences indicate that measurements of specular doubly-reflection can distinguish these forms of the autocorrelation function. We will show that Eq.(12) leads to an analytic but approximate inverse method for determining the autocorrelation function from measurements of the attenuation.

The attenuation is given by Eqs. (11-14). We limit our discussion to the extreme near-field of the transducer, i.e. we assume that

$$z_o << \frac{k_w a^2}{2}, \tag{20}$$

a condition that is readily achievable. For example at 10 MHz, $k_w = 419 / \text{cm}$. For a 1/2 inch diameter transducer and an offset z_o= 1 cm, the left-hand-side of (20) is 84 cm and the inequality is well satisfied. In the near-field limit, Eq.(12), can be rewritten

$$\frac{(\frac{\langle S_R \rangle}{S_o}\exp(\sigma^2)-1)}{(\frac{1}{2a^2}-\frac{ik_w}{4z_o})} = \int_0^\infty 2pdp\exp(-\frac{p^2}{2a^2})[\exp(-\sigma^2\Gamma(p))-1]\exp(\frac{ip^2k_w}{4z_o}). \tag{21}$$

We fix a and k_w . We then consider the right-hand-side to be a function of $v = k_w / (4\, z_o)$. Upon the further change of variables, $u = p^2$, we obtain

$$M(v) = \int_0^\infty du F(u) \exp(ivu). \tag{22}$$

Explicitly, $M(v)$ is a function determined by measuring the loss at all stand-off distances z_o and is defined by the left-hand-side of (21). The function $F(u)$ is defined by

$$F(u) = \exp(-\frac{u}{2a^2})(\exp(-\sigma^2 \Gamma(\sqrt{u})) - 1). \tag{23}$$

The function $F(u)$ is real and radially symmetric, since Γ was assumed to be radially symmetric. Hence, Eq.(22) can be inverted via an inverse Fourier transform to determine $F(u)$ from the data,

$$F(u) = \frac{1}{2\pi} \int_{-\infty}^{\infty} M(v) \cos(uv) dv \ . \tag{24}$$

Finally, Γ is inferred from $F(u)$.

The inverse method suggested in this section has not been tested numerically, and consequently its stability has not been assessed. It does, of course, exactly invert the analytic expressions for the attenuation that were derived for the Gaussian and exponential autocorrelation functions (when they are evaluated in the near-field limit). In the next sections, we will see that fitting theory to experiment enabled us to estimate the autocorrelation length of the one particular sample for which measurements have been made.

V. EXPERIMENTAL PROCEDURE

Our analysis seems to show that the total scattering-induced loss of an ultrasonic signal interacting with the same rough surface twice is substantially affected by the degree of phase-coherence between the two interactions. If the propagation distance between the first and second interactions is much greater than the coherence length of the diffuse field, the second interaction is incoherent with respect to the first one and the total scattering loss caused by the double interaction is simply twice the loss caused by a single interaction. On the other hand, if the propagation distance between the first and second interactions is much shorter than the coherence length of the diffuse field, the second interaction is coherent with respect to the first one, and the total scattering loss caused by the double interaction is four times as much as the loss caused by a single interaction. Double-interaction with the same rough surface is very typical in pulse-echo inspections for flaws below a rough water-solid interface. Previous experimental results have shown that for typical immersion geometries, when the flaw is at a sufficiently large distance from the surface, the second (backward) interaction is essentially incoherent with respect to the first (forward) one, and the total scattering loss of the doubly-transmitted specular wave can be approximated as twice the single-transmission loss[1,6]. The primary purpose of our experimental effort was to determine, in the case of coherent double-interaction with the rough surface, if the total loss is doubled; i.e. if the loss becomes four times higher than the single-transmission loss. This excess loss was easier to demonstrate for double-reflection than for double-transmission, due primarily to practical considerations of our laboratory set-up. However, our analysis suggests that many of the conclusions that can be drawn from the measured loss of the doubly-reflected signal, can be readily applied to the case of double-transmission as well.

Sample Preparation and Characterization by Acoustic Surface Profilometry

A specimen was specially designed and carefully prepared for this experiment. A 2"-thick, 4" x 4" aluminum block was first milled and then ground on both sides to provide smooth, flat and parallel surfaces. Then the previously ground surface was roughened on one side over a centered 2" x 2" square area by peening with a 1/2"-radius steel head in a hydraulic press. The remaining 1" - wide smooth frame around the roughened area was used during the profilometry measurement to align the specimen parallel to the scanning bridge. The schematic diagram of the profilometric inspection is shown in Fig. (4). The highly focused beam of an acoustic microscope was used to map the surface topography in a way that is similar to a conventional stylus profilometry but without touching the surface. In order to keep the focal spot as small as possible, we used a Panametrics V3330 50 MHz immersion transducer with a 0.25" diameter and a 0.20" focal length. The beam diameter at the focal plane is approximately 60 μm, while the focal depth is roughly 200 μm. Such a sharply focused beam can be readily used to map the surface profile of a rough surface if the rms roughness is much less than the focal depth, and the correlation length is much greater than the beam diameter. Under these conditions, the amplitude of the surface reflection is more or less independent of the local slope of the surface, while the reflection's time-of-arrival directly yields the local surface height. As a first step, the sample is carefully aligned parallel to the scanning direction by using the previously mentioned smooth frame around the roughened area. A synchronized saw-tooth generator is used as a simple time-voltage converter and changes the time-of-flight information into a voltage proportional to the depth. The ultrasonic profilometer was easily calibrated by measuring the sensitivity of the time-voltage converter. The output of the time-voltage converter was digitized with 12 bit resolution over a 1" x 1" area to produce a 200 x 200 pixel image of the surface height

distribution. Figure (5) shows a gray-scale representation of the measured two-dimensional surface height distribution.

The rms roughness (h) and the auto-correlation length (L) of the surface were obtained from the digitized surface height distribution by a two-dimensional fast Fourier transform. First, the 128 x 128 pixel center part of the distribution was Fourier transformed. Second, the resulting spectrum was high pass filtered to eliminate any slowly varying height component that might have been caused by imperfect alignment or shape of the sample. This preprocessing is common practice in surface profilometry and serves to separate the high-frequency "roughness" from the often comparable or even stronger low frequency "shape" effects. In our case, the high-pass filtering was realized by convolving the measured spectrum with the calculated spectrum of a 1/2" diameter circular aperture; the size of the aperture was chosen to correspond to the unfocused ultrasonic transducer used in the scattering experiment. Third, the square magnitude of the filtered spectrum was inverse Fourier transformed to obtain the two-dimensional autocorrelation function. For isotropic surfaces, the autocorrelation function is determined by the distance between two points but is independent of their relative orientation. Thanks to this symmetry, the two-dimensional autocorrelation can be substituted by a simple one-dimensional correlation distribution that is calculated as the average of the cross-sections of the two-dimensional distribution in different orientations. Finally, the initial part of this one-dimensional correlation function was fit by a Gaussian and the correlation length was obtained as the best least-squares fit. Figure (6) shows the measured auto-correlation function and the best fitting Gaussian distribution, for which $L = 724$ μm. High pass filtering usually has negligible effect on the measured correlation length since the transducer radius is at least one order of magnitude larger ($a >> L$). Of course, the rms roughness can be calculated from the square-root of the measured correlation function at zero separation. Our best estimate for h, after high-pass filtering, is h

=5.22 μm . The sample was, however, quite flat, as is evidenced by the fact that the inferred h was equal to 5.24 μm in the absence of high-pass filtering.

In the case of practical ultrasonic inspections the surfaces may be far from flat and the surface height may change significantly for distances larger than the transducer diameter. In these cases, the total rms roughness is the incoherent sum of the "roughness" and "shape" contributions. Good agreement between profilometric and ultrasonic scattering measurements can only be expected if both methods use the same high-pass filtering.

Scattering Induced Loss of the Singly- and Doubly-Reflected Waves

Figure 1 is a schematic diagram of the experimental technique used to measure the roughness induced scattering loss of singly- and doubly-reflected ultrasonic pulses for a normally oriented immersion transducer. In this part of the experiment, we used a Panametrics V358 1/2" collimated-beam transducer. The nominal center frequency of this transducer is 50 MHz. However, with proper damping the operating frequency range extends from 5 MHz to 50 MHz. Besides this unusually wide bandwidth, the transducer is mounted on a 1/2" -long glass buffer rod, which plays an essential role in this measurement. Schematically the experiment proceeds as follows. The wave (1) is launched by the piezoelectric element, (2) propagates through the glass buffer rod and transmits into the water; (3) reflects from the rough surface and transmits through the water back to the buffer rod (4) reflects back into the water from the buffer rod, (5) reflects from the rough surface a second time and transmits through the water back to the buffer rod, (6) transmits through the buffer rod and (7) is detected by the piezoelectric element. The face of the buffer rod acts like a good ultrasonic mirror since it is a smooth, polished water-glass interface. Of course, the reflection coefficient of the water/glass boundary is only about 80%. but, because of the

way we measure the scattering induced loss of the specular wave, the small frequency-independent loss is divided out and has negligible effect on our results. In order to measure the specular (average) part of the signal, we would, in principle, need to prepare a large number of samples and estimate the ensemble average. Instead, we calculated the spatial average of the specular wave by obtaining many reflections from all parts of the roughened area. In order to eliminate the adverse effects of possible sample misalignment, lack of sample flatness, and large scale curvature, we used a cross-correlation technique at each point to compensate for the over-all time-shift of the received echo[6]. This compensation acts like the high-pass filtering implemented for the profilometric measurement mentioned in the last subsection.

Experimental Results

Measurements of the scattering-induced loss of singly- and doubly-reflected waves were made for frequencies between 5 and 50 MHz (subject to a dynamic range of approximately 40 dB). The measurements were made for six standoff distances (from the water-glass interface to water-aluminum interface) of 2.5, 5.25, 8 , 11, 16 and 22 mm. Figures 7a-f show the plots, each for a different standoff, of the loss as a function of frequency. The solid lines show the best-fitting f^2 curves matched to the frequency-dependent loss of the first reflection. We estimated the rms roughness of the surface from these fits corresponding to different standoffs as 5.16 μm ± 3%, which is in excellent agreement with the 5.22 μm obtained from the profilometric measurement. The two dotted lines simply show twice and four times the above mentioned best-fitting f^2 loss spectrum and are expected to indicate the incoherent and coherent limits of the double-reflection loss. The open boxes indicate the measured single-reflection losses, while the open circles show the measured double-reflection losses.

Our analysis indicates that the double-reflection loss should be four times the single-reflection loss either for small standoff distances or for high frequencies. Figure 7a is for our smallest standoff distance (2.5 mm). As can be seen, the measured double-reflection losses are nearly four times the single-reflection losses over the whole frequency range. On the other hand, Fig. 7f shows the results for our largest standoff distance (22 mm). In this case the measured double-reflection losses are essentially two times the single-reflection losses over the whole frequency range. For intermediate standoff distances, the double-reflection losses are twice the single-reflection losses for low frequencies but switch to four times the single-reflection losses at high frequencies.

VI. COMPARISON OF RESULTS, DISCUSSION AND SUMMARY

The experimental measurements of the last section were least-squares fit to the theory for a Gaussian autocorrelation function. We used $a = 0.625$ cm and $h = 5.2$ μm, which were known independently. The fit shown in Fig. 8 is excellent with a small discrepancy appearing only for Fig. 8f. The fit yielded an estimate for the autocorrelation length of $L =$ 0.071 cm, which is in good agreement with the acoustic microscope measurement of 0.073 cm reported in the last section (the nearly exact agreement is probably fortuitous). Figure 9 shows the calculated losses for both Gaussian and exponential correlation functions with $L =$ 0.071 cm. The data are shown by the solid dots and more closely resemble the shape of the curve calculated from the Gaussian autocorrelation function.

The theory overestimates the loss shown in Fig. 8f, which shows the loss for the largest offset distance, 2.2 cm. We attribute the small discrepancy to the relatively small size of the sample, and the increasing effects of diffraction with offset distance. For $z_o = 2.2$ cm the beam extended slightly beyond the roughened area into the area of the smooth frame.

Phase correlation strongly affects the backscattering of waves. Up to the present time most attention has focused on the increase in the variance ("the incoherent backscattering") of the wave. This is the effect typically described as enhanced backscattering, and relates to the diffuse component of the wave. As one might expect, the average specular component of the wave is also affected and in the opposite way. Namely, the strength is reduced rather than being enhanced.

The increased loss in the average, specular signal can potentially degrade the detection of subsurface flaws such as cracks, voids and inclusions. The additional losses due to correlated retransmission are significant for depths on the order or less than, z_e,

$$z_e \approx \frac{k_s L^2 e^{-\sigma^2/5}}{4}, \tag{25}$$

for surfaces with Gaussian autocorrelation functions and for $\sigma^2 < 2$. Equation (25) can be understood as follows. The important question is whether the portion of the beam that transmits through a part of the surface, retransmits through the same part. There are two effects that divert the beam from straight line propagation: diffraction and local-focusing due to the roughness. Equation (25) roughly indicates that for small σ, z_e is determined by the near-field transition distance for a region on the size of the correlation length, L.

In summary, we have used a simple approximation to study the effects of phase correlation on double-transmission and on double-reflection. Correlation causes additional losses in the specular signal for sufficiently high frequencies or for sufficiently small dimensions. Theory was compared with experiment for a double-reflection experiment. Good agreement was obtained. Finally, we proposed a method to determine the surface autocorrelation function from the correlation-enhanced losses.

VII. ACKNOWLEDGMENT

This work was supported in part by the FAA-Center for Aviation Systems Reliability, operated by the Ames Laboratory, USDOE, for the Federal Aviation Administration under Contract No. W-7405-ENG-with Iowa State University. We thank Dr. Gabor Blaho for his valuable contributions in the development of the software and hardware tools used in the experimental work and Mrs. Suquin Meng for her valuable work in carefully preparing the experimental sample.

VIII. REFERENCES

1. P. B. Nagy and J. H. Rose, "Surface roughness and the ultrasonic detection of subsurface scatterers", J. Appl. Phys. **73**, 566 (1993).

2. J. A. Ogilvy, Theory of Wave Scattering from Random Rough Surfaces (Adam Hilger, Bristol, 1991).

3. P. Beckmann and A. Spizzichino, The Scattering of Electromagnetic Waves from Rough Surfaces, (Pergamon Press, Oxford, 1963).

4. M. deBilly and G. Quentin, " Backscattering of acoustic waves by randomly rough surfaces of elastic solids immersed in water ", J. Acoust. Soc. Am.**72**, 591 (1982).

5. M. deBilly, F. Cohen-Tennoudji, A. Jungman and G. Quentin, " The possibility of assigning a signature to rough surfaces using ultrasonic backscattering diagrams ", IEEE Trans. Sonics Ultrason. **SU-23**, 356 (1976).

6. P. B. Nagy and L. Adler, "Surface roughness induced attenuation of reflected and transmitted ultrasonic waves", J. Acoust. Soc. Am. **82**, 193 (1987).

7. C. Eckhart, " The scattering of sound from the sea surface", J. Acoust. Soc. Am. **25**, 556 (1953).

8. J. H. Rose, M. Bilgen, P. B. Nagy, and L. Adler, "Effects of surface roughness on ultrasonic backscatter," in Review of Progress in Quantitative Nondestructive Evaluation,

edited by D. O. Thompson and D. E. Chimenti (Plenum, New York, 1992), Vol. 11B, pp. 1693-1700.

9. M. Bilgen, J. H. Rose and P. B. Nagy, "Ultrasonic inspection, material noise and surface roughness," in Review of Progress in Quantitative Nondestructive Evaluation, edited by D. O. Thompson and D. E. Chimenti (Plenum, New York, 1993), Vol. 12B, pp. 1767-1774.

10. P. B. Nagy, L. Adler and J. H. Rose, "Effects of acoustic scattering at rough surfaces on the sensitivity of ultrasonic inspection," in Review of Progress in Quantitative Nondestructive Evaluation, edited by D. O. Thompson and D. E. Chimenti (Plenum, New York, 1993), Vol. 12B, pp. 1775-1782.

11. Y. A. Kravtsov and A. I. Saichev, "Effects of double passage of waves in randomly inhomogeneous media," Sov. Phys. Usp. **25**, 494-508 (1982).

12. E. Jakeman, "Enhanced backscattering through a deep random phase screen," J. Opt. Soc. Am. A **5**, 1638-1648 (1988).

13. J. W. Goodman, Introduction to Fourier Optics (McGraw-Hill, New York, 1969).

14. I. S. Gradshteyn and I. M. Ryzhik, Tables of Integrals, Series and Products, (Academic Press, New York, 1980).

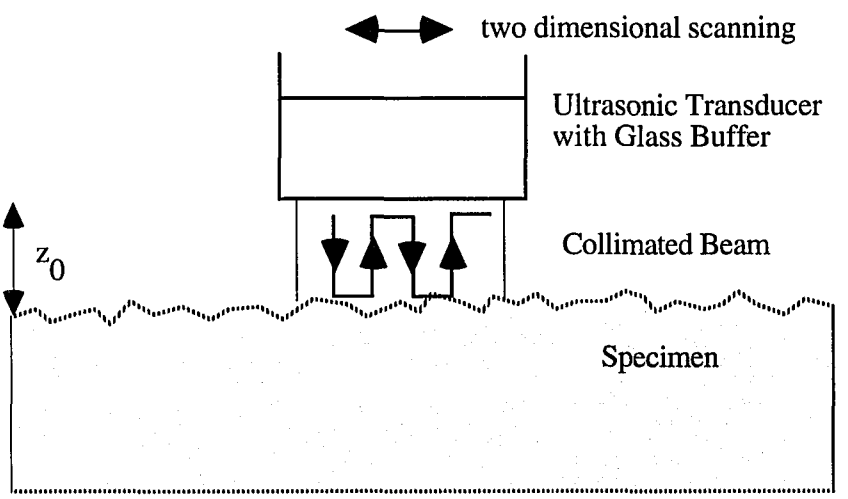

Figure 1. Schematic representation of the geometry of the double-reflection measurement.

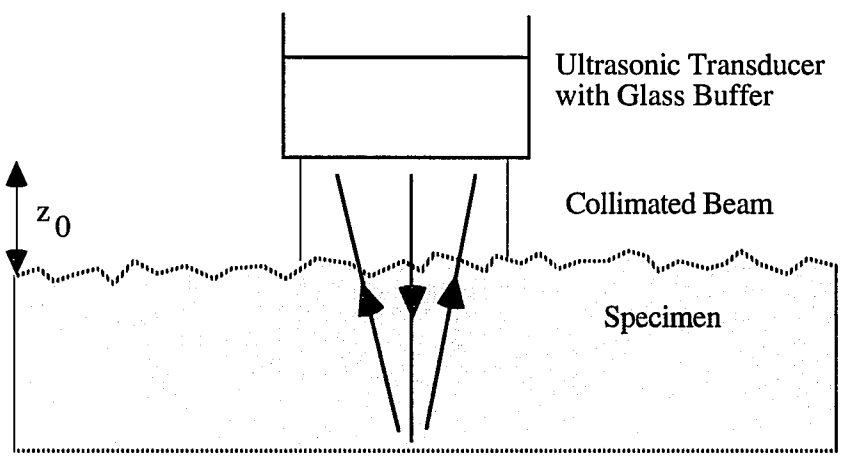

Figure 2. Geometry of double transmission experiment. The signal is generated by the echo from the back surface of the roughened plate.

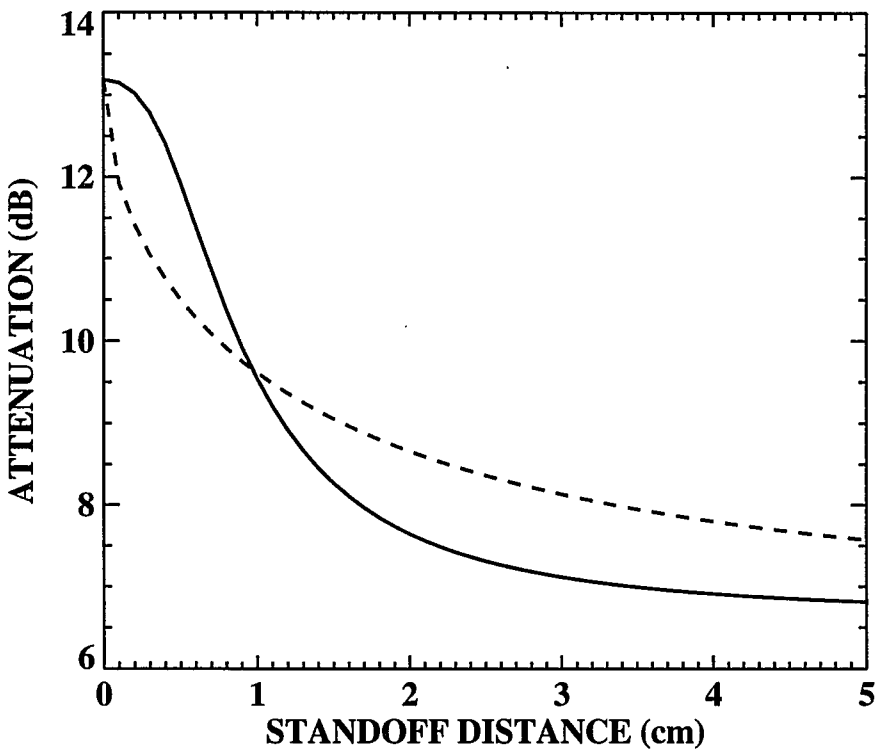

Figure 3. Predicted loss for a Gaussian and an exponential autocorrelation function as a function of the distance between the transducer and the surface for an unfocused transducer. The parameters are $f = 20$ MHz, $L = 0.071$ cm, $h = 5.2$ μm and $R = 0.635$ cm.

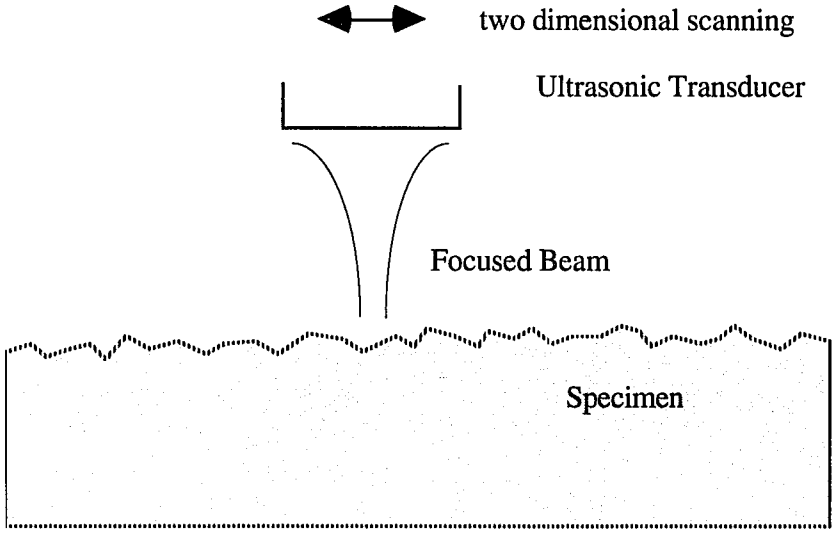

Figure4. Schematic diagram of the acoustic profilometer.

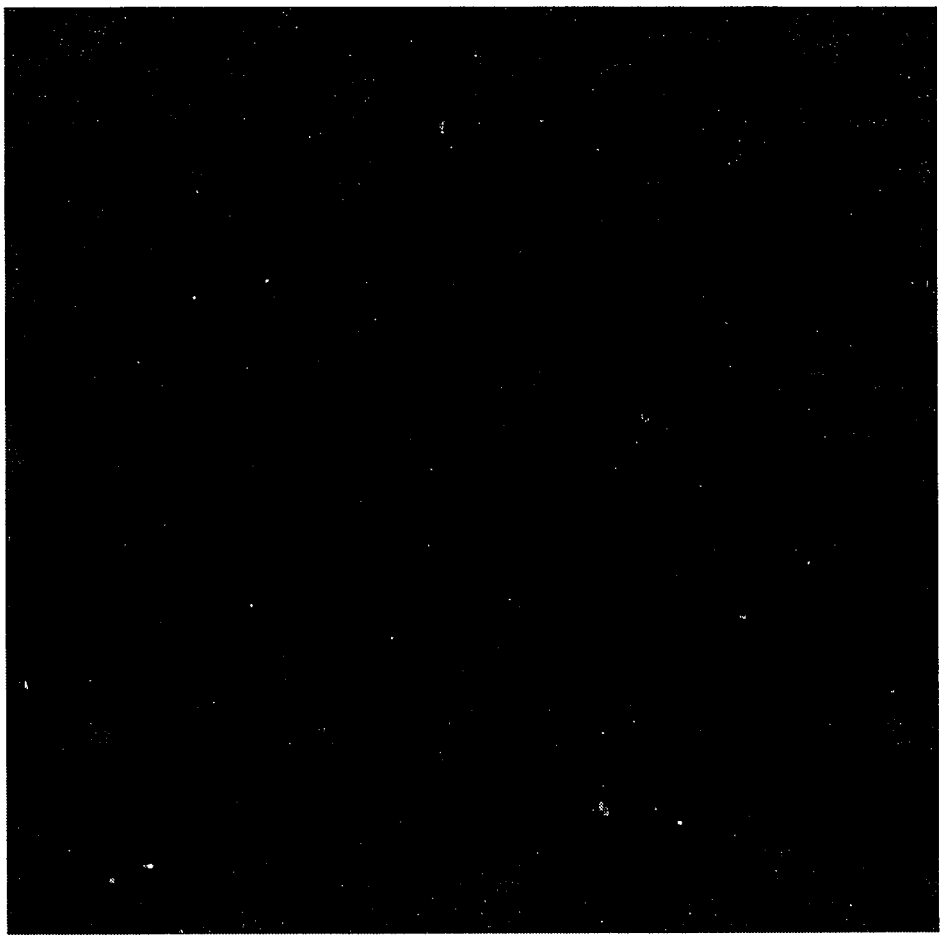

Figure 5. Gray-scale representation of the surface height of a centered 1" x 1" area of the sample.

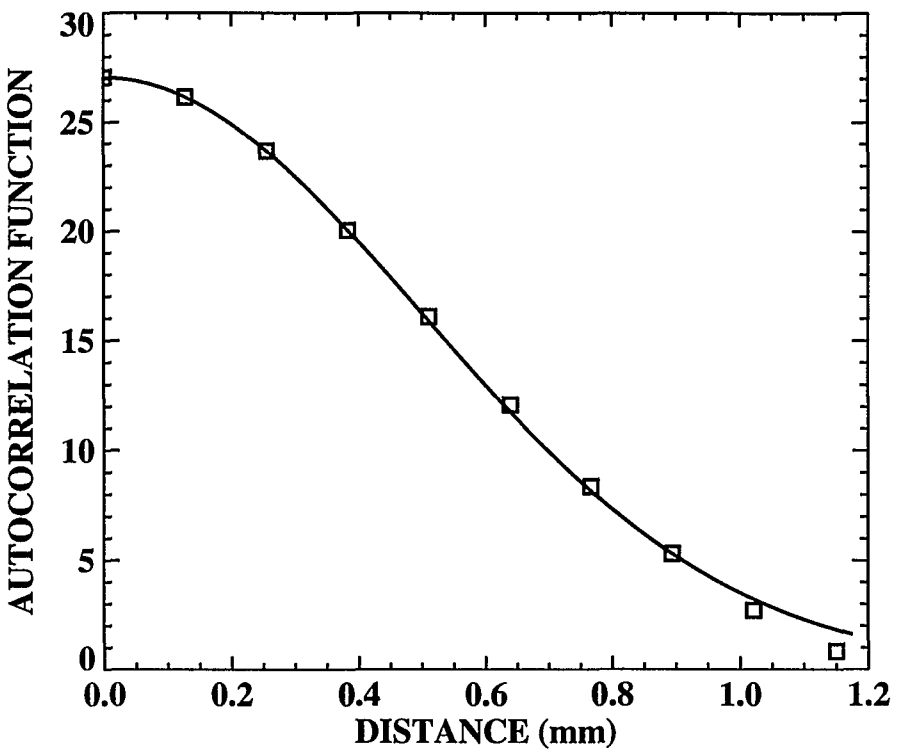

Figure 6. Measured autocorrelation function and the best fit Gaussian, which had parameters L = 724 μm and h = 5.22 μm.

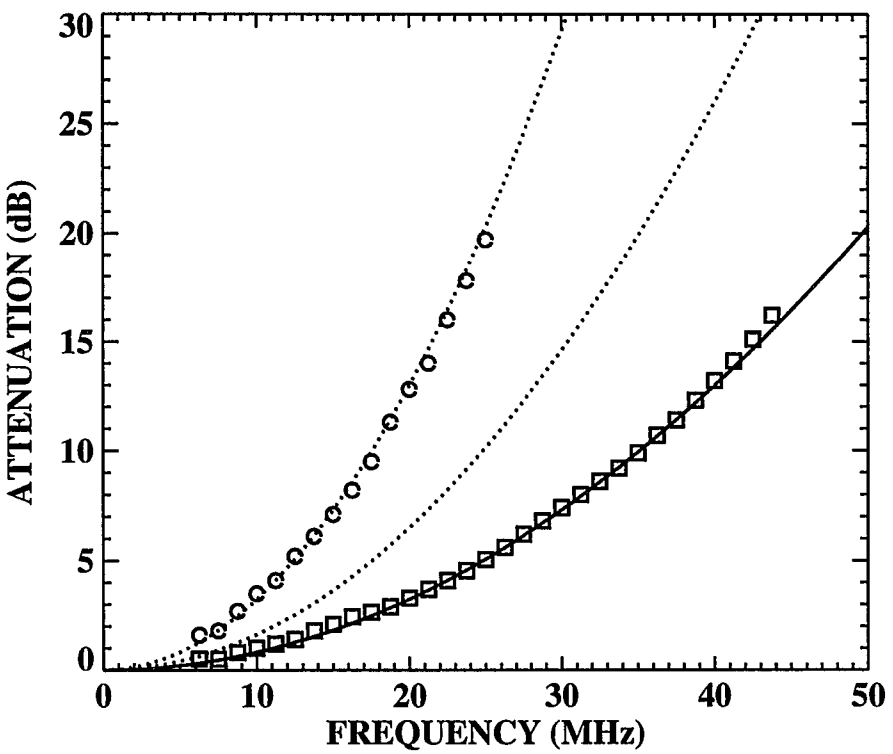

Figure 7a. Measurement of losses for single- and double-reflections. The stand off distance is 2.5 mm.

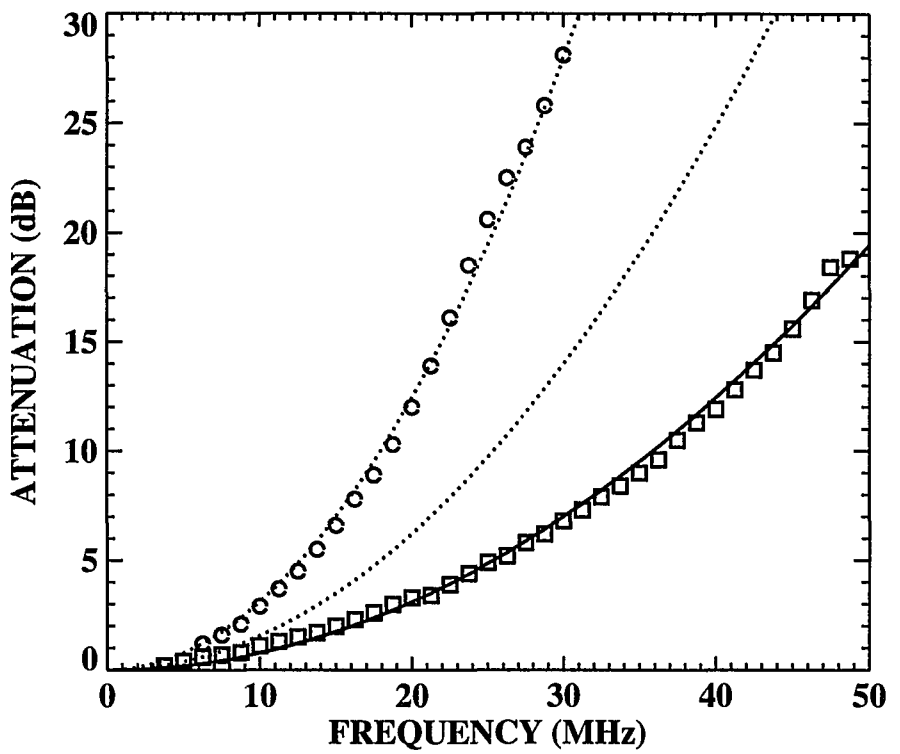

Figure 7b. Measurement of losses for single and double-reflections. The stand off distance is 5.25 mm.

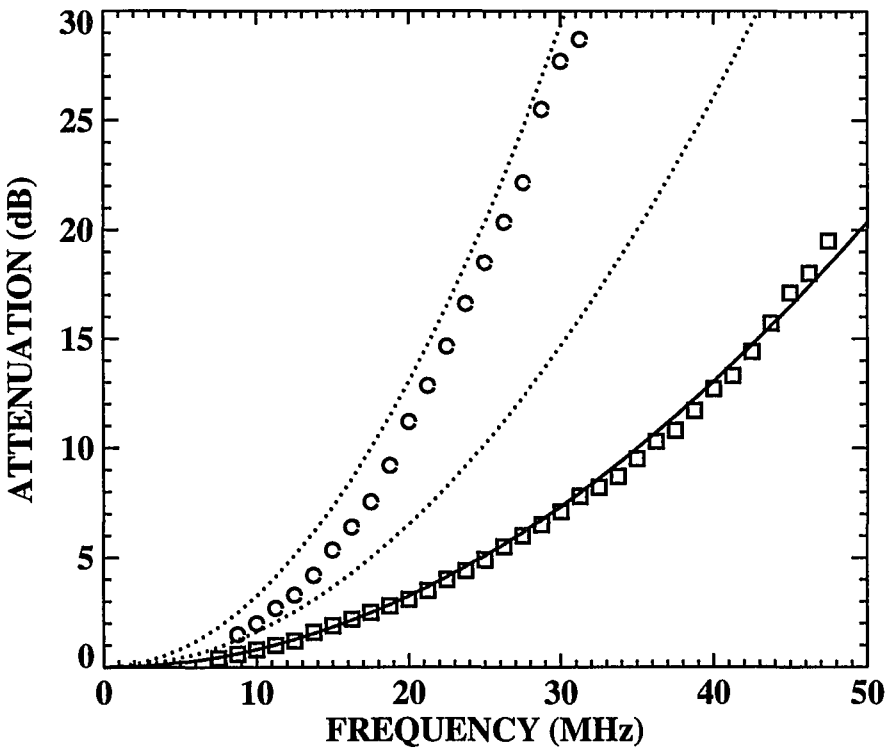

Figure 7c. Measurement of losses for single and double-reflections. The stand off distance is 7.9 mm.

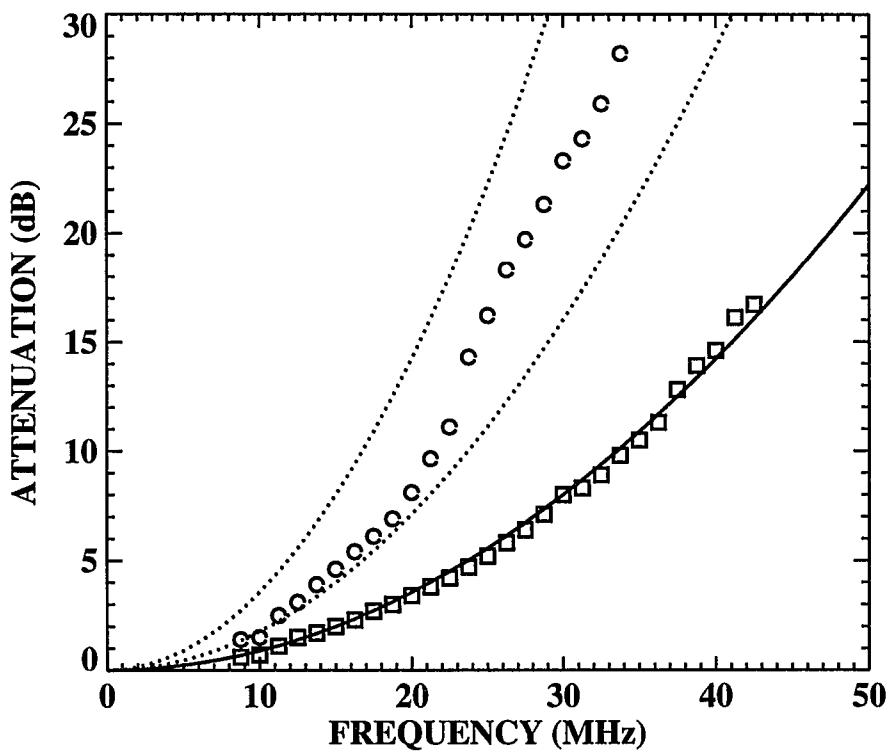

Figure 7d. Measurement of losses for single and double-reflections. The stand off distance is 11.0 mm.

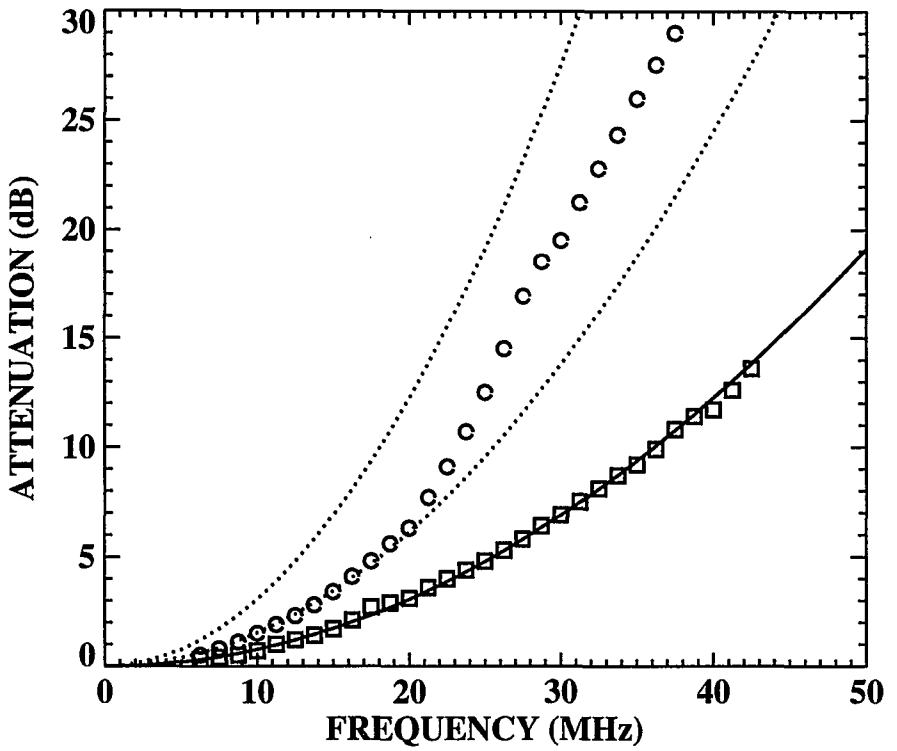

Figure 7e. Measurement of losses for single and double-reflections. The stand off distance is 16.0 mm.

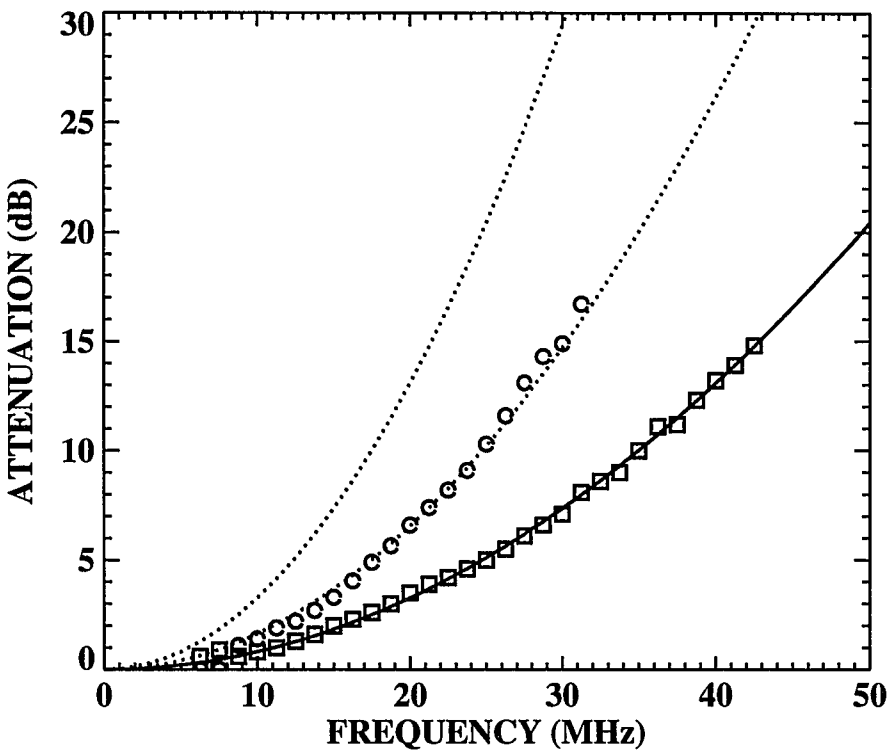

Figure 7f. Measurement of losses for single- and double-reflections. The stand off distance is 22.0 mm.

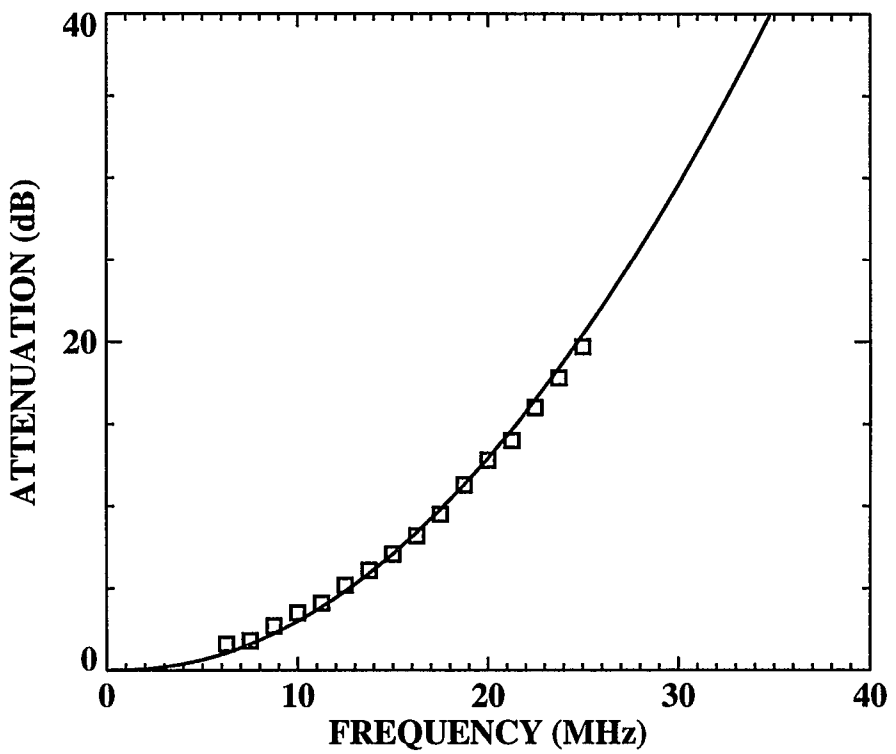

Figure 8a. Compares measured double-reflection loss with theory for a Gaussian autocorrelation function with h = 5.2 μm and L = 710 μm. The standoff distance is 2.5 mm.

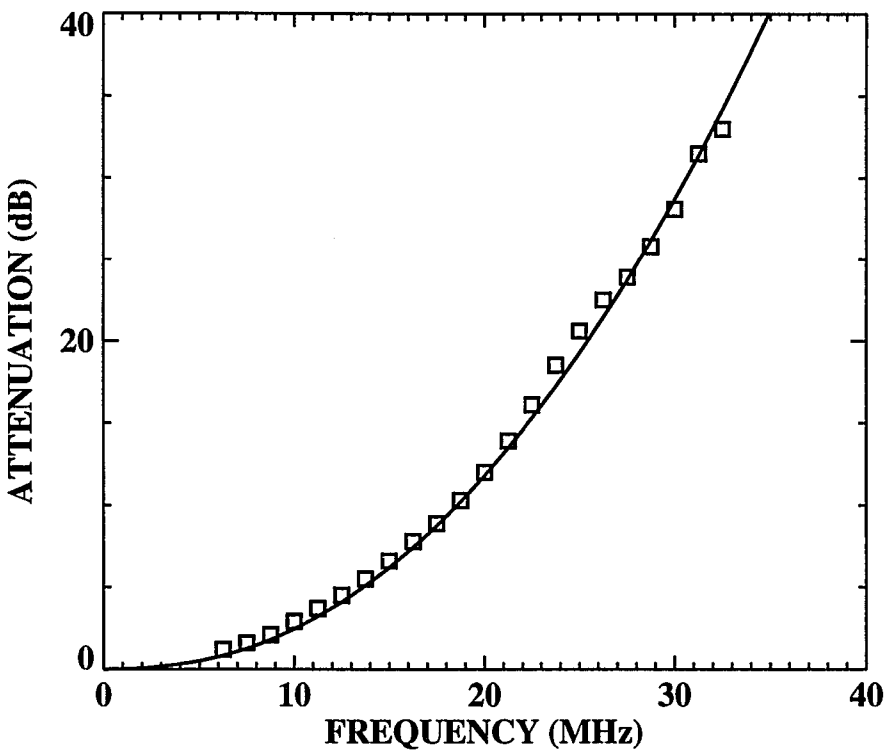

Figure 8b. Compares measured double-reflection loss with theory for a Gaussian autocorrelation function with h = 5.2 μm and L = 710 μm. The standoff distance is 5.25 mm.

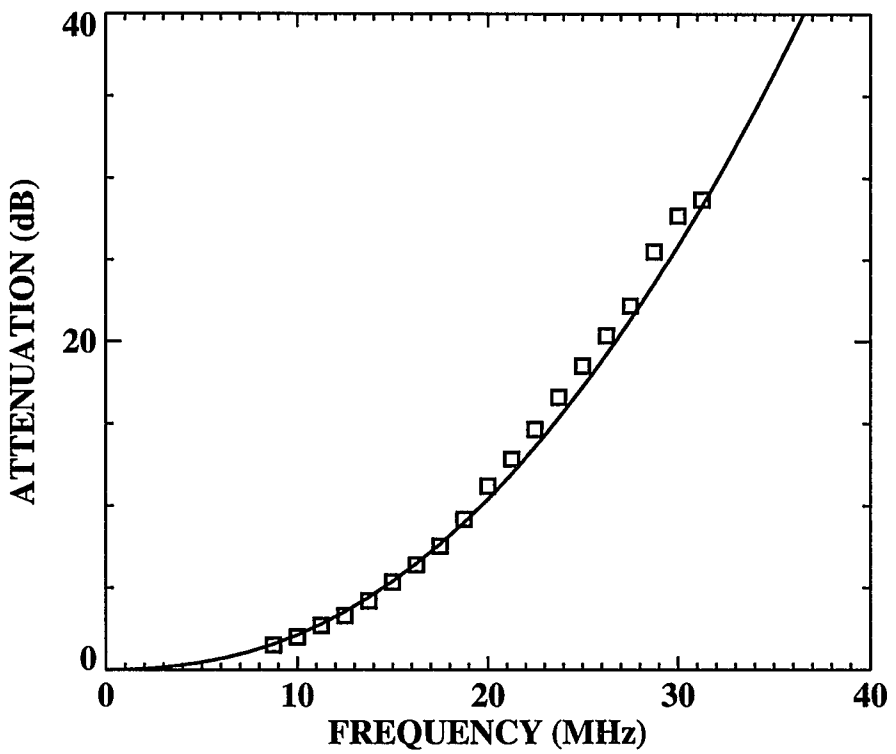

Figure 8c. Compares measured double-reflection loss with theory for a Gaussian autocorrelation function with h = 5.2 μm and L = 710 μm. The standoff distance is 7.9 mm.

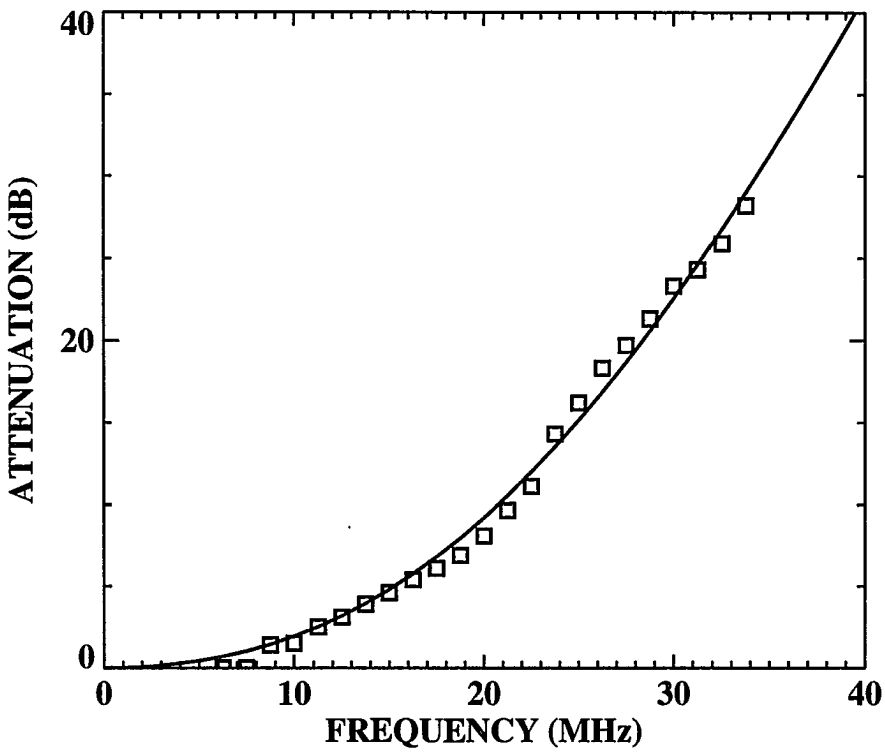

Figure 8d. Compares measured double-reflection loss with theory for a Gaussian autocorrelation function with h = 5.2 μm and L = 710 μm. The standoff distance is 11.0 mm.

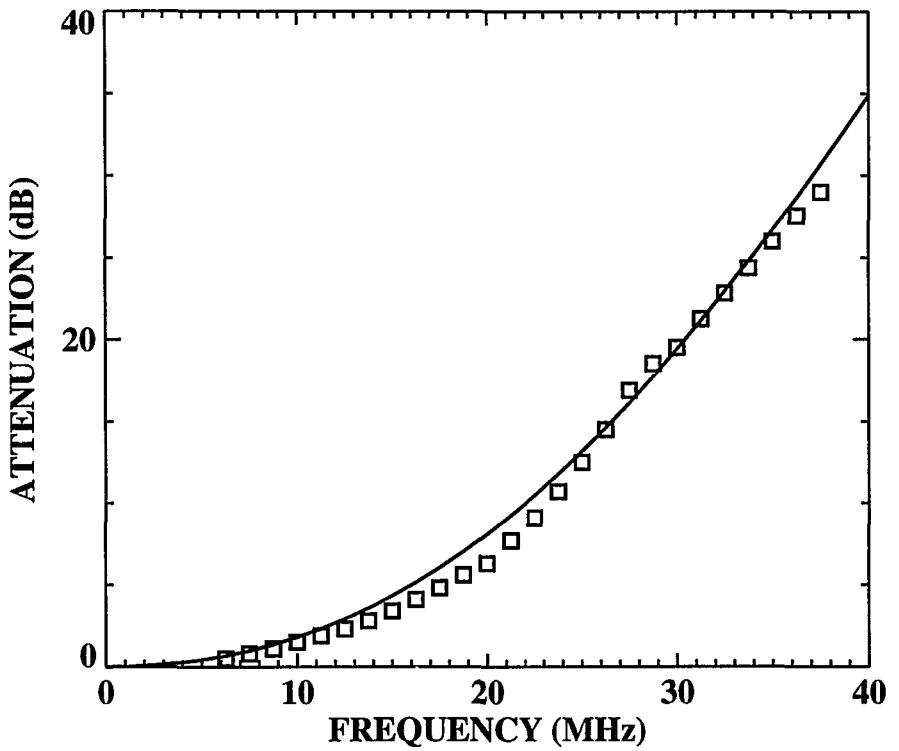

Figure 8e. Compares measured double-reflection loss with theory for a Gaussian autocorrelation function with h = 5.2 μm and L = 710 μm. The standoff distance is 16.0 mm.

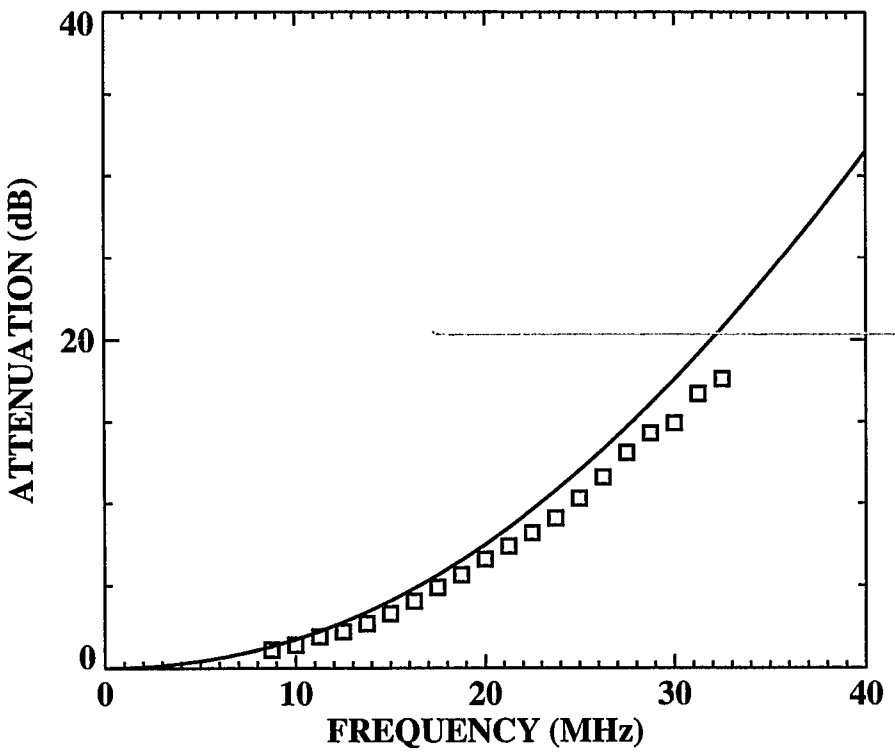

Figure 8f. Compares measured double-reflection loss with theory for a Gaussian autocorrelation function with h = 5.2 μm and L = 710 μm. The standoff distance is 22.0 mm.

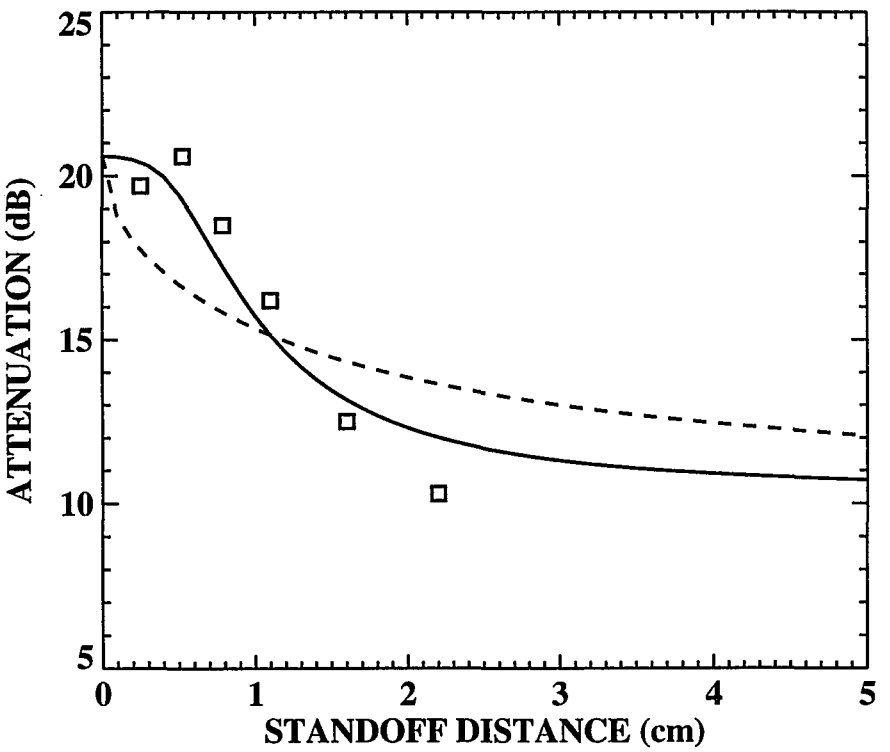

Figure 9. Compares measured loss at 25 MHz as a function of standoff distance and compares it with the theory for both Gaussian and exponential autocorrelation functions with h = 5.2 μm and L = 710 μm.

GENERAL CONCLUSIONS

The objective of this dissertation was to determine the effects of randomly rough surfaces on ultrasonic inspection. The dissertation accomplished this objective by developing robust theories for quantitative inspection of industrial parts with rough surfaces. These theories provide a concrete understanding of the physics of the ultrasonic signal, and establishes a basis for detecting interior defects, e.g. cracks, voids and inclusions, predicting material noise, and characterizing material properties, e.g. grain sizes, and to estimate surface features, e.g. rms height and correlation function. They also provide a basis for the development of experiments and the interpretation of measurements.

Some major results of this dissertation can be summarized as follows 1) observation of a near surface dead-zone for the flaw signal (due to substantially increased attenuation for near-surface flaws), 2) a substantial reduction in roughness-induced noise for focused probes 3) and a consequent improvement in the signal-to-noise ratio, 4) characterization of randomly rough surfaces (the determination of surface statistics from ultrasonic reflections) and 5) comparison of the theoretical results with the available experimental measurements. This dissertation studied the simple but uncontrolled phase-screen approximation in detail and tested its validity against benchmark calculations of the integral equation method. It has demonstrated that this approximation describes the basic physics of wave reflection or transmission fairly accurately at rough surfaces (many circumstances satisfying $k_S h<.5$ and $h/L<.1$).

The theories presented are general for most parts and may be applied to other disciplines that involve randomly rough surfaces. Such applications, for example, arise in the fields of biomedical imaging, remote sensing, optics, electromagnetics and oceonography.

BIBLIOGRAPHY

1. J. W. Goodman. Introduction to Fourier Optics. New York: McGraw-Hill 1969.

2. P. M. Morse and H. Feshback. Methods of Theoretical Physics. Part II. New York: McGraw-Hill Book Company, 1953.

3. B. A. Auld. "General electromechanical reciprocity relations applied to the calculation of elastic wave scattering coefficients." Wave Motion 1 (1979): 3-10 .

4.J. A. Kong, L. Tsang and R. Shin. Theory of Microwave Remote Sensing. New York: Wiley Interscience, 1985.

5. J. C. Stover. Optical Scattering: Measurement and Analysis. New York: McGraw-Hill, 1990.

6. C. Eckart. "The scattering of sound from the sea surface." J. Acoust. Soc. Am. 25 (1953): 566-570.

7. P. Beckmann and A. Spizzichino. The Scattering of Electromagnetic Waves from Rough Surfaces. Oxford: Pergamon, 1963.

8. F. G. Bass and I. M. Fuks. Wave Scattering from Statistically Rough Surfaces. Oxford: Pergamon, 1979.

9. J. Shen and A. A. Maradudin. "Multiple scattering of waves from random rough surfaces." Phys. Rev. B 22 (1980): 4234-4240.

10. M. deBilly and G. Quentin. "Backscattering of acoustic waves by randomly rough surfaces of elastic solids immersed in water." J. Acoust. Soc. Am. 86 (1982): 591-601.

11. E. I. Thorsos. "The validity of the Kirchhoff approximation for rough surface scattering using a Gaussian roughness spectrum." J. Acoust. Soc. Am. 83 (1988): 78-92.

12. D. K. Dacol and D. H. Berman. "Sound scattering from a randomly rough fluid-solid interface." J. Acoust. Soc. Am. 84 (1988): 292-302 .

13. E. I. Thorsos and D. R. Jackson. "The validity of the perturbation approximation for rough surface scattering using a Gaussian roughness spectrum." J. Acoust. Soc. Am. 86 (1989): 261-277.

14. Ö. Bozma and R. Kuc. "Characterizing pulses reflected from rough surfaces using ultrasound." J. Acoust. Soc. Am. 89 (1991): 2519-2531.

15. M. Blakemore. "Scattering of acoustic waves by the rough surface of an elastic solid." Ultrasonics 31 (1993): 161-174.

16. J. A. Ogilvy. Theory of wave scattering from random rough surfaces. Brostol: Adam Hilger, 1991.

17. W. A. Kuperman and H. Schmidt. "Self-consistent perturbation approach to rough surface scattering in stratified elastic media." J. Acoust. Soc. Am. 86 (1989): 1511-1522.

18. P. B. Nagy and L. Adler. "Surface roughness induced attenuation of reflected and transmitted ultrasonic waves." J. Acoust. Soc. Am. 82 (1987): 193-197.

19. P. B. Nagy and J. H. Rose. "Surface roughness and the ultrasonic detection of subsurface scatterers." J. Appl. Phys. 73 (1993): 566-580.

20. C. Pecorari, D. A. Mendelsohn, G. Blaho and L. Adler. "Investigation of ultrasonic wave scattering by a randomly rough solid-solid interface." J. Non. Eval. in press.

21. Y. A. Kravtsov and A. I. Saichev. "Effects of double passage of waves in randomly inhomogeneous media." Sov. Phys. Usp. 25 (1982): 494-508.

22. E. Jakeman. "Enhanced backscattering through a deep random phase screen." J. Opt. Soc. Am. A 5 (1988): 1638-1648.

ACKNOWLEDGEMENTS

I am grateful to Dr. James H. Rose for providing all the guidance, encouragement and insights over the years. I have greatly benefited from working with him. I would like to thank my thesis committee members Dr. William H. Brockman, Dr. Satish S. Udpa, Dr. Hsien-Sen Hung, Dr. David Carlson and Dr. Fritz Keinert for their comments and suggestions. I am grateful to the Center for NDE at Ames for providing me the opportunity to work on this project and greatly value the association made with the people there over the years.

Over all, I would like to thank my family for the support at all times.